



EIDESSTATTLICHE ERKLÄRUNG

Ich erkläre an Eides statt, dass ich die vorliegende Arbeit selbstständig verfasst, andere als die angegebenen Quellen/Hilfsmittel nicht benutzt, und die den benutzten Quellen wörtlich und inhaltlich entnommenen Stellen als solche kenntlich gemacht habe. Das in TUGRAZonline hochgeladene Textdokument ist mit der vorliegenden Masterarbeit identisch.

Datum

Unterschrift

“Es gibt nichts Praktischeres als eine gute Theorie”

Immanuel Kant

Josef und Margarethe Luiprecht,
meinen Großeltern

Abstract

Within this thesis the design and application of a self-regulating hydrogen generation system, capable to release significant amounts of hydrogen from borohydride solutions via non-noble metal catalysts, are presented. Ultimately, this system is able to supply polymer electrolyte membrane fuel cells for portable applications in the power range of 100 W.

Hydrolysis reaction of stabilized borohydride solutions is achieved by non-noble metal catalysts. Using a modified electro-less plating method, a cobalt-tungsten-boron based catalyst is deposited on a nickel foam support material through reduction of the respective metal salts. The resulting catalysts undergo thermal treatment to further improve their catalytic activity. Investigations concerning both deposition as well as the calcination process in order to optimize the catalytic performance have been conducted.

Due to their superior hydrogen storage capacity and long-term stability, borohydride based ionic liquids present a promising replacement for sodium borohydride in the near future. At ambient conditions alkaline media are required to keep borohydride solutions stable and prevent degasification. In cooperation with proionic GmbH, various organic compounds have been examined regarding their hydrogen release behaviour under the influence of a Co-W-B/Ni-foam catalyst.

A passive and self-regulating hydrogen release system is demonstrated on a lab-scale basis.

Kurzfassung

Innerhalb dieser Masterarbeit werden Design und Anwendung eines selbstregulierenden Systems zur Erzeugung von Wasserstoff vorgestellt. Dieses System ist dazu in der Lage signifikante Mengen an Wasserstoff mithilfe von unedlen Metallkatalysatoren aus Borhydrid haltigen Lösungen freizusetzen und ist somit in der Lage Polymer-Elektrolyt-Membran Brennstoffzellen für portable Anwendungen zu versorgen.

Die Hydrolyse-Reaktion von stabilisierten Borhydrid-Lösungen wird dabei mittels unedlen Übergangsmetallkatalysatoren bewerkstelligt. Über die Reduzierung der entsprechenden Metallsalze kann ein Katalysator, basierend auf den Elementen Kobalt, Wolfram und Bor, auf einem Supportschaum aus Nickel abgeschieden werden. Dazu wird eine modifizierte Form der chemischen bzw. autokatalytischen Plattierung verwendet. Zur Steigerung der katalytischen Aktivität werden die so erzeugten Katalysatoren einer thermischen Behandlung unterzogen. Untersuchungen sowohl zur chemischen Abscheidung, als auch zum Kalzinierungsprozess wurden durchgeführt, um die katalytische Performance zu optimieren.

Zukünftig gelten ionische Flüssigkeiten auf Borhydrid-Basis aufgrund ihrer ausgezeichneten Wasserstoff-Speicherkapazität und Langzeitstabilität als vielversprechender Ersatz für Natriumborhydrid. Damit Borhydrid in Lösung bei Umgebungsbedingungen stabil ist, sind alkalische Lösungsmittel vonnöten. In Zusammenarbeit mit proionic GmbH wurden verschiedene organische Komponenten auf ihre Fähigkeit Wasserstoff katalytisch mittels Co-W-B/Ni-Schaum Katalysator freizusetzen, untersucht.

Zusätzlich wird ein passives und selbstregulierendes Freisetzungssystem für Wasserstoff im Labormaßstab präsentiert.

Acknowledgements - Danksagung

Zuvorderst gilt mein Dank meinen Großeltern, Josef und Margarethe Luiprecht, die mir mein Studium mit ihrer selbstlosen und langjährigen finanziellen und persönlichen Unterstützung überhaupt erst möglich gemacht haben. Von ganzem Herzen: Vergelt's Gott!

Des Weiteren möchte ich mich bei meinen Eltern bedanken, die mir in jeder etwaigen Notlage mit Rat und Tat zur Seite gestanden sind und niemals gezweifelt oder gezögert haben, egal in welchen Belangen. Überhaupt möchte ich meiner gesamten Familie herzlichen Dank aussprechen für all die Liebe und Beteiligung an meinem beruflichen Werdegang seit früher Kindheit. Ganz besonderer Dank gilt hier Marlen Luiprecht, die mehr Zeit und Energie in mich und meine Bildung investiert hat als jede andere Person. Durch ihr liebevolles Zutun wurde meine Liebe zur Wissenschaft überhaupt erst erweckt. Dankeschön!

Auch bei meinen Freunden und Studienkollegen möchte ich mich aufrichtig bedanken für all die gemeinsamen Stunden und euren Beistand in den vergangenen Jahren. Ohne euch wäre mein Studium deutlich härter, einsamer und langweiliger gewesen. Ohne euch wäre es "all work and no play" gewesen. Allen voran möchte ich an dieser Stelle meinen Betreuer Dr. Christoph Grimmer erwähnen, der sowohl durch beeindruckende fachliche Kompetenz, als auch durch innige Freundschaft tiefe Eindrücke hinterlassen und mein Studium mit Zuckerbrot und Peitsche vorangetrieben hat. Danke Besti!

Großer Dank gilt auch Assoc.-Prof. Dipl.Ing. Dr. Viktor Hacker für das herzliche Willkommen Heißen in seiner Arbeitsgruppe, seine Begleitung, Unterstützung und sein Entgegenkommen während meiner Masterarbeit.

Vielen lieben Dank natürlich auch an alle Kolleginnen und Kollegen am Labor für Brennstoffzellensysteme für diese großartige, lehrreiche Zeit und all die unvergesslichen Erfahrungen.

Nicht zuletzt gilt meine tiefste Dankbarkeit der Liebe meines Lebens, Estha-Maria Sackl, meinem Gefährten im ursprünglichen Sinn, Martin Schinagl, seiner Gattin Sigrid Elisa Pliessnig, sowie meiner zweiten Familie, Familie Karl, Gerda und Thomas Hutter aus Villach.

Ohne euch wären die kommenden Seiten und alles damit Verbundene undenkbar gewesen!

...DANKE!

Table of contents

1. Introduction	3
2. Hydrogen Storage	5
2.1 General aspects	5
2.2 Hydrogen storage technologies	6
2.2.1 Physical storage technologies	6
2.2.2 Chemical storage technologies.....	8
2.2.3 Borohydride hydrolysis.....	12
2.2.4 Hydrolysis catalysts	13
2.2.5 Borohydride storage systems.....	14
3. Fuel Cells	15
3.1 General aspects	15
3.2 Polymer Electrolyte Membrane Fuel Cell (PEMFC)	17
3.2.1 Composition	17
3.2.2 Efficiency and its limits	19
3.2.3 Advantages of PEM fuel cells	21
4. Experimental	23
4.1 Catalyst fabrication	23
4.1.1 Support material preparation	23
4.1.2 Catalyst deposition	23
4.1.3 Thermal treatment	24
4.2 Characterization	25
4.2.1 Electrochemical performance characterization	25
4.2.2 Volumetric performance characterization	28
4.2.3 Long-term stability	30
4.2.4 Self-regulating Compact Hydrogen Expression System	31
4.2.5 SEM.....	35
5. Results and Discussion	36
5.1 Catalyst optimization	36
5.1.1 Electrochemical deposition	36
5.1.2 Thermal treatment	39
5.2.1 Long-term stability	42
5.2 Ionic liquid characterization	45

5.2.1 Volumetric performance characterization	45
5.2.2 Temperature related performance determination	48
5.3 Self-regulating Compact Hydrogen Expression System	56
5.3.1 Continuous operation.....	57
5.3.2 Discontinuous operation	61
6. Conclusion and Outlook	64
7. References	66
8.1 Results of hydrogen release experiments using the self-regulating system.....	71
8.1.1 NaBH ₄ in 0.1 M NaOH.....	71
8.1.2 DMMorBH ₄ in 0.1 M DMMorOH	77
8.2 Complementary Information	81
8.3 List of figures	81
8.4 List of tables	84

1. Introduction

Environmental impacts of anthropogenic climate change have become more and more drastic and a serious threat to human society over the past decades: Reports of ice caps melting in the Antarctica, sea level rise and the occurrence of heavy natural catastrophes have been increasing sharply. The sea level has been rising 2-3 mm per year since 1993 and is still showing an upward trend [1]. Furthermore, the unnatural increase in catastrophes already claimed a distressingly high toll in the recent past, finding its climax in the 138.000 casualties, caused by cyclone Nargis [2]. Speaking about global warming, the mean earth temperature gained another 0.85 K from 1980 to 2012 [3] due to humanly added greenhouse gases, which does not seem a lot, but considering that during the last ice time the mean temperature on this planet has only been about 5 K lower, gives a different perspective. These facts and numbers demonstrate that global warming has a lot of immanent and latent hazard-potential and needs to be addressed now, before it spirals out of control. The largest part of the responsible greenhouse gases consists of carbon dioxide, making it the biggest lever to pull concerning global warming issues.

Combustion of fossil fuels yields CO₂ as a by-product, which when released to the atmosphere causes up to 26 % of man-made climate change. About 50% of the CO₂ remains in the atmosphere with an average residence time of around 120 years. The most important reason to address this issue as soon as possible is the fact that the three major phenomena considering global warming generate positive feedback, enhancing themselves and one another. They consist of: the water vapour feedback, the ice-albedo feedback and the CO₂ feedback regarding solubility in the oceans. The water vapour feedback states that the warmer a planet is, the more H₂O is found in its atmosphere, which in turn heats up the planet again [4]. The ice-albedo feedback explains the absorption of infrared radiation from different surfaces and how less ice creates an even warmer surface. With rising temperatures more ice sheets are melting, which normally reflect large amounts of heat. Darker, heat absorbing surfaces are exposed, generating a warmer ambient [5]. Lastly, CO₂ interacts with the oceans depending on the temperature. Warm water can dissolve less CO₂ than cold water and releases more of the greenhouse gas into the atmosphere. This self-sustaining processes, combined with atmospheric residence time of carbon dioxide are inhibiting a fast depletion of CO₂ from the atmosphere, even if emissions are reduced or completely stopped.

To prevent even greater, long-lasting climatic problems for the generations to come, greenhouse gas emissions have to be dealt with as soon as humanly possible. This is of course easier said than done, especially with politics acting very slow, setting appropriate targets not before a quite distant future and lacking in consequences for violation of said targets [6]. However, it is possible to take fast and precise measurements against man-made environmental concerns and counteract a global problem in

time, as the Montreal Protocol showed on substances which deplete the ozone layer almost 30 years ago [7]. Kofi Annan declared the Montreal Protocol as “perhaps the single most successful international environmental agreement to date”, however the challenges for CO₂ are considerably bigger.

The most promising and independent way of accelerating a necessary and distinct ecological improvement, concerning the role of CO₂ in global warming, is by revolutionizing the entire energy chain through the development of an alternative, economically lucrative energy carrier and thus paving the way for politics and industry. Science is advancing on a very auspicious path to deliver functioning and economically feasible alternatives to replace common energy-sources and finally relieve the environment. The following thesis gives an insight in a zero-emission technology, representing a promising approach to satisfy ecological claims.

2. Hydrogen Storage

2.1 General aspects

As fossil fuel reserves become more and more scarce, inconvenient to harvest and more expensive in the years to come, not to mention the accompanying environmental impact of the emitted greenhouse gases, a change in energy economy is needed. Changing the energy industry is a formidable task, which has to happen at a large scale, considering that the infrastructure needs to adapt as well. To date hydrocarbons from fossil fuel make up the majority in terms of energy storage and transportation. Those two terms are the key aspects when thinking of advancing to an era of new energy carriers.

The first and lightest element on the periodic table and the most abundant one in the entire universe has been under investigation as a potential energy carrier for decades. Elemental hydrogen is highly reactive and does not exist in nature, therefore it has to be produced by mankind. Although a substitution of hydrocarbons by hydrogen would result in pure water as waste product instead of CO₂, if fossil energy is used to synthesize the gas, the economic value would diminish drastically. Therefore, hydrogen has to be produced from green resources in order to antagonize the greenhouse effect and counteract global warming effectively. Hydrogen has the highest energy per unit weight of any known compound, but very low energy content per unit volume. Compared to gasoline (44 MJ/kg lower heating value), hydrogen (120 MJ/kg lower heating value) contains almost three times as much energy per unit weight, meaning an average fill-up of approx. 40 kg gasoline, would only account for 15 kg for hydrogen, but would need a volume of 1200 L at about 15 MPa, whereas gasoline requires 54 L at ambient pressure [8]. Due to the higher efficiency of the fuel cell system, 1 kg of hydrogen yields a range of 100 km. Modern fuel cell vehicles contain 5 kg of H₂ stored at 70 MPa.

Finding a sophisticated storage medium for hydrogen has proven to be very challenging, since it is everything but trivial to balance weight, volume, energy content and energy input for storage, as this example shows. Many efforts have been made in the years in the search of an economic solution.

A third of the US oil-assets flow into the transportation sector, which means the development of an alternative, green energy storage medium for the automobile industry would have a tremendous impact on both economy and environment. Together with the fact that the US Department of Energy (DOE), the main furtherer of hydrogen storage research in the USA, prioritizes the transportation industry strongly, explains why the prime focuses of hydrogen studies lie on mobile applications and meeting the DOE's demands [8].

2.2 Hydrogen storage technologies

Probably the longest-known option for hydrogen storage is its absorption by a metal. Palladium has the highest absorption rate for hydrogen of all elements and can absorb from 900 times (solid metal) up to 3000 times (colloidal Pd-solution) its own volume in H₂, creating PdH_x by filling its interstitial holes in the metal lattice up with hydrogen [9]. Of course Palladium was never up for discussion because of expense reasons. The next material investigated, one with an even higher absorption rate for hydrogen, was found in 1970 in the form of the intermetallic compound LaNi₅ [10]. With a hydrogen storage capacity of 1.4 wt.%, 360 kg of LaNi₅ would be necessary to store 5 kg of H₂. Many interstitial hydrides have been studied since, and many different approaches have been discovered, exceeding the pure concept of absorption. Today's hydrogen storage technologies can be subdivided into physical storages and chemical storages.

2.2.1 Physical storage technologies

The physical storage technologies include [11]:

- CGH₂ (compressed gaseous hydrogen), 35–70 MPa, room temperature
- LH₂ (liquid hydrogen), 0.1–1 MPa, circa -253 °C
- Cryo-adsorption on high-surface-area materials, 0.2– 0.5 MPa, approx. -193 °C

Compressed gaseous hydrogen

Since hydrogen is not an ideal gas, the volume deviates from the ideal volume with increasing pressure. At a pressure of 60-70 MPa the increase in volume compared to an ideal gas is approx. 20 %, which means compressing will become less efficient at higher pressures. Conveniently enough the mechanical energy content of this system, which gives information about the energy required to bring the gas from ambient conditions to 35-70 MPa, is 18 MJ/kg of H₂ at 70 MPa (considering real mechanical losses), or 14.5 MJ/kg of at 35 MPa. For pressures above 70 MPa the energy demand rises drastically and becomes economically unviable [11].

System costs, fuel costs, volumetric storage density and the gravimetric storage density are still suboptimal considering the DOE targets [12], but nevertheless the CGH₂-system is currently the most applicable technology for mobile application. Due to the simple concept, no temperature issues occur and fill-up times below three minutes are the state-of-the-art as demonstrated in the form of the first fuel cell-cars (Toyota Mirai, Hyundai ix35).

Liquid hydrogen

The significant decrease in volume by liquefying hydrogen at 0.1 MPa, causes a much higher mass density compared to compressed gaseous hydrogen, but it does not change the major drawback of using a -253 °C cold fuel at ambient temperature. The huge temperature difference and the very low phase-change enthalpy of approx. 0.45 MJ/kg between liquid and gaseous H₂ lead to evaporation and thereby an expansion of the stored hydrogen. This overpressure needs to be released periodically and results in significant energy losses. Additional evaporation losses come from filling up the tank at the station. These losses combined with the huge engineering challenges, the loss of a third of the immanent chemical energy by liquefaction and the relatively high system costs, render liquid hydrogen obsolete.

Cryo-Adsorption

Cryo-adsorption is categorized as part of the physical storage technologies, since most materials used bind molecular hydrogen weakly at their surface by physisorption, instead of splitting hydrogen into protons, which then diffuse into the material. Near the millennium various carbon structures were investigated (e.g. nanotubes, multiwall nanotubes, graphites, etc.) and brought promising results, but reproducibility was an issue and many of the early results have been related to impurities, such as water [13], until carbon was rendered unable to store decent amount of hydrogen and fell out of the competition [14]. Zeolites, that are aluminosilicates with a highly porous structure, have got some attention too, but none could convince with a decent storage density above 2.5 wt.%. Polymers with intrinsic microporosity (PIMs) are in the same hydrogen storage range. Another mentionable group of physisorption-materials are the so-called MOFs. These metal-organic frameworks consist of polymers with metal ions in the centres, which are connected by organic molecules. They show three dimensional, crystalline structures and exhibit surface areas >5000m²/g [11]. Within the MOF-structure many parameters can be varied (metal ion, more than one type of metal, length and polarizability of the ligands, etc.), which leads to different adsorption properties and makes MOF research worthwhile. Apparently they reach storage capacities of >10 wt.% at high pressures and -196 °C, while only being able to keep in 1-2 wt.% at room temperature [15].

Although cryo-adsorption technologies show much favourable phase-change enthalpy behaviour and therefore do not struggle with as high evaporation losses as LH₂-technologies, the low temperature brings high costs and the volumetric storage densities are still insufficient regarding DOE requirements [12].

2.2.2 Chemical storage technologies

Chemical storage technologies can be subdivided into [11]:

- Amine-Borane adducts
- Amide/Imide
- Liquid organic hydrogen carriers
- Hydrocarbons
- Methanol
- Glass microspheres
- Hydrides

Amine-Borane adducts

The two most promising amine-borane adducts are BH_3NH_3 and $\text{NH}_3\text{B}_3\text{H}_7$ with 19.6 wt.% and 17.8 wt.% H_2 content respectively. If all the hydrogen from BH_3NH_3 is released, the end product is boron nitride (BN), which is isostructural with diamond and accordingly hard to rehydrogenate. By a two-step partial hydrogen elimination to BHNH , 13 wt.% H_2 can be generated, but side products such as diborane (B_2H_6), ammonia (NH_3) and borazine ($\text{B}_3\text{H}_6\text{N}_3$) are highly toxic for humans and/or fuel cells. $\text{NH}_3\text{B}_3\text{H}_7$ releases hydrogen through hydrolysis, but faces similar issues regarding fuel cell poisoning. Product control or gas cleaning processes enhance are necessary, which either decreases the storage capacity or increases the costs.

Since the hydrogen release reaction is exothermic at 130°C for BH_3NH_3 and requires a catalyst for $\text{NH}_3\text{B}_3\text{H}_7$, reversible hydrogen storage for mobile application is not feasible.

Amide/Imide

In 2002 Chen et al. researched the reversible storage of hydrogen by Li_3N following a three step reaction [16]:



Considering equation 2, the reaction from lithium amide to the imide form generates 6.4 wt.% hydrogen gas at 200°C . Higher amounts of hydrogen could be released from the system, but at much

higher thermodynamic demands. Nevertheless, the high reaction enthalpy of 60 kJ/mol for the rehydrogenation reaction (at 250 °C and 0.1 MPa) and the problem of ammonia evolution at higher temperatures render this system not very well suited for PEMFC.

Liquid organic hydrogen carriers

Liquid organic hydrogen carriers, such as cyclohexane (C₆H₁₂), methylcyclohexane (C₇H₁₄) or decalin (C₁₀H₁₈) have shown significant gravimetric (between 6.1 and 7.2 wt.%) and also volumetric (between 47 and 65 kg/m³) hydrogen storage capacities, are already available at relatively low costs and even the required dehydrogenation catalyst is already developed to a point of very satisfactory activity, stability and life time [11]. Because of high temperatures between 250 and 300 °C, which are necessary to liberate the stored H₂ and the lack of on-board rehydrogenation technology, this system cannot be used for mobile applications. For the mobile sector carbazoles (C₁₂H₉N), which have gravimetric storage capacities of 4-6 wt.%, could be of more interest, if the high melting point issues can be resolved without losing too much storage. Otherwise the material remains solid under ambient temperature, but both decomposition and rehydrogenation need the material in its liquid form in order to take place.

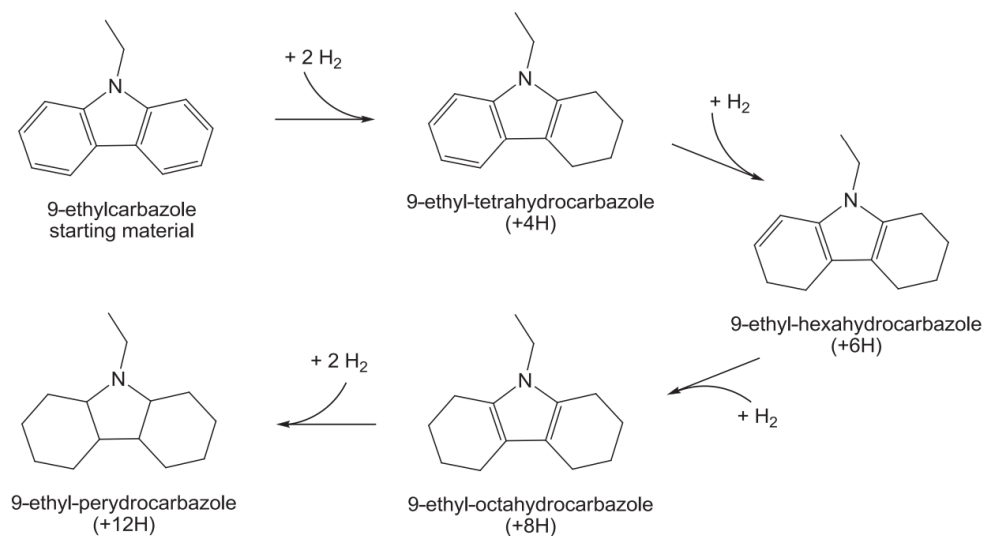


Figure 1: Hydrogenation/dehydrogenation of 9-ethylcarbazole as an example for LOHC [17].

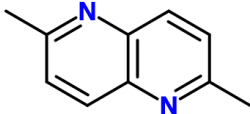
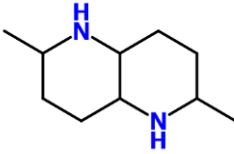
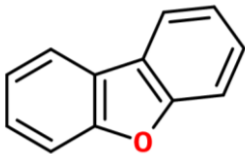
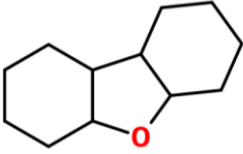
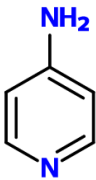
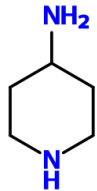
Quality	Dehydrogenated	Hydrogenated
Name	2,6-dimethyl-1,5-naphthyridine	2,6-Dimethyldecahydro-1,5-naphthyridine
Structure		
Theoretic H ₂ storage density		6.0 wt.%
Name	Dibenzofuran	Perhydrodibenzofuran
Structure		
Theoretic H ₂ storage density		6.7 wt.%
Name	4-aminopyridine	4-Aminopiperidine
Structure		
Theoretic H ₂ storage density		6.1 wt.%

Table 1: Examples for liquid organic hydrogen carriers [18].

Hydrocarbons

Hydrocarbons are our main energy carrier at the moment and as such very well understood. They are very well suited for hydrogen storage, as gravimetric hydrogen density as well as volumetric hydrogen density are quite high (e.g. 25 wt.% H₂ for methane). Eberle et al. reported that methane systems are best suited for stationary applications, gasoline and diesel fuel systems have been developed for mobile application and liquefied petroleum gas systems for portable applications [11]. Through steam reforming, partial oxidation or a combination of the two hydrogen can be generated with CO or CO₂ as a side product respectively. Using hydrocarbons for H₂ storage does not solve the ecological problem our current energy industry presents, it could however be of temporary benefit to minimise local emissions. Steam reforming yields high hydrogen concentrations (70-80%), but has longer start-up and general response times (e.g. around 4 minutes for a potential mobile application), partial oxidation on the other hand is less efficient (40-50%).

In general hydrocarbons produce CO₂ emissions and are not the best fit for the automotive industry, since mobile reformers struggle with issues like size, proper heat management and the removal of carbon species, which are poisonous for both the reforming catalyst and the PEMFC.

Methanol

On one hand, reforming of methanol is generally less complicated than reforming other hydrocarbons, because it requires relatively low temperatures (250-300 °C) and yields more hydrogen and less CO. On the other hand, it faces the same challenges as hydrocarbons in addition to the lack of already existing infrastructure [19]. The technology gained ground for portable applications, although it stands in competition with DMFCs.

Glass microspheres

Glass microspheres show surprisingly high gravimetric storage capacities of over 30 %, but lack in volumetric storage density, need high loading and release temperatures and suffer from hydrogen losses at ambient conditions.

Hydrides

The first hydrides investigated for hydrogen storage have been transition metal hydrides, which accumulate hydrogen within the interstitial holes in the crystal lattice. Due to the high molecular weight of those metals they cannot reach appropriate storage capacities. Lighter materials have been found in the form of binary hydrogen compounds, such as Lithium, Beryllium, Magnesium and Boron, but the disadvantages could not be overcome yet.

(Lithium hydride shows a high storage capacity of almost 13 wt.%, but the ionic Li-H-bond is very strong and does not allow decomposition only at very high temperatures. The same goes for Magnesium. BeH₂ is able to store even more hydrogen and due to covalent bonding releases it at much softer conditions. But beryllium is too costly and too toxic for usage. Diborane could store even more hydrogen, but is also highly toxic and pyrophoric in air.)

Close to the millennium, complex hydrides became the focus of attention of reversible hydrogen storage research, after Ti-doped NaAlH₄ with a theoretical storage capacity of 7.5 wt.% was developed [20]. Not all four hydrogen-atoms can be released in an economical way, which diminished the storage capacity to 5.6 wt.%, but in the following years the reaction temperature could be lowered from 200 °C to 80 °C [21]. Replacing sodium with lithium shows overall faster kinetics and lower decomposition temperature [22]. Replacing the aluminium with boron, thus leading to LiBH₄, brings very high storage capacity (18.5 wt.%), but the lithium species struggles with rehydrogenation [23]. Both lithium

borohydride and sodium borohydride excel in theoretical storage capacity, however their high stability and the possibility of PEMFC-poisoning boranes as side products have to be considered.

A future outlook for hydrogen storage is not easy to make. For stationary applications liquid hydrogen is and will be dominant for some time, for mobile application high pressure storage represents still the state-of-the-art technology. Reforming technologies will probably not find any implementation bigger than transportable size.

In general, it is safe to assume that physical storage systems have almost reached their potential limits, while chemical storage systems seem rather promising for meeting DOE targets in a not so distant future. A modern fuel cell car with any kind of chemical hydrogen storage would need a very sophisticated heat management system to maximize the efficiency and will be quite challenging for both chemists and engineers.

2.2.3 Borohydride hydrolysis

Sodium borohydride

Sodium borohydride exhibits an interesting property: the colourless solid is soluble in water and releases hydrogen upon contact with a heterogeneous catalyst [24]. The solution is stable at alkaline pH with a half-life period of over a month at pH = 13, significantly longer half-life at pH 14 and the release can be managed very easily. Considering the decomposition of two molecules of water, NaBH₄ has a gravimetric storage density of 10.6 wt.% [25]. Because the by-product NaBO₂ precipitates as dihydrate (NaBO₂ · 2H₂O) or tetrahydrate (NaBO₂ · 4H₂O), less water is available for hydrolysis or dissolution of NaBH₄. The storage capacity decreases thus from 10.6 wt.% (theoretical value, educts only) to 2.1 wt.% (practical value, considering solubility limits of NaBO₂), which does not meet the DoE requirements for mobile applications, resulting in a no-go recommendation in 2007 [26].

Ionic liquids

Ionic liquids (IL) are liquids that consist only of ions, or rather liquids salts. The difference between an ionic liquid and a molten salt is determined by the melting point; if the material is liquid below 100 °C it is an ionic liquid, which can be used as solvent [27].

If the sodium in NaBH₄ is replaced by an organic cation, the resulting material exhibits ionic liquid-like behaviour and counteracts some issues of sodium borohydride as a hydrogen storage material. Methoxyethyl-trimethyl-ammonium borohydride (METMABH₄) and Dimethyl-morpholinium borohydride (DMMorBH₄), developed by our research partner Prolonic GmbH, both show increased long term stability at milder conditions as well as higher storage capacity in solution [28], [29].

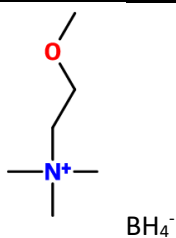
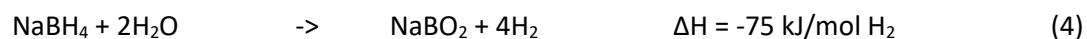
Name	Abbreviation	Theoretic H ₂ storage density	Real H ₂ storage density	Structure
Methoxyethyl-trimethyl-ammonium borohydride	METMA BH ₄	6.0 wt.%	4.7 wt.%	
Dimethyl-morpholinium borohydride	DMMor BH ₄	6.1 wt.%	4.8 wt.%	

Table 2: Properties of the ionic liquids METMABH₄ and DMMorBH₄ [28], [29].

Unfortunately, the viscosity increases during hydrogen release and the overall HRR kinetics are compromised at the expense of higher long term stability [30].

2.2.4 Hydrolysis catalysts

Hydrolysis of BH₄⁻ can be achieved through strong acid, noble-metal catalysts such as palladium or platinum, as well as non-noble transition metal catalysts such as cobalt or iron [31]. The hydrogen release reaction (HRR) is straightforward [24]:



Three key aspects are important regarding catalysts in general and apply for hydrolysis catalysts as well: activity, stability and costs.

Noble metal catalysts, especially platinum and ruthenium on LiCoO₂-support are undeniably ahead in terms of activity and stability. Non-noble metal catalysts are able to release hydrogen at activities around 10.000 ml/min per gram catalyst, while noble metal catalysts still outperform them with activities up to 30 times higher [32]. As for the stability reliable long term data is scarce. More data is available for non-noble metal catalyst, but coherent deductions are risky. It seems like noble metal-catalyst have also better long term stability, but both systems exhibit nowhere near sufficient stability for market maturity. In terms of costs however, the transition metals are far superior with a price of approx. 10 \$ per vehicle compared to 170-560 \$ for precious metal catalysts [32].

2.2.5 Borohydride storage systems

Probably the most researched hydrogen storage system is similar to the one first published by Amendola et al. in 2000. It is in general a continuous flow reactor for NaBH_4 solution, looking more or less as shown below:

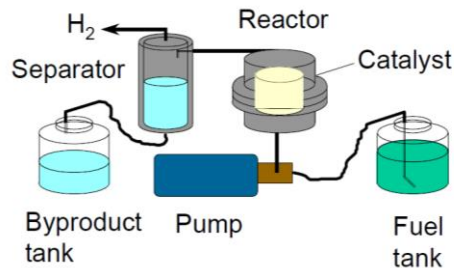


Figure 2: Scheme of continuous flow hydrogen generator [33].

Though high hydrogen storage capacities of up to 6.3 wt.% could be achieved, the results can probably be attributed to excessive amounts of ruthenium catalyst used [34]. Furthermore, the hydrogen storage capacities were calculated on educts-basis only, which means the weight of the vessel and other hardware was not considered. The DoE-targets include those however. As stated above, due to solubility issues resulting in low storage capacities, the DoE rendered $\text{NaBH}_4/\text{NaBO}_2$ solutions obsolete. Another approach using steam at 110 °C to hydrolyse solid NaBH_4 was investigated, but the outcome of 1.9 wt.% H_2 was unsatisfying [35]. By mixing solid NaBH_4 with HCL (3 M) and adding only enough water for stoichiometry 10 wt.% (educts-only) H_2 storage was achieved by Murugesan et al. [36]. The concept of blending small amounts of catalyst precursor to the solid NaBH_4 , leading to an in-situ catalyst development when liquid is added, did exhibit storage capacities over 6 wt.% H_2 [37]. The gravimetric and volumetric hydrogen storage density was successfully increased in order to meet DoE requirements. However, it seems all the other DoE target have been overlooked.

By using acid or catalyst precursor for HRR, these components have to be refilled at every fill up causing much higher cost. Additionally, the fast response time, easy handling and overall “ultra-safety” from the liquid NaBH_4 systems do not apply. Response times are severely lagging, especially for precursor catalyst systems, thus being harder to predict and being at risk of thermal runaway with too much water [38].

3. Fuel Cells

3.1 General aspects

Invented around 1839 by William R. Grove and Christian F. Schönbein, the fuel cell is a tertiary galvanic cell which converts chemical energy directly into electrical energy [39]. This occurs through the oxidation of the fuel at the anode, at which electrons are generated.

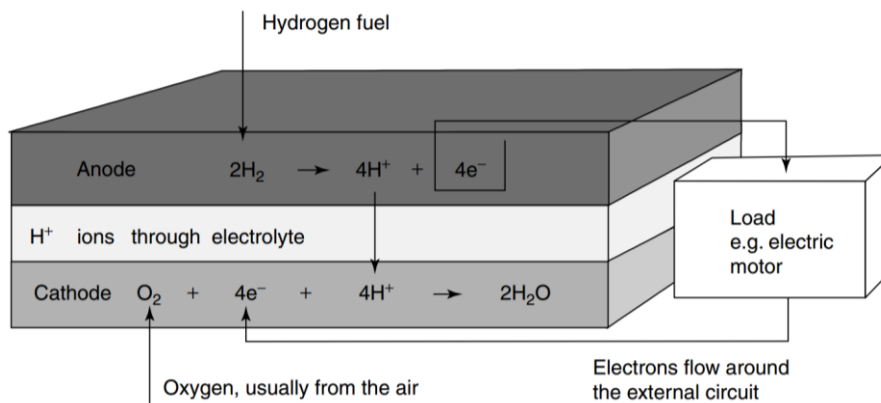
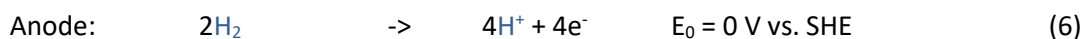


Figure 3: Scheme for an acid electrolyte fuel cell [40]

Theoretically any substance that can be oxidized at an electrode and does not impair any part of the fuel cell system could be used as fuel. Practically Methane, Ammonia, Methanol, Ethanol, Gasoline, etc. are employed as energy carriers for the different fuel cell types, although hydrogen is the most typical and most commonly used fuel [40], [41]. At the cathode oxygen serves as the oxidant, resulting in following electrode reactions [39]:



Oxygen in pure form or the oxygen content in the air is the oxidant for any type of fuel cell. The different types of fuel cells can be distinguished by three criteria: operating temperature, fuel and electrolyte.

Operating temperature:

Low temperature fuel cells	->	operating temperature < 100 °C
Medium temperature fuel cells	->	operating temperature = 100-250 °C
High temperature fuel cells	->	operating temperature > 400 °C

Fuel:

Hydrogen	->	end product = water
Alcohol (methanol, ethanol...)	->	end product = water and carbon dioxide
Syngas from steam reforming	->	end product = water and carbon dioxide

Electrolyte:

Acidic fuel cell	->	mobile ion = proton
Alkaline fuel cell	->	mobile ion = hydroxide ion
Molten carbonate fuel cell	->	mobile ion = carbonate ion
Solid oxide fuel cell	->	mobile ion = oxygen anion

Another possibility for dividing fuel cells is by looking at the application:

Stationary	->	HT-PEMFC, MCFC, SOFC
Mobile	->	LT-PEMFC, SOFC
Portable	->	DMFC, LT-PEMFC

Today, the highest developed fuel cell is the so-called polymer electrolyte membrane fuel cell (PEMFC). It stands out by very high power densities, good long-term endurance and fast dynamic response, amongst other things.

3.2 Polymer Electrolyte Membrane Fuel Cell (PEMFC)

3.2.1 Composition

A common PEMFC consist of:

- Current collector plates or bipolar plates
- Electrodes
- Membrane
- Catalyst

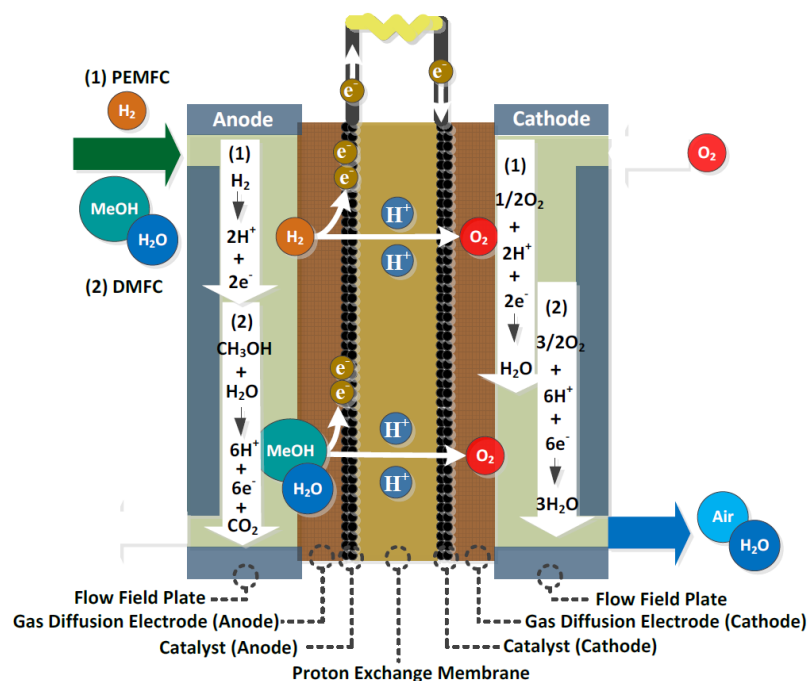


Figure 4: Scheme of a PEMFC (1) and of a DMFC (2) [42].

Current collector plates or bipolar plates:

The end plates are made from electrically conductive materials and keep the fuel cell compressed from both sides. They are necessary to deviate the current from the bipolar plates and can also help to control the temperature. The bipolar plates connect the current collector plates and the electrodes and supply them with hydrogen and oxygen through engraved flow fields. Made from graphite-material or metal, they are used to collect the current produced in the fuel cell and to control the temperature of the system.

Electrodes:

The electrodes consist of carbon-based materials, since they need to be electrically and thermally conductive, mechanically and chemically stable and water repellent. The part contacting the electrolyte is called the active layer. Within the active layer, at the so-called three-phase-boundary, fuel gas, electrolyte and catalyst meet (fig. 6). The active layer has a very fine structure, and a big, catalyst enriched, active surface. The other part, which is in contact with the bipolar plates, is called the gas diffusion layer and has a coarse structure to allow gas to pass through and to remove product water.

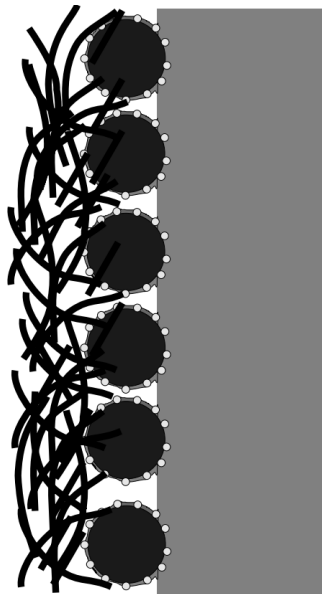


Figure 5: Scheme of a PEMFC electrode with gas diffusion layer (left), active layer (middle) and electrolyte (right) [40].

Membrane:

The membrane is made up from a fluoroethylene polymer with sulfonated functional groups.

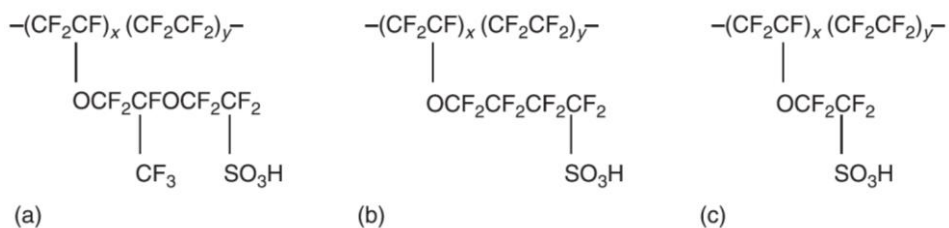


Figure 6: Example structure of Nafion® (a), 3MTM-PFSA (b) and Aquivion® (c) [41].

The first one provides mechanical and chemical stability and is very hydrophobic (product water gets purged), while the end groups are strongly acidic and thus create hydrophilic regions which allow protons to freely move. The most common perfluorosulfonic acid-based ionomer is Nafion[®] from Dupont and exists since the 1960s [40], other important ones are Aquivion[®], Flemion[®] and Aciplex[®] [42], [41].

Furthermore, the membranes need to be very thin (10-100 μm) but a barrier for hydrogen and electrons at the same time [43].

Catalyst:

The most widely used PEMFC catalyst is platinum and should be dispersed on the carbon particles as fine as possible to ensure a big active area. This is where the electrode reactions take place. Catalyst particles and loading should be as small as possible, around 3-10 nm in size and around 0.15 mg/cm² in loading [44].

3.2.2 Efficiency and its limits

For thermal engines the efficiency is limited by the difference in temperature of the operating heat engine and the temperature at the exhaust. The so-called Carnot efficiency is:

$$\mu_C = \frac{T_1 - T_2}{T_1} \quad (8)$$

T₁ -> Temperature of working engine

T₂ -> Temperature at exhaust

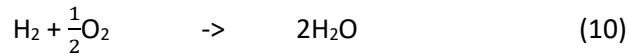
Therefore, the theoretical efficiency of an internal combustion engine is approx. 54 %. Since fuel cells are not limited by the Carnot efficiency, efficiencies of over 90% are possible.

Thermodynamically spoken, the efficiency can be calculated by using the change of enthalpy and the change of entropy of the electrode reactions, resulting in:

$$\mu_{th} = 1 - \frac{T \Delta S}{\Delta H^0} \quad (9)$$

-ΔH⁰ -> Change of enthalpy of formation

Depending on the physical condition of the product water there are two possible values for ΔH^0 :



$$\Delta H^0_{\text{LHV}} = -241.83 \text{ kJ mol}^{-1} \quad (\text{g}) \quad E_{\text{th}} = 1.25 \text{ V}$$

$$\Delta H^0_{\text{HHV}} = -285.84 \text{ kJ mol}^{-1} \quad (\text{l}) \quad E_{\text{th}} = 1.48 \text{ V}$$

ΔH^0_{LHV} is called the lower heating value and ΔH^0_{HHV} is called the higher heating value. The difference between those two is the molar vaporisation enthalpy of water [45]. Since the reaction above is not reversible, which means a loss in energy due to entropy, the total electrical energy available is equal to the change in Gibbs free energy:

$$\mu_{th} = \frac{\Delta G}{\Delta H^0_{\text{HHV}}} * 100 \quad (11)$$

At room temperature (25 °C) and for liquid product water this equals a theoretical efficiency of 83%. Some other theoretical efficiency limits are shown in fig. 8:

Form of water product	Temperature [°C]	ΔH^0 [kJ/mol]	Max. EMF [V]	Efficiency limit [%]
Liquid	25	-237.2	1.23	83
Liquid	80	-228.2	1.18	80
Gas	100	-225.2	1.17	79
Gas	200	-220.4	1.14	77
Gas	400	-210.3	1.09	74
Gas	600	-199.6	1.04	70
Gas	800	-188.6	0.98	66
Gas	1000	-177.4	0.92	62

Table 3: Efficiency limits based on HHV for hydrogen fuel cells [40].

The electrical efficiency of a fuel cell is always below the theoretical efficiency and can amount up to 70% [46]. By relating the actual measured voltage to the Gibbs free energy, which is the open cell voltage of a fuel cell, the electrical efficiency can be defined:

$$\mu_{el} = \frac{-zFE}{\Delta H^0} = \frac{E}{E_0} \quad (12)$$

- z -> Number of exchanged protons
- F -> Faraday constant = 96485 C/mol
- E -> Measured cell voltage
- E₀ -> Open cell voltage

3.2.3 Advantages of PEM fuel cells

The general advantages of fuel cells compared to other energy technologies are considerable.

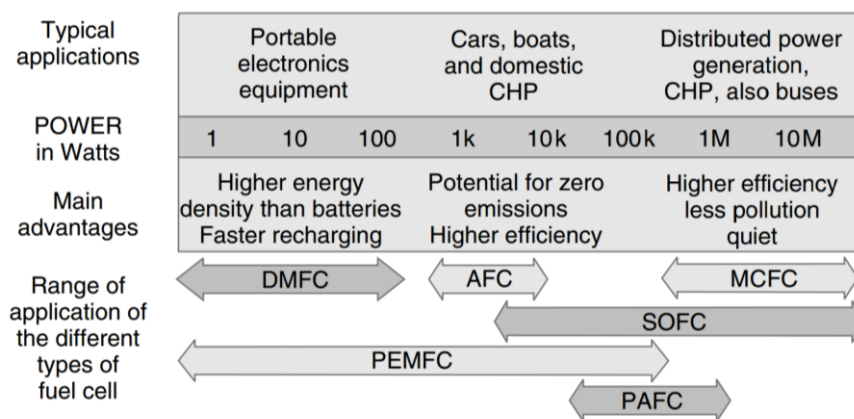


Figure 7: Advantages and applications of different types of fuel cells [40].

On the other hand, there are two major issues at this time: the missing infrastructure for hydrogen and the overall cost-efficiency. A closer look at PEM fuel cells reveals many very promising aspects, which are the reason for the extensive research in past and present:

- Emissions By using hydrogen from green sources as fuel, the end product is water and hence the PEMFC becomes a possible zero emission energy generator.
- Efficiency Fuel cells convert chemical energy directly into electrical energy, which leads to a high overall efficiency (>60%), as well as very high partial load efficiency.

- Flexibility
The range of possible applications is very wide: fuel cells can produce energy from a few watts up to a megawatt and are hence suited for portable, mobile and stationary systems.

- Simplicity
Due to the simple build-up, fuel cells are very compact systems with no moving parts and therefore slow abrasion and high lifetimes. The sealing and cooling technology is also quite trivial, because the operation temperature is low and the electrolyte is solid. Furthermore, since the electrolyte is solid, there comes no hazard from highly corrosive, liquid electrolytes.

- Dynamic
Another advantage of a low operation temperatures and a compact system is the dynamic handling, which allow a fast start up/shut down, as well as swift load changes.

- Silence
The formation of water from hydrogen and oxygen does not make any noise and even with the implementation of a fuel processor and a cooling circle, the system is still very silent.

4. Experimental

4.1 Catalyst fabrication

The catalysts for hydrogen release were fabricated via an electro-less plating method described by Dai et al. and consisted of cobalt, tungsten and boron on nickel foam [47]. Due to the much higher catalytic activity reported for thus prepared catalysts, this modified electro-less plating method was chosen over conventional methods for the preparation of the Co-W-B catalysts used in this thesis.

4.1.1 Support material preparation

A piece of commercially available nickel foam (by Alantum, GER) was cut up by scalpel to the desired size, weighted and submerged into EtOH abs. The solution containing the pieces of foam was then put into an ultrasonic bath for 10-15 minutes in order to purge it from greasy residues. Afterwards, the foam was rinsed with aqua dest. and immersed into a 10 % HCl-solution for another 10 minutes to reduce the oxidized surface area of the support material.

Prior to this thesis a short laboratory project has been conducted to determine the best parameters for nickel foam as support material. The following table shows the parameters chosen for all nickel-foams within this work:

Producer	Thickness [mm]	Porosity [%]	Pore size [μm]	Area density [g/cm^2]	Purity [%]
Alantum	1.6	95	800	460 ± 30	95

Table 4: Parameters of nickel foam support material.

4.1.2 Catalyst deposition

For the deposition of cobalt, tungsten and boron, the cations of the respective salts had to be reduced to their elemental state. Therefore, two solutions were prepared: one containing cobalt and tungsten salts, the other containing sodium borohydride both as reducing agent and as boron source. Then, 2 ml of the two previously prepared solutions were poured onto the foam, first solution A and approx. 20 seconds later solution B to start the deposition reaction. The evolution of hydrogen could be observed as the catalyst has been deposited on the nickel foam. Composition and concentration of the two solutions are given in the table below:

Solution A	Concentration [g/L]
CoCl ₂ 2H ₂ O	50
Na ₂ WO ₄ 2H ₂ O	15
NH ₄ Cl	80
NH ₃ H ₂ O	45
Solution B	
NaBH ₄	40
NaOH	10

Table 5: Composition of the two solutions used for electrochemical deposition of the catalyst [47].

The following chemical reactions were involved in forming the Co-W-B-catalyst:



During the deposition solution A, which had shown a brownish colour at the beginning, changed its colour to a light red and finally to a deep black. The reaction was completed after approx. 15-20 minutes, when hydrogen evolution, which could be observed as bubbling, had stopped completely. Afterwards the catalyst was cleaned with aqua dest. and the whole deposition was repeated. The number of depositions steps regarding hydrolysis activity has been investigated within this thesis, leading to a reduction from 3 overall steps for the first generation of catalysts to 2 steps for the second generation.

4.1.3 Thermal treatment

To conclude the catalyst preparation a temperature treatment under inert atmosphere (N₂) has been conducted. The Co-W-B/Ni foam catalyst was put into an oven at 250°C for 2 hours to enhance the catalytic activity. Dai et al. stated an improved performance after calcination, due to an enlarged active surface area and the precipitation of nanocrystalline cobalt [47].

The figure below shows the raw support material, the deposition steps and the Co-W-B/Ni-catalyst after annealing:

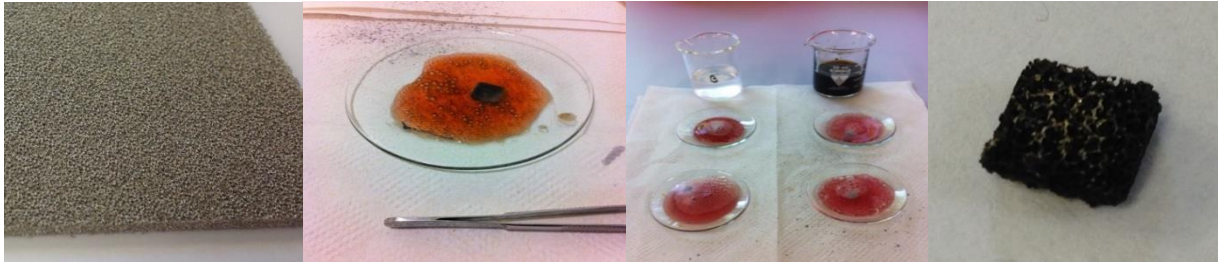


Figure 8: Raw nickel foam (left), during catalyst deposition (middle) and catalyst after calcination on nickel foam (right).

4.2 Characterization

4.2.1 Electrochemical performance characterization

4.2.1.1 Setup

The hydrogen release reaction rate determines the activity of the catalyst and was measured with an electrochemical method. After the Co-W-B/Ni-foam was put in an especially designed, in-house fabricated and temperature controlled acrylic glass cell (fig. 9), the whole system was flushed with inert N_2 gas for approx. 15 minutes.

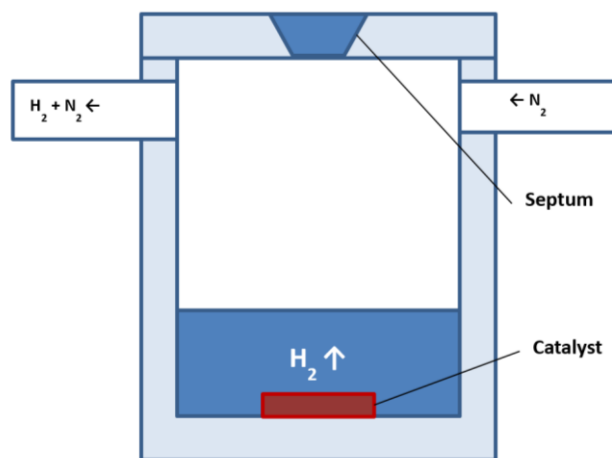


Figure 9: Scheme of the in-house made hydrogen release cell.

Once all the air had been purged from the system, a standard $NaBH_4/NaOH$ -solution was injected with a syringe through a septum at the top of the cell and the hydrogen evolution started instantly. The newly released hydrogen was carried by the applied N_2 stream through a washing flask (filled with H_2SO_4 to rinse the gas from amine impurities) to a fuel cell, where the H_2 has been oxidized. The resulting current was measured with a Zahner potentiostat using Thales software.



Figure 10: In-house made hydrogen release cell; spare parts (left) and assembled cell (right).

4.2.1.2 Method

To determine the activity or rather the amount of hydrogen liberated through the catalyst, an internally fabricated PEM fuel cell with an active area of 25 cm^2 had been connected to a power potentiostat from Zahner. The former was needed to oxidise hydrogen, thus generating current; with the aid of the latter the resulting current could be measured. This measurement has been topic of a publication in the International Journal of Hydrogen Energy [48].

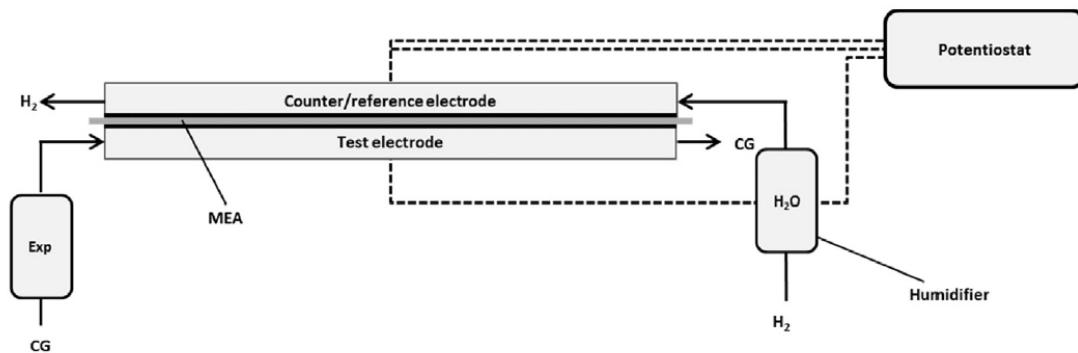
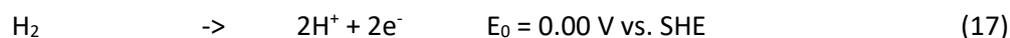


Figure 11: Measurement setup consisting of: hydrogen release cell, fuel cell and potentiostat [48].

The fuel cell itself consisted of a commercially available MEA (membrane electrode assembly), graphite flow fields, gold bathed copper current collectors and stainless steel end plates [49]. Using the cathode of the electrochemical cell as our test electrode, the anode as counter and pseudo reference electrode, hydrogen could be detected. Catalytically released H₂ was carried (by a nitrogen stream) to the test electrode, to which an over potential of 430 mV regarding the hydrogen oxidation reaction was applied

by the potentiostat. Therefore, oxidation of the delivered elemental hydrogen occurred, leading to the generation of protons and electrons:



Those H^+ cations crossed over to the counter electrode and reacted back to elemental hydrogen, the electrons from the same reaction were registered. Conveniently enough, the counter electrode of the same fuel cell could be used as pseudo reference electrode, when flushed with H_2 from the tap.

4.2.1.3 Settings

Unless specifically stated in the results and discussion section below, the following setting parameters have been used for the herein performed hydrogen release rate measurements:

Temperature	[°C]
Fuel cell	65
Humidifier	59.9
Gas pipes	70-74
Release cell	30
Gas flow	[ml/min]
Working electrode N_2	40
Counter electrode H_2	40

Table 6: Parameters for HRR measurements.

Humidifier and gas pipes were integrated in the in-house assembled measuring station and could be controlled via Labview. If the measuring station was not available, a simple water-filled washing flask has been implemented into the setup between hydrogen gas tap and fuel cell to keep the MEA moistened and the PEMFC efficient.

4.2.1.4 Equipment

The following table lists the operation equipment for the hydrogen release rate experiments executed during this work:

Equipment	Hardware	Software
Potentiostat	Zahner IM6 combined with a PP240	Thales
In-house built measuring station	Complex heating and piping system	Labview
In-house made release cell	Acrylic glass frame and silicon gaskets	-
Thermostat	Julabo ME	-

Table 7: Equipment used for HRR measurements.

For measuring samples with volumina bigger than 1 ml, the release cell could be expanded, if another acrylic glass piece was added. For even bigger volumina the cell had to be replaced by a double-walled three-way round bottom flask, which yielded similar properties.

4.2.1.5 Setup for performance characterization at different temperatures

Activity measurements at different temperatures have been conducted using the method outlined above. However, to compare different bases for ionic liquid dissolution, a slightly modified setup has been used. The hydrogen release cell (see section 4.2.1.1) has been replaced by a 100 ml triple-neck round bottom flask, which was half-way submerged into an open Julabo for thermostatzation. Nothing else was changed within the normal setup, but the release chamber.

4.2.2 Volumetric performance characterization

4.2.2.1 Setup

A very long known, but still widely used standard method for hydrogen quantification is the water displacement method [50], [51]. By channelling the released hydrogen via hose into an upside down, water-filled glass cylinder (or U-shaped tube), the amount of gas could be determined by simply reading the meter. The advantages were simplicity and thus low error rates, the drawbacks consisted of the possibility of human error, as well as fewer and less precise values.

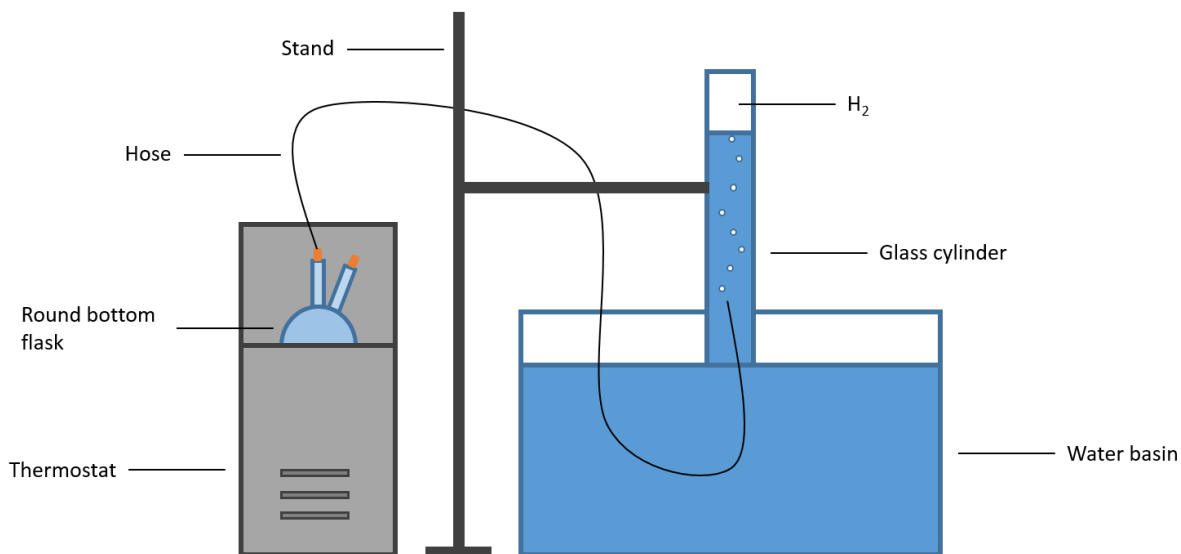


Figure 12: Setup for volumetric water displacement method.

As shown above, a 100 ml double-neck round bottom flask, which was half-way submerged into the tempered water of an open thermostat, was implemented as hydrogen release cell. Because no carrier gas flow was needed, a double-neck flask, instead of a triple-neck round bottom flask has been used.

4.2.2.2 Equipment

For hydrogen quantification via water displacement method the following equipment was used:

Equipment	Specification
4 x Glass cylinder	Volume = 0.5 L
Water basin	Volume = 50 L
Thermostat	RMS Lauda
4 x double neck round bottom glass flask	Volume = 100 ml
Piping	Silicon hoses

Table 8: Equipment for volumetric water displacement method.

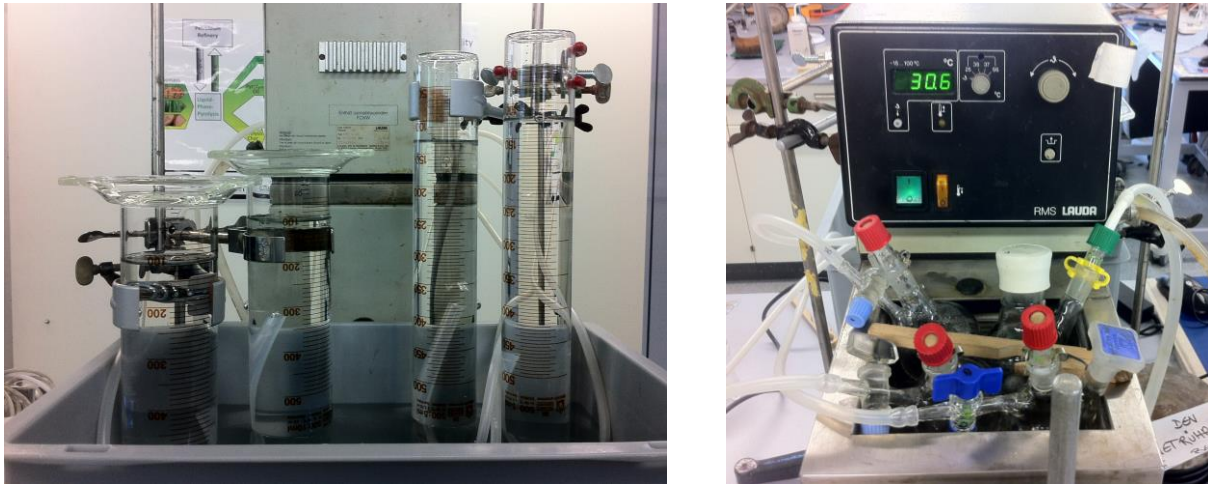


Figure 13: Glass cylinders during the measurement (left), double-neck flasks submerged into the thermostat (right).

4.2.3 Long-term stability

4.2.3.1 Setup

The setup for long-term stability measurements was straightforward: the activity of a catalyst has been examined (as specified in section 4.2.1) before and after non-stop operation over a certain time period, or rather at the begin of lifetime (BOL) and the end of lifetime (EOL). To simulate permanent operation conditions, the catalyst was put in a 2 L glass beaker, filled with approx. 1 L of sodium borohydride solution. If the visible bubbling and thus the HRR regressed, the solution was replaced with fresh NaBH_4 solution.

4.2.3.2 Equipment used

For the simulation of non-stop operation over a defined period of time, only 3 items were required:

Equipment	Specification
Glass beaker	Volume = 2 L
Watch glass (to cover the beaker)	Diameter = 200 mm
NaBH_4 in 1 M NaOH	1 wt.% H_2

Table 9: Equipment used for the simulation of non-stop operation.

4.2.4 Self-regulating Compact Hydrogen Expression System

4.2.4.1 Setup

The final aim of this thesis has been the design and development of a compact hydrogen storage system, able to produce significant amounts of hydrogen on demand, comprising one key feature: the system should be self-regulating without the help of any external power device like a pump or a stirrer. Consisting of some safety valves and two in-house made acrylic glass cells, i.e. a borohydride tank and a hydrogen release chamber, the herein presented device met those requirements.

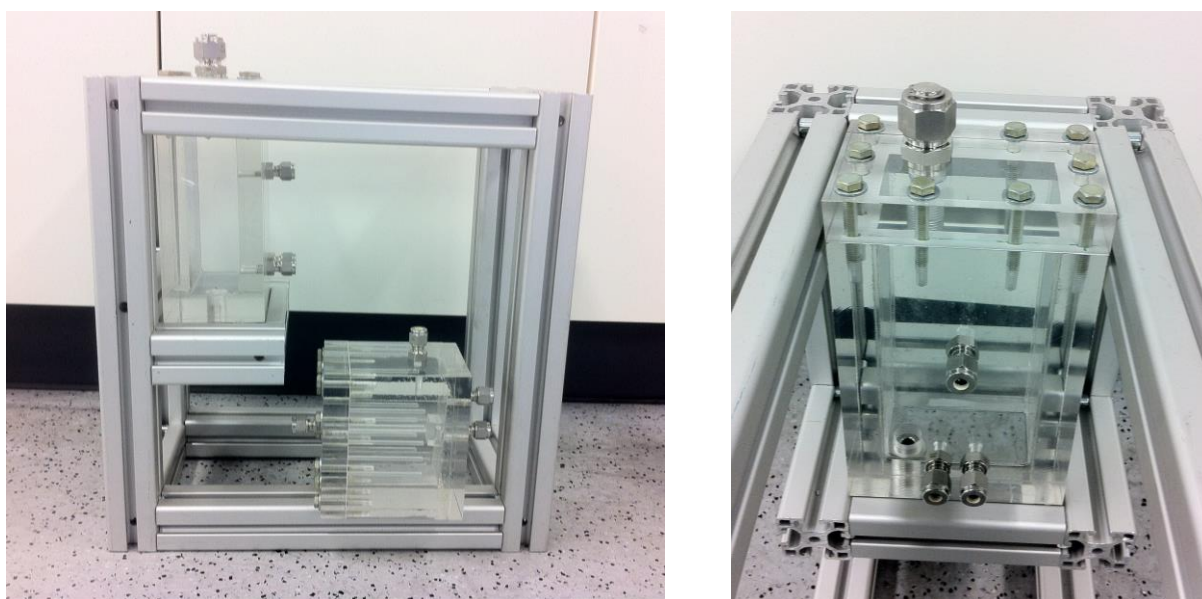


Figure 14: Profile of hydrogen storage and hydrogen release chamber (left), front of hydrogen storage chamber (right), without piping and pressure controlling implemented.

Both chambers were made from 2 cm thick acrylic glass to withstand pressure and have been sealed with silicon gaskets. They each featured four in/outlets: two for connecting one with the other, one for filling/gas exhaust and one for safety/convenience respectively. Tank and reaction chamber were connected over two hoses, or rather Teflon-pipes for pressure reasons. Within those pipes, safety valves were implemented, allowing the liquid borohydride to flow only one-way: one connection led from tank to reaction chamber, the other from the reaction chamber to the tank.

At the gas outlet of the hydrogen release cell a three-way crossing was installed, ending in a pressure gauge, a safety outlet and a H₂-quantifier respectively. For quantifying the produced hydrogen, a commercially available mass flow-controller (MFC) from Bronkhorst was used. Since catalytically generated hydrogen from liquid sources is always quite humid, a drying tube was inserted before the MFC. The product gas had to be thoroughly dried, due to the sensitivity of the mass flow controller, therefore a large drying tube filled with approx. 1.5 L SiO₂ was implemented.

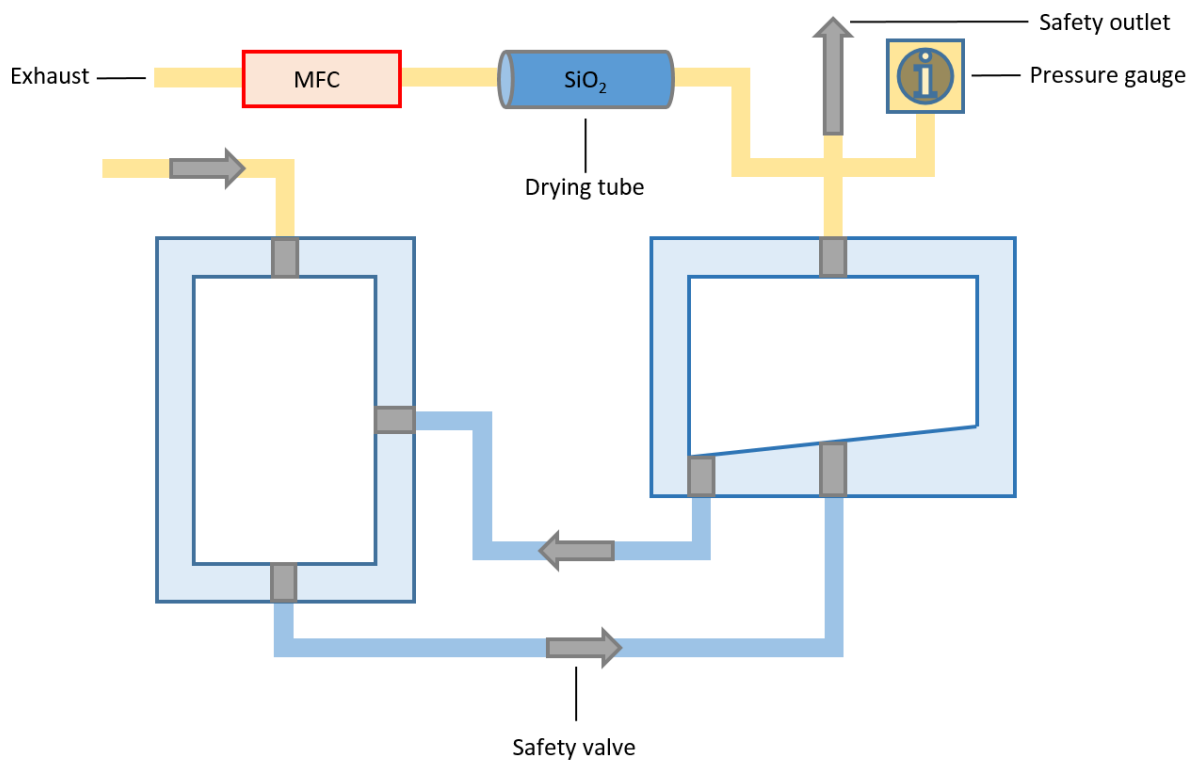


Figure 15: Scheme of the system setup, with borohydride tank (left) and hydrogen release chamber (right).

4.2.4.2 Functionality

After filling up the tank with a borohydride solution, 4.5 bar of N₂ pressure have been applied externally with nitrogen from the gas tap. On the other side, the hydrogen release chamber has been filled with catalyst and then inflated with H₂ to the same extend. To prevent the gases to cross over to the other cell during fill-up, the two stopcocks between the chambers had been closed previously. Upon reaching the same pressure levels, those stopcocks together with a third one right before the MFC were opened and the system was ready to start operation. The scheme below represents the system in this stadium:

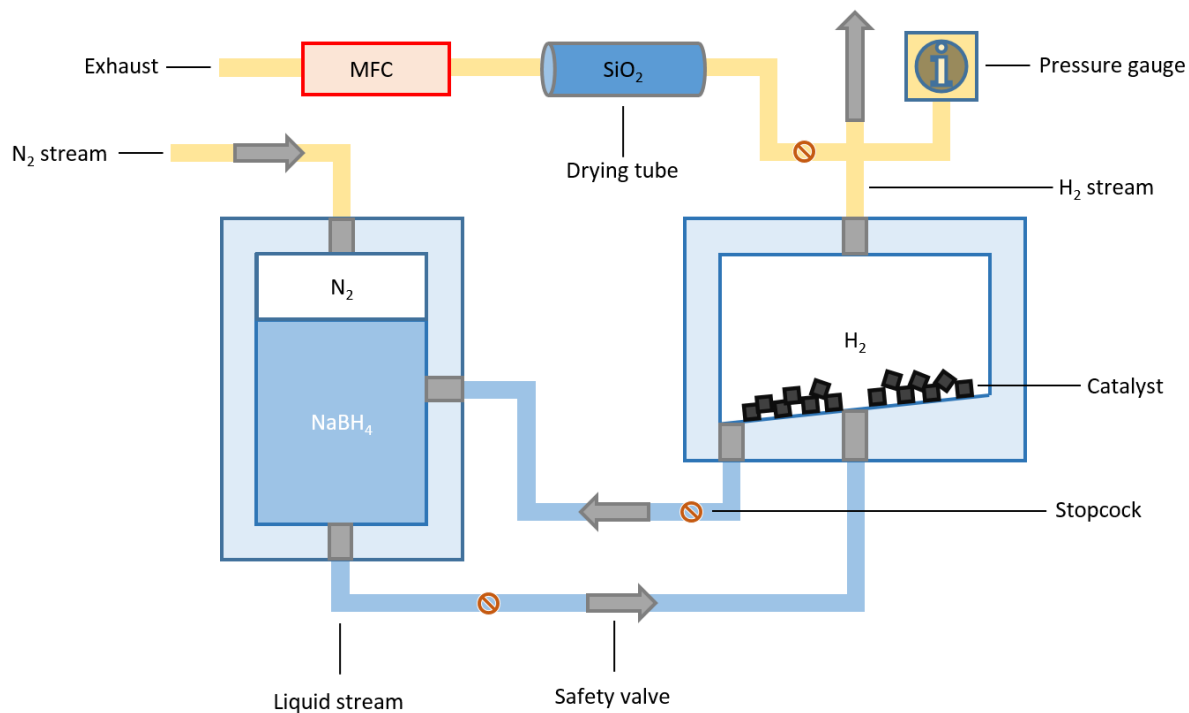


Figure 16: Scheme of the self-regulating hydrogen supply system before the start of hydrogen evolution.

By setting the MFC to a certain hydrogen usage, the H_2 -pressure inside the reaction chamber has been starting to decrease until a certain pressure difference was reached. The safety valve implemented in direction of the release cell opened and borohydride solution could cross. Driven by the small pressure difference between the two chambers, liquid borohydride has been pumped slowly to the reaction cell. Once the solution came in touch with the catalyst, the hydrogen release reaction started within seconds, thus increasing the H_2 pressure again. Therefore, the difference in pressure began to regress, leading to less borohydride cross-over.

If the hydrogen demand was tuned back or shut down completely, the safety valve closed due to lack of pressure difference. Additionally, if the pressure within the release chamber became significantly bigger than the pressure inside the tank, the other safety valve opened and borohydride was pushed back into the tank, hence the reaction came to an end. On the other hand, if hydrogen demand was increased drastically, the pressure within the reaction chamber diminished faster, resulting in a higher pressure difference. This had the effect of a much faster flow of borohydride from tank to release cell, therefore increasing the amount of liquid in touch with catalyst and enhancing the amount of hydrogen generated. In summary: If more hydrogen is present in the system, less hydrogen is produced; if less hydrogen is present in the system, more hydrogen is produced, thus being a negative feedback. Negative feedback depicts the premise of a self-regulating system.

The figure below represents the operation mode, with open stopcocks and constant hydrogen expression:

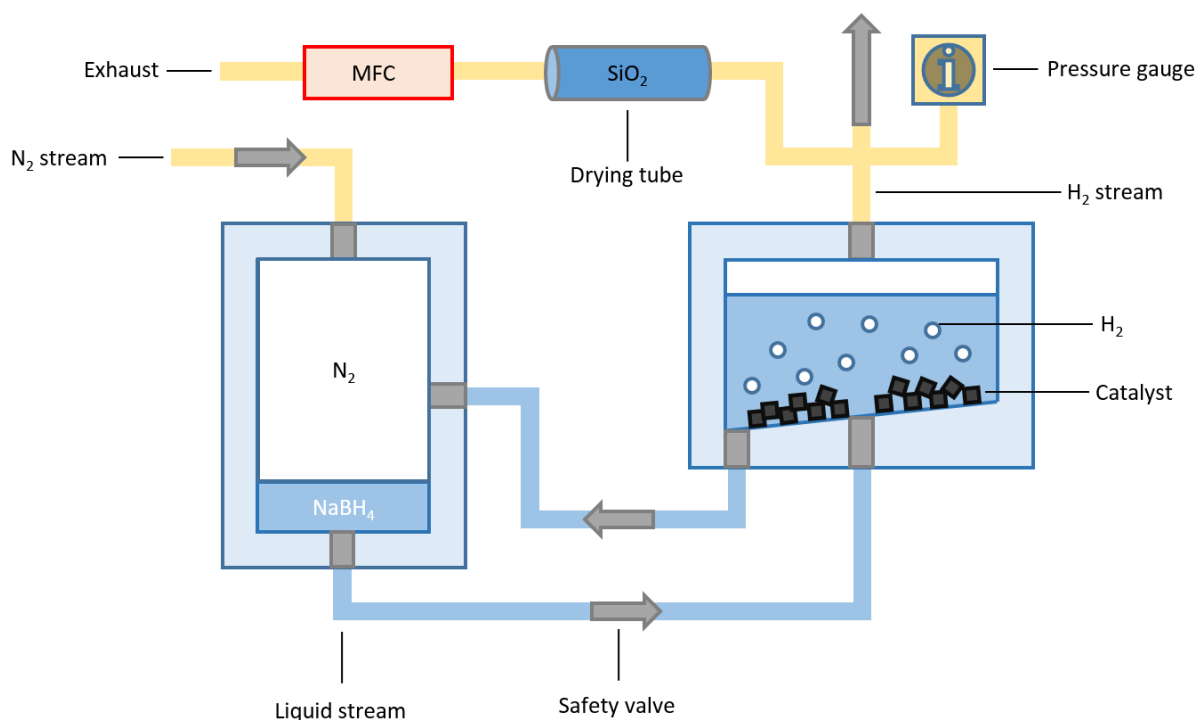


Figure 17: Scheme of the self-regulating hydrogen supply system during operation.

4.2.4.3 Settings

The settings at the start of every measurement are listed in the following table:

Starting pressure	Gas (from tap)	[bar]
Tank chamber	N_2	4.5
Reaction chamber	H_2	4.5
Safety valve	Pressure [psi]	Pressure [bar]
from tank to reaction chamber	10	0.7
from reaction chamber to tank	3	0.2
Catalyst	Mass [g]	Catalyst loading [g]
Co-W-B/Ni-foam	~1.8	~1.7

Table 10: Setting parameters used for on demand hydrogen production.

The actual starting pressure varied in the range of +0.4 bar from experiment to experiment, but has always been the same for the two cell chambers. As for the masses regarding catalyst usage, the values have been interpolated from smaller catalysts.

4.2.4.4 Equipment

Specifications for the equipment used to generate hydrogen on demand are summarized in the table below:

Equipment	Hardware	Software
In-house made hydrogen release system	Piping system with various safety valves, in/outlets and stopcocks	-
Mass flow-controller	Bronkhorst, F-201CV-020, 1000 ml/min)	Bronkhorst software
Flow tracker	NATEC Sensors GmbH, M-1SLPM-D/CV, 1000 SmLPM	Integrated

Table 11: Equipment used for on demand hydrogen production.

The flow tracker was rather an extra precaution to check the steadiness of the MFC. Eventually the MFC was replaced by the newly acquired flow tracker, due to its higher reliability. Without MFC the hydrogen demand had to be adjusted manually via needle valve, which worked surprisingly well and didn't change the functionality.

4.2.5 SEM

Scanning electron microscopy (SEM) images were recorded via a Zeiss Ultra 55 microscope to compare the surfaces of the raw support material, the freshly manufactured catalyst and the catalyst after a distinct operation period. The images have been taken at an acceleration voltage of 5 kV.

5. Results and Discussion

5.1 Catalyst optimization

5.1.1 Electrochemical deposition

Within the scope of optimizing the hydrolysis catalyst, the impact of the number of loading cycles or rather deposition steps had been investigated. Electro-less deposition had been executed as mentioned in section 4.1.2, with 1-4 deposition steps for the various catalysts. Images of the surface of the raw Ni-foam and the completed catalyst surface show the result of the electro-less plating:

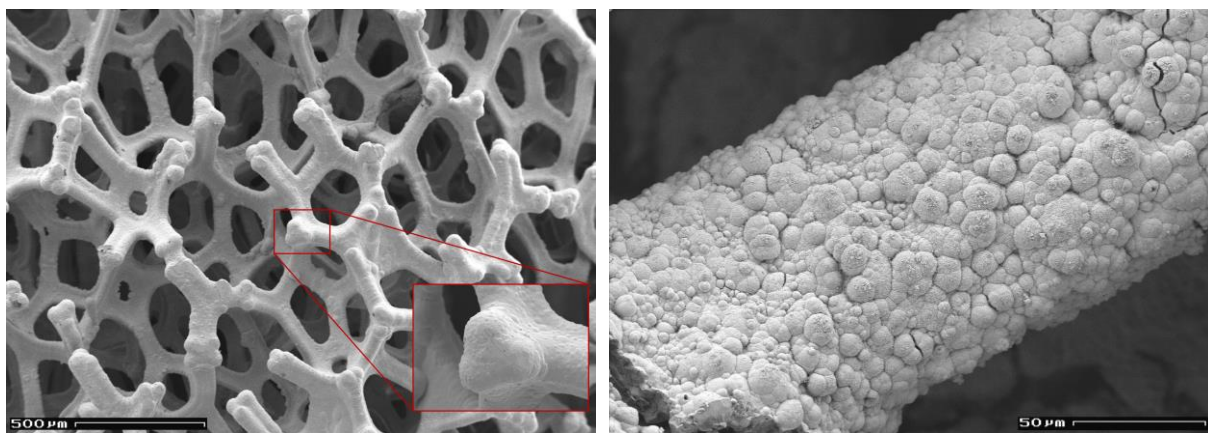


Figure 18: SEM images of the raw nickel foam support material (left) and the completed Co-W-B/Ni-foam catalyst (right) [52].

Due to the fact that these catalysts were the afore specified standard catalysts, they are henceforth called first generation catalysts and marked with an elevated “1st” after their names. The catalyst parameters can be seen in the following table:

Name	Size [cm ²]	Deposition steps	m (Ni-foam) [mg]	m (catalyst) [mg]	m (loading) [mg]
CGr60 ^{1st}	0.25	1	13.7	21.3	7.6
CGr61 ^{1st}	0.25	2	14.8	28.0	13.2
CGr62 ^{1st}	0.25	3	12.8	26.1	13.3
CGr63 ^{1st}	0.25	4	13.2	33.7	20.5

Table 12: Parameters of the catalysts for electrochemical deposition optimization.

Surprisingly enough, CGr61^{1st} and CGr62^{1st} exhibited almost the exact same catalyst loading, although the latter should have had a higher loading of approx. 50 % or around 7 mg. Instead CGr63^{1st} showed the expected loading of 3 deposition steps, when being plated 4 times. Since the electro-less plating

was done simultaneously, meaning in the first rotation all four catalyst got treated together, in the second rotation CGr61^{1st}, CGr62^{1st} and CGr63^{1st} together etc., it seems like the third plating rotation did not have any effect on them at all. Although no peculiarities could be observed during the deposition steps the catalyst loadings for CGr62^{1st} and CGr63^{1st} are about 7 mg too low respectively. For determining the influence of multiple plating cycles on the effectiveness of the catalysts, performance tests have been conducted to compare the various hydrogen release rates. Therefore, the setup of section 4.2.1 and 10 ml of a standard NaBH₄ solution respectively were used. The properties of the standard solution are listed in the table below.

NaBH ₄ solution conc.	m NaBH ₄ [mg]	Solvent	NaOH conc.	Volume [ml]
1 wt.% H ₂	477	NaOH	1 M	10

Table 13: Parameters for HRR measurement regarding electro-less deposition optimization.

The results of the performance characterization via electrochemical measurements are depicted in the figures below:

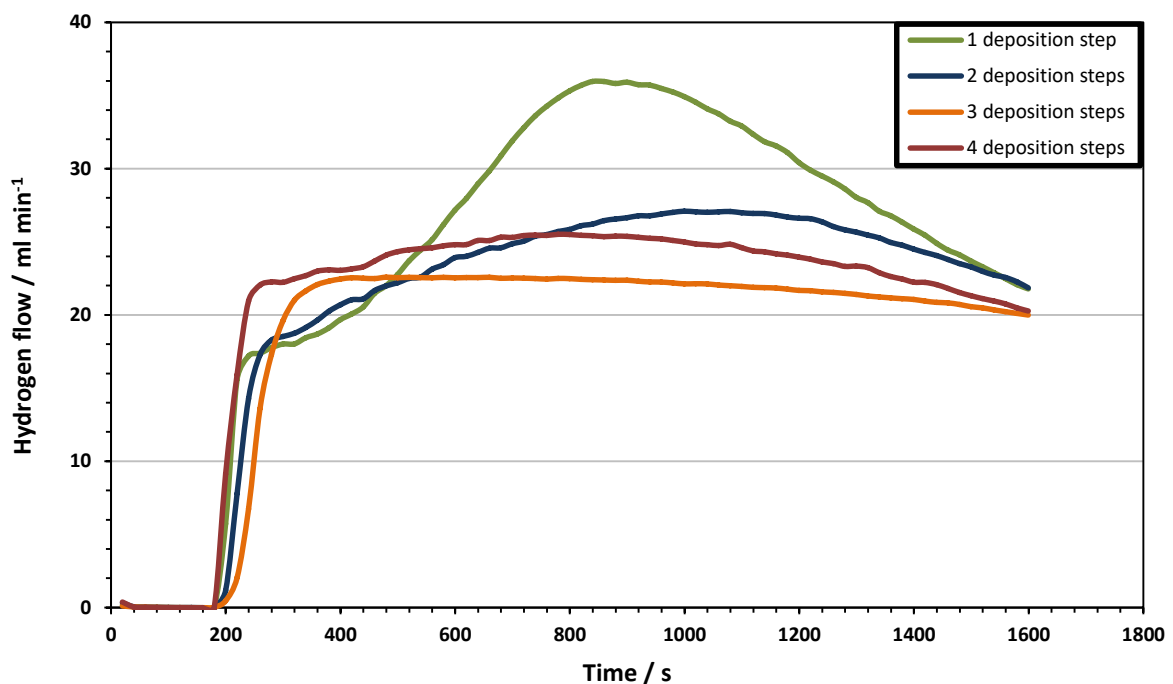


Figure 19: HRR from NaBH₄ solution (1 wt.% H₂) with four differently loaded Co-W-B/Ni-foam catalysts at 30°C, analysed by electrochemical approach.

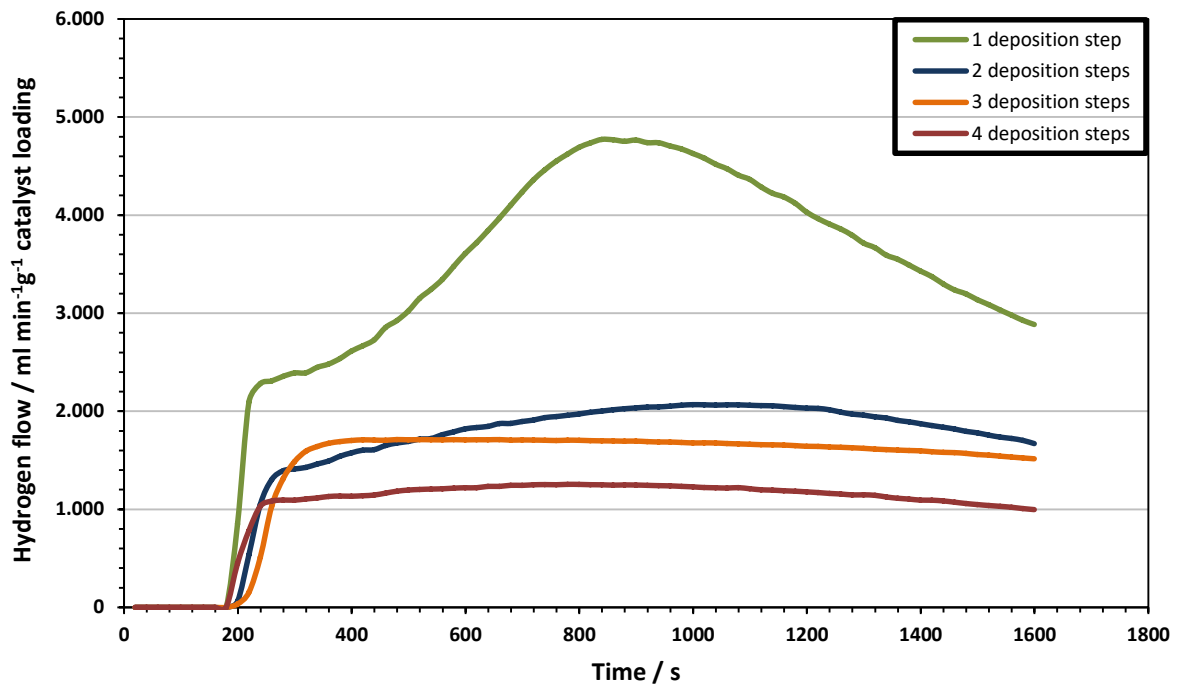


Figure 20: HRR per gram catalyst from NaBH₄ solution (1 wt.% H₂) with four differently loaded Co-W-B/Ni-foam catalysts at 30°C, analysed by electrochemical approach.

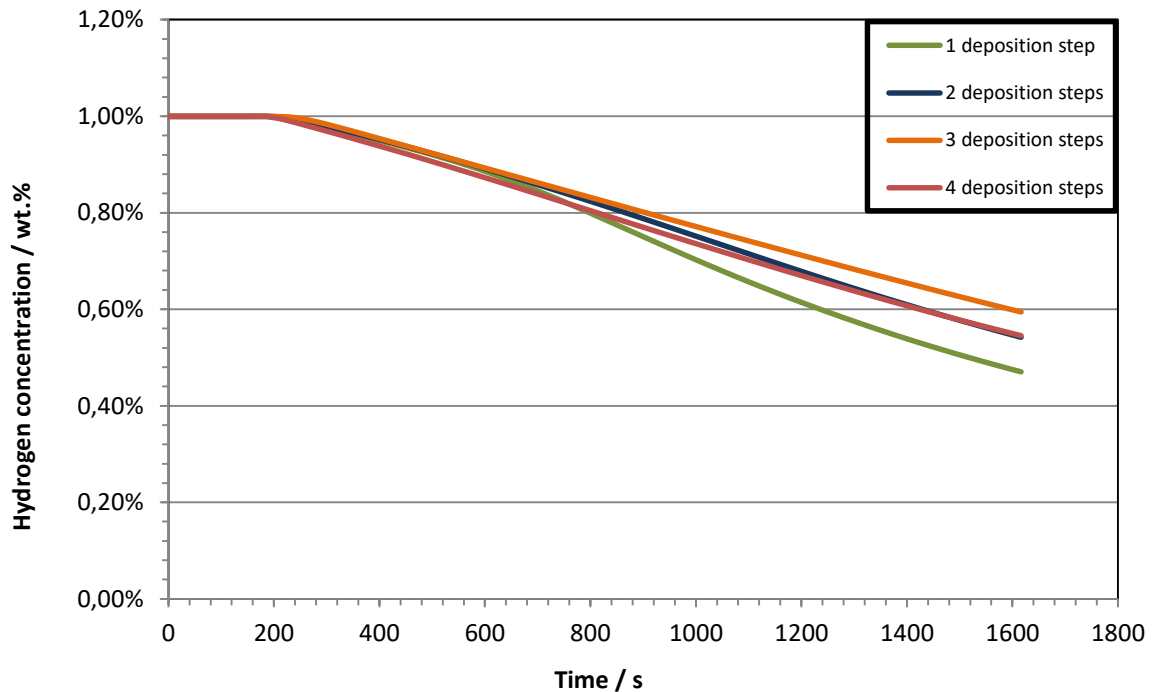


Figure 21: Concentration profile of NaBH₄ solution (1 wt.% H₂) during hydrogen release of four differently loaded Co-W-B/Ni-foam catalysts at 30°C, analysed by electrochemical approach.

Figure 19 summarizes the performance tests of the four different catalysts. The results have been plotted as hydrogen flow in millilitre per minute versus time. CGr60^{1st}, which got only plated once,

exhibited the highest hydrogen release rate of all the catalysts of approx. 36 ml/min, thus showing an activity higher than 130 % compared to the rest. About 5-6 minutes after the start of the test, CGr60^{1st}s HRR began to surpass the others, although having the weakest starting activity. Furthermore, this was the catalyst with the sharpest activity peak. Since the HRR is highly dependent on the borohydride concentration of the solution, the loss in activity after 13-14 minutes is probably connected to the diminished concentration (Figure 21).

A higher hydrogen generation rate of a catalyst with only one deposition step over catalysts with multiple steps does not concur with literature [47]. Dai et al. stated a significant increase of activity with each deposition step up until three steps. More deposition steps are accompanied by a higher catalyst loading, which in turn goes along with higher activity. However, looking at the HRR per gram catalyst loading, CGr60^{1st} maximum activity is over twice as high (ca. 4800 ml/min per gram Co-W-B) as the second best (ca. 2100 ml/min per gram Co-W-B). This is comparable with literature values for non-noble transition metal catalysts [32]. Due to the fact that the single deposition step catalyst yielded the best results by far, for the second generation of Co-W-B/Ni-foam catalysts only one electro-less plating step per catalyst was determined.

5.1.2 Thermal treatment

The next working point for catalyst optimization was the temperature ramp during calcination. Maximum temperature and holding time have already been investigated by other scientist, but the heating rate did not get any attention thus far. Therefore, the 2nd generation catalysts underwent annealing under different heating values per minute and the HRRs of the finished catalysts were observed to identify any positive or negative effects of the varied tempering conditions.

Name	Size [cm ²]	Heating rate [°C/min]	m (Ni-foam) [mg]	m (catalyst) [mg]	m (loading) [mg]
CGr68 ^{2nd}	0.25	0.5	11.5	17.4	5.9
CGr69 ^{2nd}	0.25	1	11.1	16.8	5.7
CGr70 ^{2nd}	0.25	2	10.6	16.4	5.8
CGr71 ^{2nd}	0.25	4	10.9	16.5	5.6

Table 14: Parameters of the catalysts for thermal treatment optimization.

The table above depicts Co-W-B-loadings of under 6 mg for this batch of catalysts, which was a considerably lower yield than the previous batch had shown. Since no variations regarding the recipe were conducted and no exceptional incidents during the electro-less plating have occurred, no

explanation could be found. Outcomes of the performance tests using electrochemical measurements are plotted in the figures below:

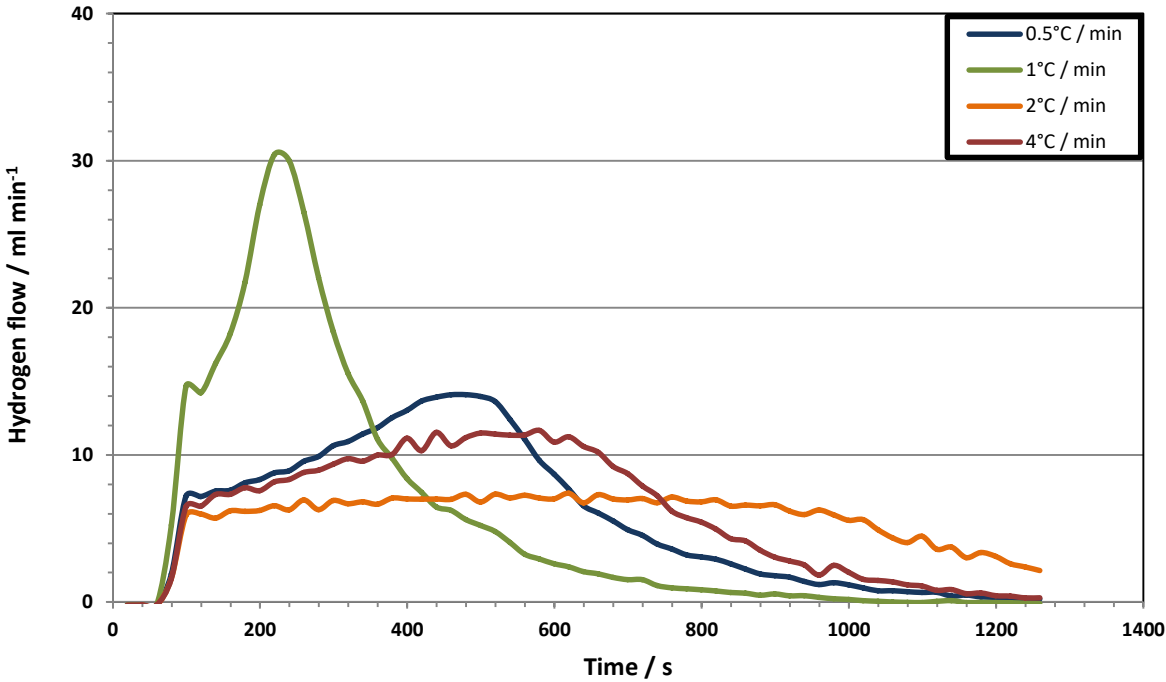


Figure 22: HRR from NaBH₄ solution (1 wt.% H₂) with four differently calcined Co-W-B/Ni-foam catalysts at 30°C, analysed by electrochemical approach.

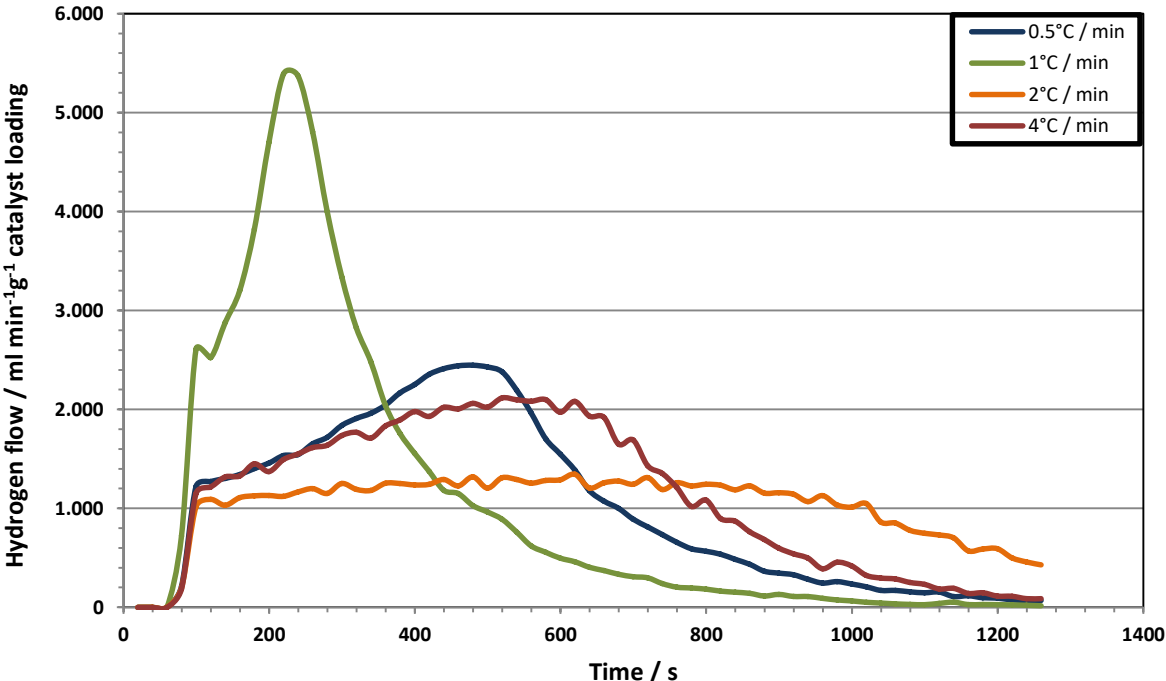


Figure 23: HRR per gram catalyst from NaBH₄ solution (1 wt.% H₂) with four differently calcined Co-W-B/Ni-foam catalysts at 30°C, analysed by electrochemical approach.

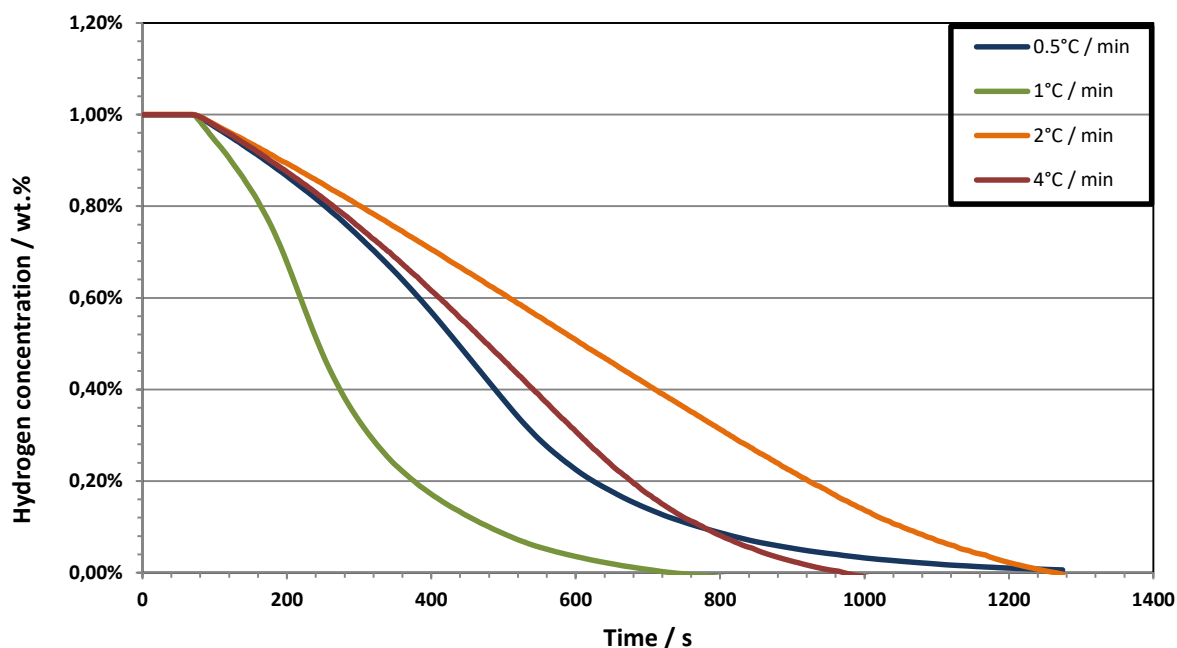


Figure 24: Concentration profile of NaBH₄ solution (1 wt.% H₂) during hydrogen release of four differently calcined Co-W-B/Ni-foam catalysts at 30°C, analysed by electrochemical approach.

In order to determine the impact of different heating rates on the activity of the catalysts, performance tests have been conducted to compare the various HRRs. For this test series only 1 ml NaBH₄ instead of 10 ml has been used. The exact parameters for the solutions can be found in the table below.

NaBH ₄ solution conc.	m NaBH ₄ [mg]	Solvent	NaOH conc.	Volume [ml]
1 wt.% H ₂	47.4	NaOH	1 M	1

Table 15: Parameters for HRR measurement regarding thermal treatment optimization.

As could be expected from the poorer Co-W-B-loading, the overall activities have been decreasing as well. Due to the fact that a loading of about 7.6 mg non-precious metal catalyst or less is quite low and only one plating step could be unreliable, especially with the measured loadings for CGr62^{1st} and CGr63^{1st} (see table 12), for the third generation of Co-W-B/Ni-foam catalysts two electro-less plating steps per catalyst were determined.

Looking at the varying outcomes in the latter three figures, it appears that slower heating ramps result in higher maximum activity values. This effect is either related to a larger active surface area or to a difference in nature of the catalytically active species, which is presumably associated with the precipitation and structure of the nanocrystalline Co [53]. With a maximum HRR of around 30 ml/min, or rather over 5400 ml/min per gram Co-W-B, CGr69^{2nd} is over twice as active than the other catalyst of this generation. Since the Co-W-B-loading of this generation was more or less identical, the values

for HHR and HHR per gram catalyst are quite similar, but compared to the first generation the maximum activity per gram catalyst loading did further improve.

5.2.1 Long-term stability

Since long term stability is one of the three most important properties of every catalyst, long term-HRR experiments had been performed as the last catalyst characterization test. Both Begin-of-lifetime (BOL) and end-of-lifetime (EOL) performance have been investigated, as well as the surface structure before and after a certain period of non-stop operation via SEM. For this purpose, a catalyst of the third generation has been used. Because a lot of catalyst has been prepared in a bulk procedure and was cut into corresponding pieces afterwards, only the output weight is known.

Name	Size [cm ²]	Heating rate [°C/min]	m (Ni-foam) [mg]	m (catalyst) [mg]	m (loading) [mg]
CGr80_1 ^{3rd}	0.25	1	~17	35.1	~18

Table 16: Parameters of the catalysts for long-term experiments, m (foam) and M (loading) have been estimated.

NaBH ₄ solution conc.	m NaBH ₄ [mg]	Solvent	NaOH conc.	Volume [ml]
1 wt.% H ₂	90.6	NaOH	1 M	2

Table 17: Parameters for BOL and EOL HRR measurement.

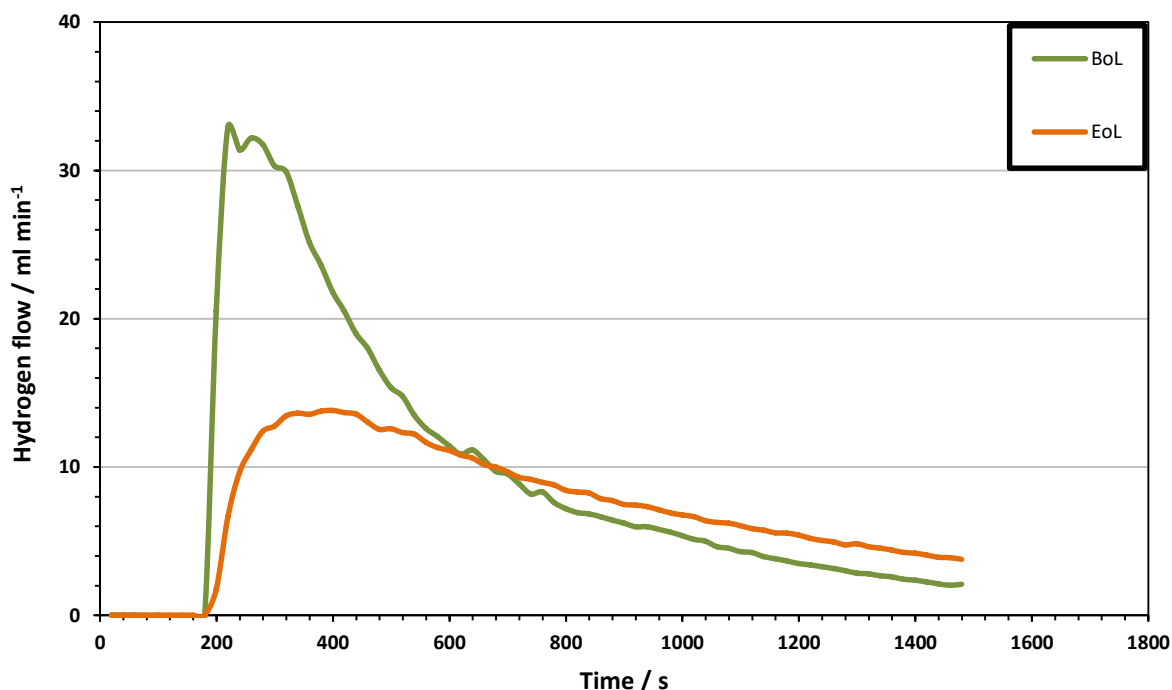


Figure 25: HRR from NaBH₄ solution (1 wt.% H₂) of the Co-W-B/Ni-foam catalysts at BOL and after 720 hours of non-stop operation at EOL, analysed by electrochemical approach at 30°C.

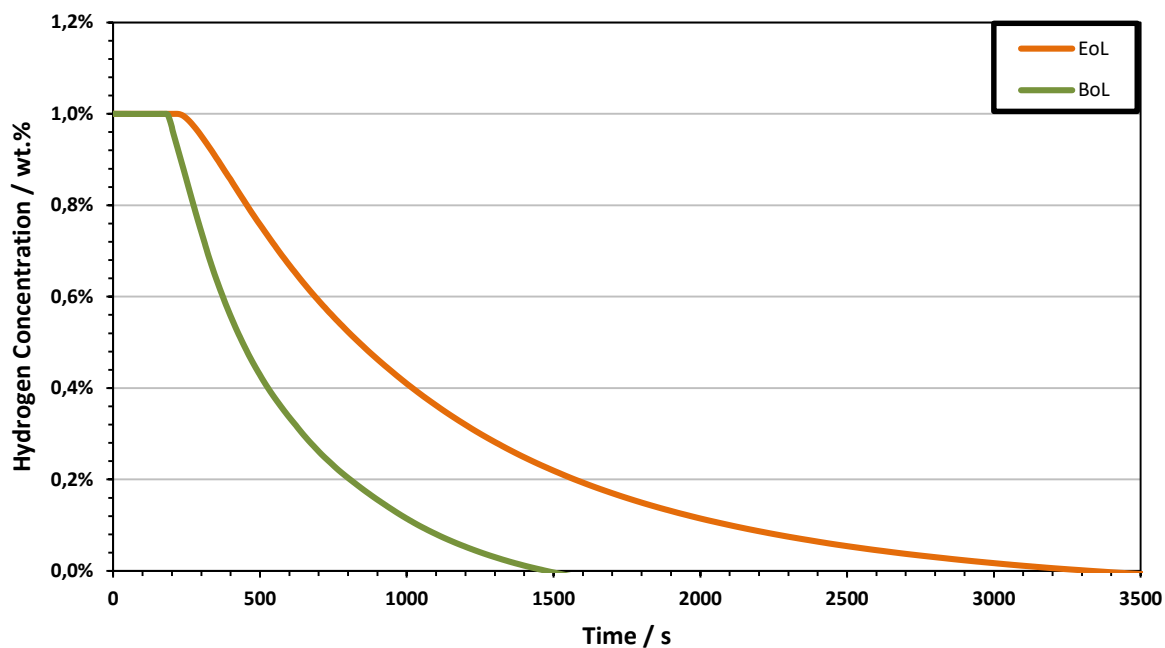


Figure 26: Concentration profile of NaBH_4 solution (1 wt.% H_2) during hydrogen release of the Co-W-B/Ni-foam catalysts at BOL and at EOL, analysed by electrochemical approach at 30°C.

Figure 25 depicts the HRR from CGr80_1^{3rd} at BOL and EOL respectively. The catalyst had been under non-stop operation for 720 hours or 4 weeks, which led to a decrease in max. activity of approx. 42 %. While the freshly produced catalyst showed a HRR of up to 33 ml/min, the same catalyst could not produce more than 14 ml/min after a month of permanent operating conditions. Therefore, the duration for complete hydrogen release was extended from only 20 minutes at BOL to over 50 minutes after long-term operation (fig. 26).

Since catalysts for hydrogen generation from borohydride solutions seem to diminish rather fast and substantial, these results concurred with previously published outcomes. Various degradation tests resulted in activity drops of 25-80 % of the initially measured values [54], [55], [56]. This degradation resulted probably from a loss of active surface area, which has also been reported previously [57].

Scanning electron microscopy images have been recorded to take a closer look at the surface effects of long-term operation. Examination under the microscope exhibited small cracks all over the surface of the catalyst before and after non-stop operation. These crack are probably results of the heat applied during thermal treatment. Weighing the catalyst at BOL and EOL did not bring any difference in mass, which meant no active material was lost and agreed with the SEM records shown in figure 27.

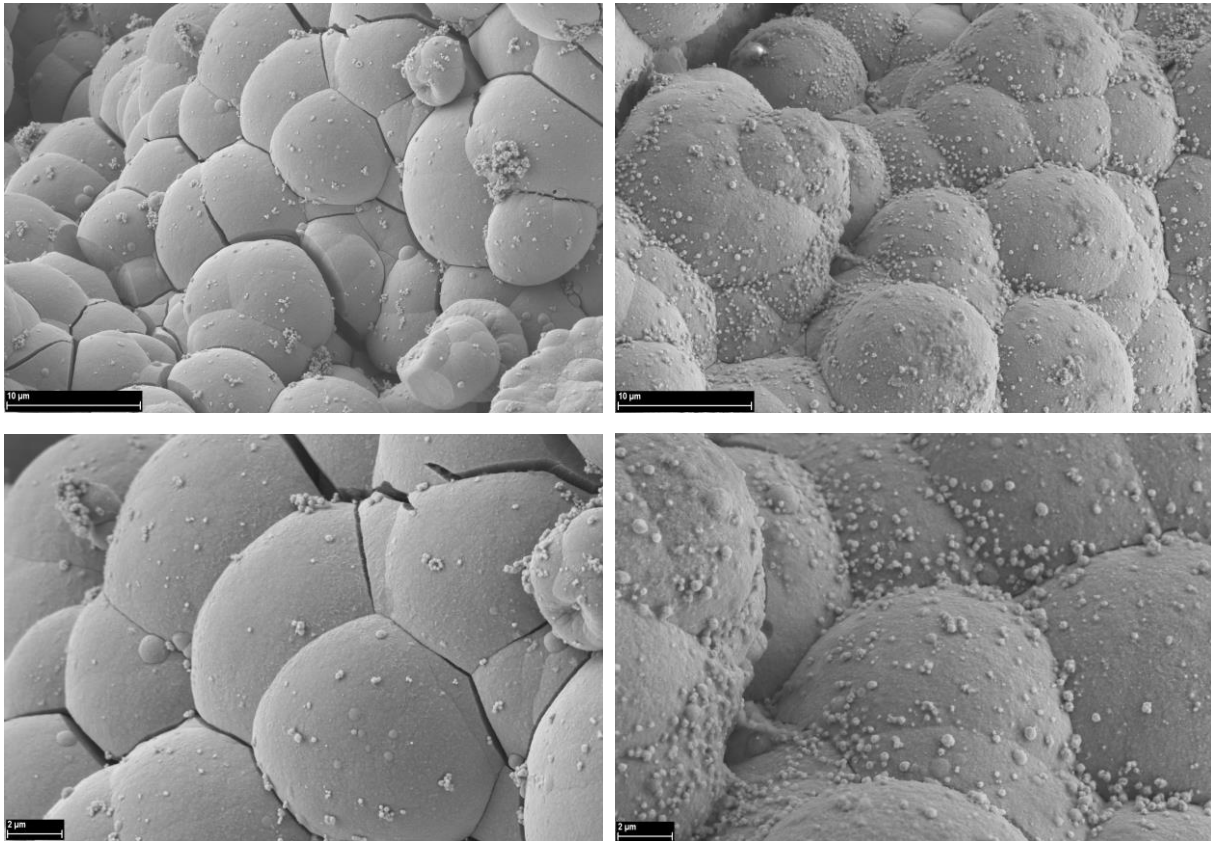


Figure 27: SEM images of a freshly manufactured catalyst at BOL (left) and after 720 hours of operation at EOL (right) [52].

However, one major disparity after only 30 days of permanent hydrogen production was distinctly observable: Nano sized, spherical depositions have been formed on the surface. A later realised EDX analysis, which is not shown in this work, identified the surface depositions as iron enriched cobalt spheres [52]. An explanation as to how the iron-containing depositions were formed has yet to be found, especially since there shouldn't be any iron within the catalyst or the borohydride solution. Contaminations within the chemicals used for catalyst fabrication are assumed to be the cause of this, but those assumptions could not be proven yet.

5.2 Ionic liquid characterization

5.2.1 Volumetric performance characterization

Due to the previously mentioned increased long term stability as well as higher storage capacity in solution, ionic liquids have been investigated. At the beginning different bases have been employed for dissolving DMMorBH₄ and the effects on hydrogen release reaction has been examined. For these measurements a standard Co-W-B/Ni-foam catalyst of the third generation was applied and the performance was tested in a volumetric way (see section 4.2.2), using the water displacement method. Like the catalysts from the CGr80^{3rd}'s series, CGr81^{3rd} was cut out from a larger piece of catalyst and hence the exact Co-W-B-deposition was not known.

Name	Heating rate [°C/min]	m (Ni-foam) [mg]	m (catalyst) [mg]	m (loading) [mg]
CGr81 ^{3rd}	1	~16	30.8	~15

Table 18: Parameters of the catalyst used for volumetric performance characterization

5.2.1.1 DMMorBH₄ in various 0.1 M bases

The results of the measurements at ambient conditions is shown in the figures below:

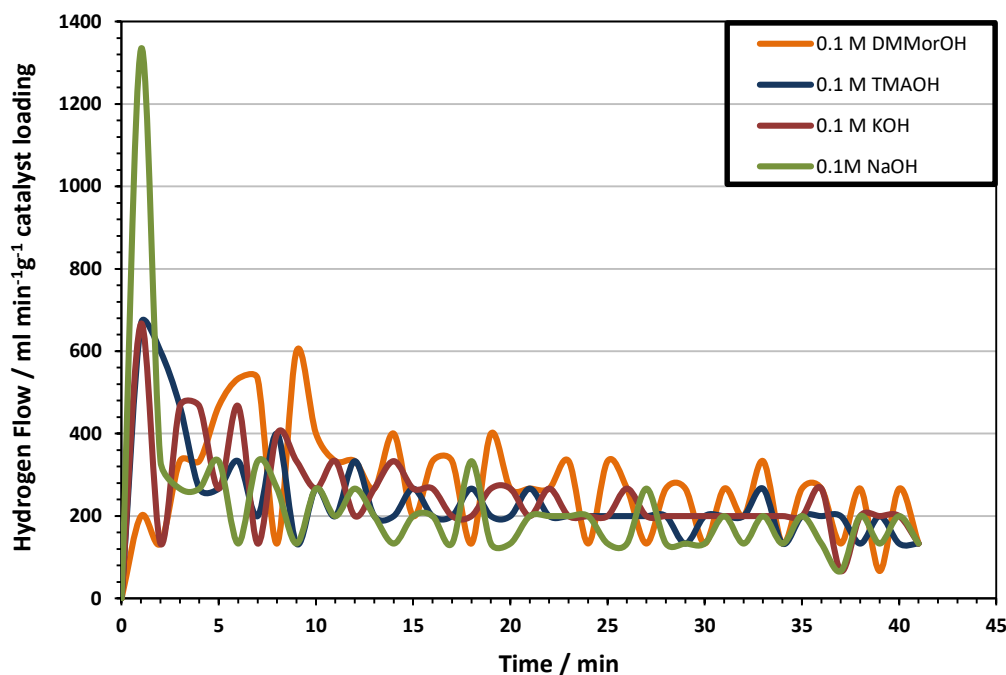


Figure 28: HRR per gram catalyst from DMMorBH₄ solution (3 wt.% H₂) with different bases at ambient conditions, analysed by water displacement method.

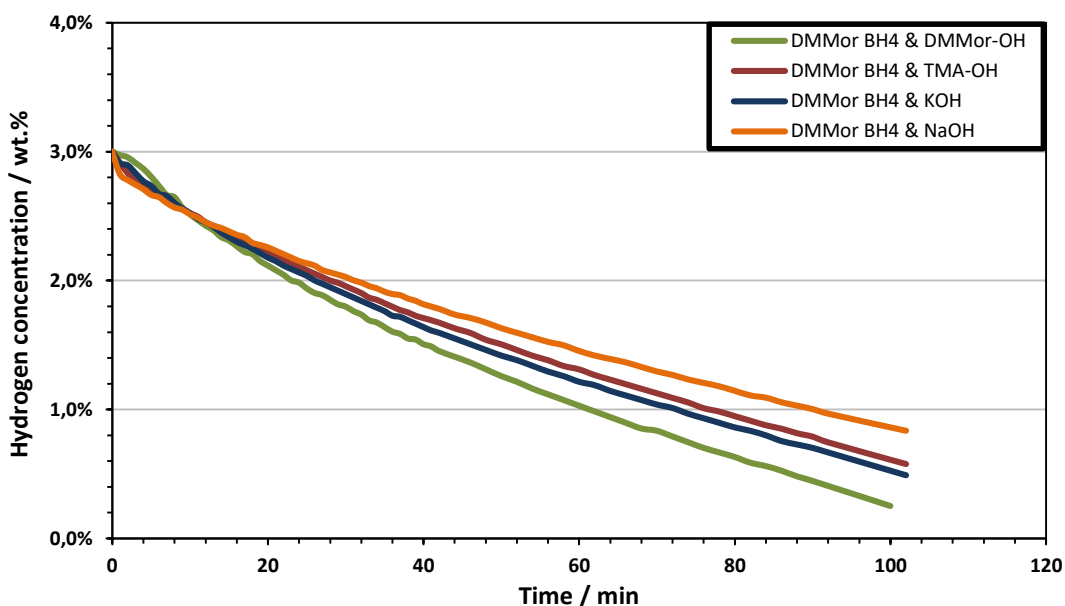


Figure 29: Concentration profile of DMMorBH₄ solutions (3 wt.% H₂) made from different bases during hydrogen at ambient conditions, analysed by water displacement method.

The experiments have been conducted using 1 ml of the following solutions respectively:

DMMorBH ₄	m DMMorBH ₄ [g]	Solvent	Base conc.	m solution [g]
3 wt.% H ₂	498.2	DMMorOH	0.1 M	1.0134
3 wt.% H ₂	510.7	TMAOH	0.1 M	1.0304
3 wt.% H ₂	514.2	KOH	0.1 M	1.0428
3 wt.% H ₂	514.0	NaOH	0.1 M	1.0381

Table 19: Parameters of the various DMMorBH₄ solutions investigated.

Figure 28 shows the activities of the catalyst relative to the various DMMorBH₄ solutions per gram of Co-W-B-loading. The overall HRRs are lower than those measured with sodium borohydride. Ionic liquids are more stable at ambient conditions; hence kinetics are less favourable for hydrogen release. With a max. activity of approx. 1350 ml/min per gram catalyst, DMMorBH₄ in 0.1 M NaOH seemed twice as willing to release H₂ than DMMorBH₄ in other bases. However, the activity peak was sharp and narrow and upon taking a closer look at the concentration profiles in figure 29, the NaOH containing solution exhibited the slowest degasification over a longer period of time. After 100 minutes DMMorBH₄ in 0.1 M DMMorOH has been releasing the most hydrogen, with only 0.2 wt.% remaining in solution, while the NaOH solution still contained approx. 0.8 wt.% H₂. Since the overall activity is more important than the max. activity for a very short time period, DMMorOH was chosen as base for the subsequent temperature related testing.

5.2.1.2 METMABH₄ in various 0.1 M bases

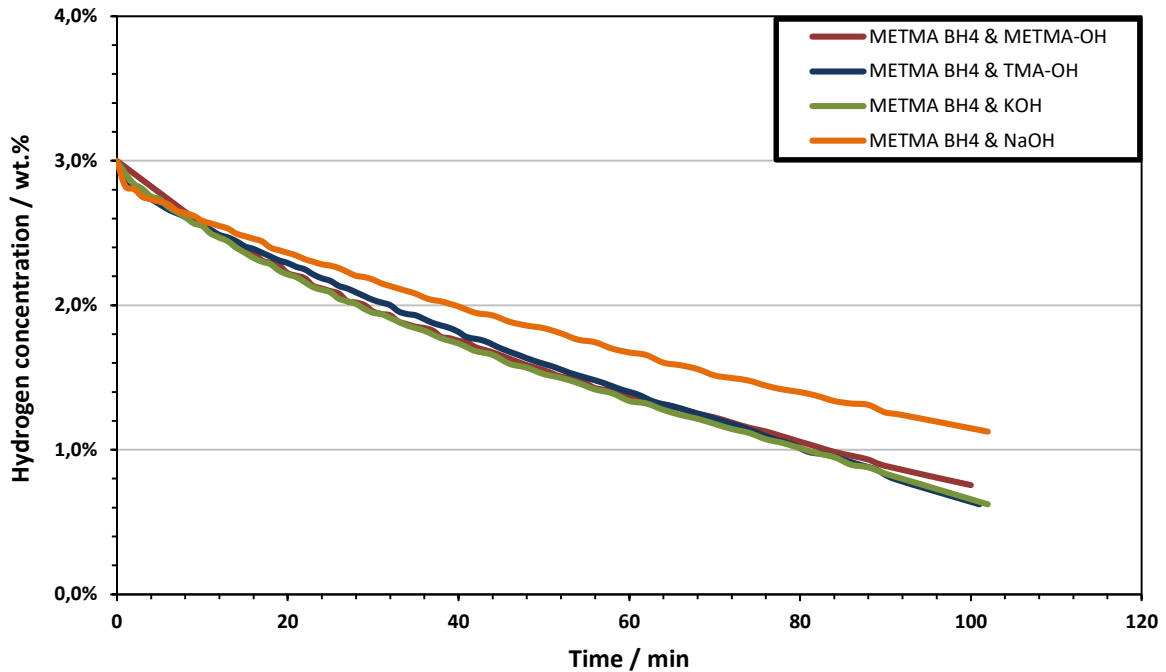


Figure 30: Concentration profile of METMABH₄ solutions (3 wt.% H₂) made from different bases during hydrogen at ambient conditions, analysed by water displacement method.

METMABH ₄	m METMABH ₄ [g]	Solvent	Base conc.	m solution [g]
3 wt.% H ₂	495.0	METMAOH	0.1 M	0.9891
3 wt.% H ₂	475.2	TMAOH	0.1 M	0.9361
3 wt.% H ₂	497.5	KOH	0.1 M	0.9825
3 wt.% H ₂	578.4	NaOH	0.1 M	1.1365

Table 20: Parameters of the various METMABH₄ solutions investigated.

From the previous DMMorBH₄ tests could be conducted that concentration profiles give probably more reliable results regarding overall performance than the max. HRR activity. Therefore, the best suited base for METMABH₄ solutions were determined by consulting figure 30. After 100 minutes TMAOH and KOH have been releasing the most hydrogen, with only approx. 0.6 wt.% remaining in solution. METMABH₄ in KOH was chosen for temperature related tests, because KOH is cheaper and abundantly available, while apparently resulting in very similar hydrogen release behaviour as TMAOH. In general, METMABH₄ seemed to be a little more reluctant considering hydrogen expression, leading to an overall slower degasification compared to DMMorBH₄.

5.2.2 Temperature related performance determination

In order to be time efficient the following temperature dependant measurements have been conducted by gradually increasing the temperature, using a larger volume of borohydride solution. Hence, the in-house made acrylic glass cell had to be replaced by a larger three-way round bottom flask. To prevent fluctuations in the N_2/H_2 gas stream due to the larger headspace, the gas flows at working and counter electrode have been increased to 100 ml/min each. Also the concentration of the bases was elevated from 0.1 M to 0.5 M to investigate potential effects.

5.2.2.1 DMMorBH₄ in 0.5 M DMMorOH

After a short standby time, the temperature was set to 30°C and at the same time the catalyst has been added to the borohydride solution to start the reaction. Once a stable current (potentiostat) could be maintained for a few minutes, the temperature was adjusted to the next higher level. Figure 31 represents the results of the thermal impacts on HRR regarding Co-W-B/Ni-foam catalyst with DMMorBH₄ in 0.5 M DMMorOH. Tables 21-23 summarize the parameters of solution, catalyst and settings used for this experiment.

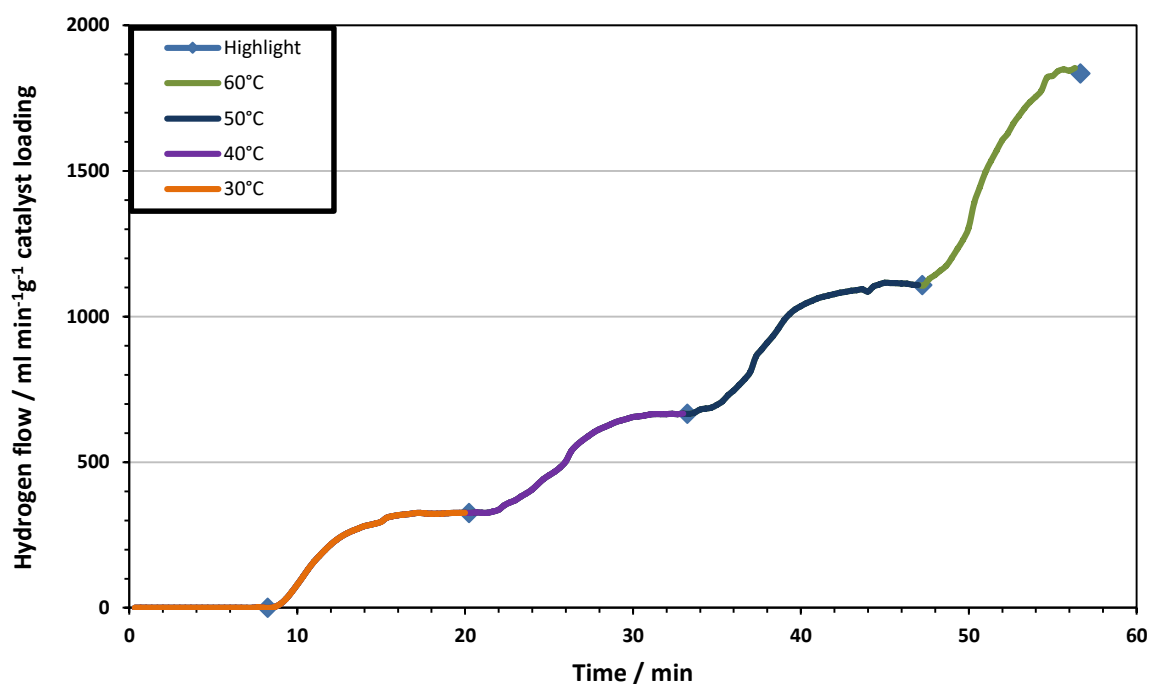


Figure 31: HRR per gram catalyst from DMMorBH₄ solution (3 wt.% H₂) with Co-W-B/Ni-foam catalysts at different temperatures, analysed by electrochemical approach.

Name	Size [cm ²]	Heating rate [°C/min)	m (Ni-foam) [mg]	m (catalyst) [mg]	m (loading) [mg]
CGr80_10 ^{3rd}	1	1	~13	37.2	~24

Table 21: Parameters of the catalysts used.

DMMorBH ₄	m DMMorBH ₄ [g]	Solvent	DMMorOH conc.	m solution [g]
3 wt.% H ₂	8.9800	DMMorOH	0.5 M	18

Table 22: Parameters of the ionic liquid investigated.

Temperature [°C]	Time [min]
30	8
40	20
50	33
60	47
Gas flow	[ml/min]
Working electrode N ₂	100
Counter electrode H ₂	100
Catalyst added	minute 8

Table 23: Setting of the DMMorBH₄ investigation at different temperatures.

At 30°C approx. 320 ml/min hydrogen per gram catalyst could be released, which did fit the previous outcomes quite well, when considering that a lower base concentration of 0.1 M leads to a less stable solution and hence is more prone to release hydrogen. Therefore, a lower HRR for the 0.5 M base measurement was expected. With every 10°C-step the HRR was gaining more activity than with the step before, up until 60°C when the test had to be stopped due to a distinct drop in borohydride concentration. Because a large percentage of the immanent H₂ had already been released at the end of the experiment, the hydrogen expression started to decrease on its own, hence compromising comparability.

From the amount of H₂ produced per minute at different temperatures the subsequent Arrhenius plot could be obtained:

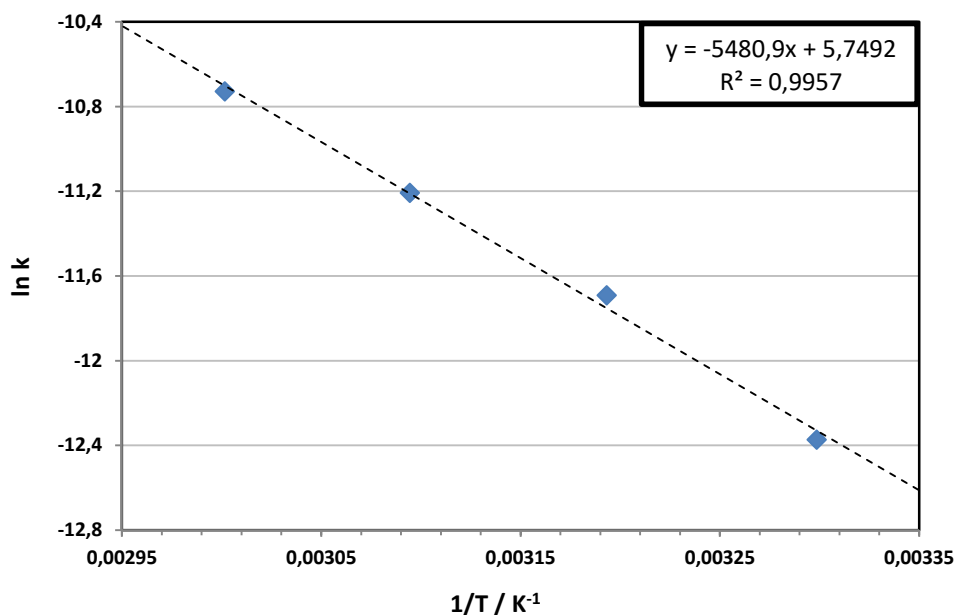


Figure 32: Arrhenius plot of DMMorBH₄ hydrolysis with Co-W-B/Ni-foam catalyst at 30°C, 40°C, 50 °C and 60°C.

By implementing the slope of the Arrhenius plot into the Arrhenius equation,

$$k = A \cdot e^{-\frac{E_A}{RT}} \quad (18)$$

- k -> reaction rate [mol·min⁻¹]
- T -> Temperature [K]
- R -> Universal gas constant = 8,314 J [mol⁻¹·K⁻¹]
- A -> Pre-exponential factor

the activation energy of DMMorBH₄ in 0.1 M DMMorOH could be calculated:

Activation Energy (E _A) per mol H ₂ [kJ/mol]	Activation Energy (E _A) per mol BH ₄ [kJ/mol]	Standard deviation
45.6	182.3	+/- 0.70

Table 24: Activation energy of DMMorBH₄ hydrolysis via Co-W-B/Ni-foam catalyst.

This was in the range of the previously determined activation energy of sodium borohydride and did fit literature quite well, even more so when considering one fact [58]: ionic liquids are usually more viscous, since they are essentially salts in a liquid state. This property decreases with increasing

temperature, as was thoroughly investigated for some ionic liquids by the partner prolonic GmbH and is depicted as an example for DMMorBH₄ in figure 33:

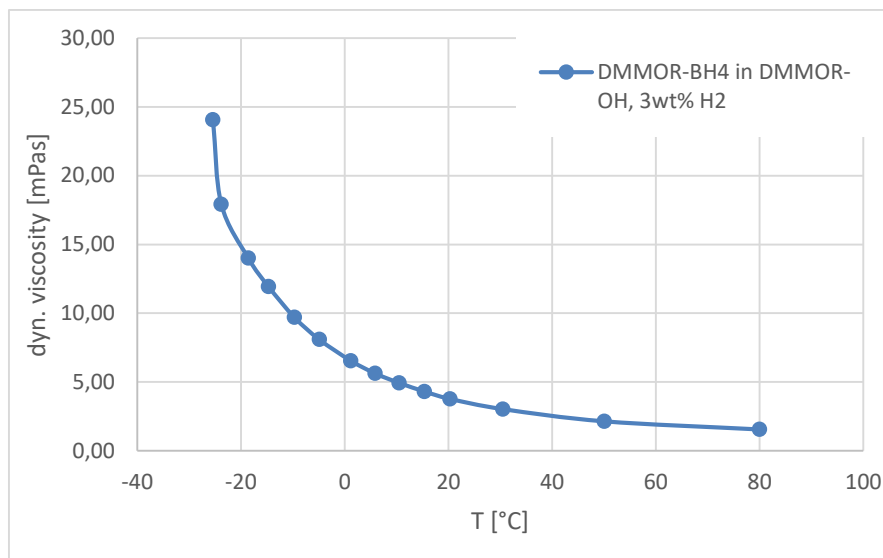


Figure 33: Viscosity behaviour in dependence of the temperature of DMMorBH₄ in DMMorOH (figure provided by Theo Friedrich from prolonic GmbH).

With diminishing viscosity, the mass transportation within the solution and thereby also the diffusion to the active sites of the catalyst are enhanced, resulting in a higher HRR. The higher reaction rate leads to a lower assumed activation energy when calculating said energy with the aid of the slope of the Arrhenius plot.

5.2.2.2 METMABH₄ in 0.5 M KOH

The same temperature dependant measurements have been conducted for METMABH₄ in 0.5 M KOH, since KOH appeared to be one of the more promising bases for borohydride dissolutions beforehand. With a minimum HRR activity of under 100 ml/min per gram catalyst at 30°C and a maximum HRR of approx. 280 ml/min at 70°C the performance was a quite underwhelming. Due to the slow degasification the temperature could be elevated up to 70°C, instead of terminating the experiment at 60°C, as had to be done previously. In general, METMABH₄ usually yields poorer outcomes than DMMorBH₄ regarding hydrogen expression. The results can be seen in figure 34:

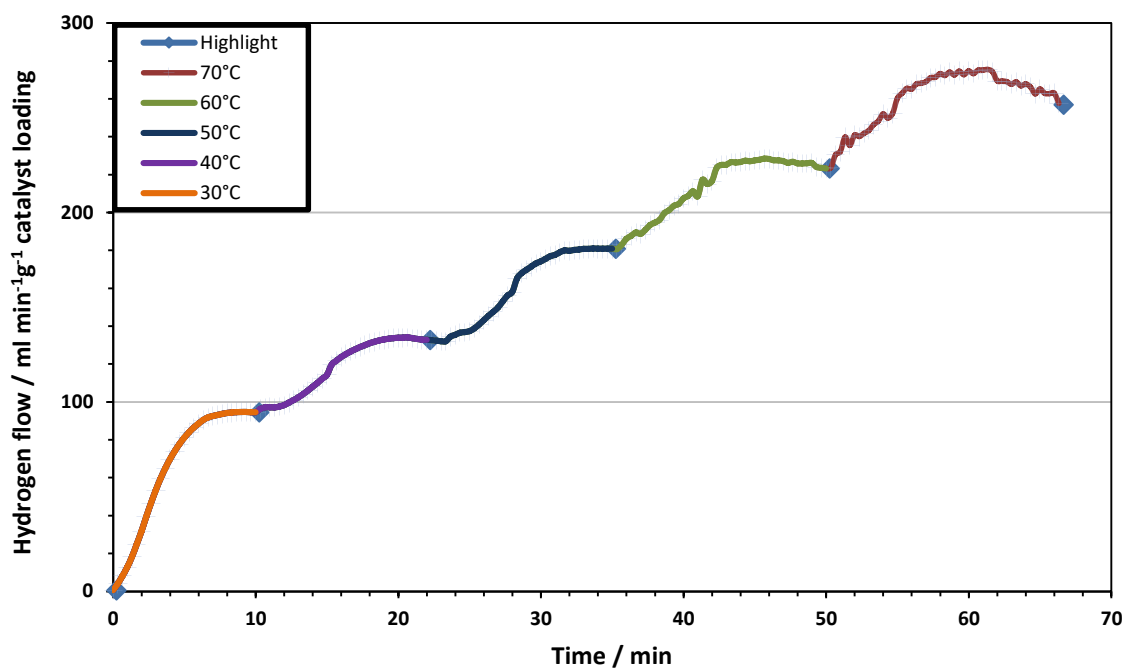


Figure 34: HRR per gram catalyst from METMABH₄ solution (3 wt.% H₂) with Co-W-B/Ni-foam catalysts at different temperatures, analysed by electrochemical approach.

Tables 25-27 summarize the parameters of solution, catalyst and settings used for investigating thermal impacts on HRR regarding Co-W-B/Ni-foam catalyst with METMABH₄ in 0.5 M KOH:

Name	Size [cm ²]	Heating rate [°C/min]	m (Ni-foam) [mg]	m (catalyst) [mg]	m (loading) [mg]
CGr80_10 ^{3rd}	1	1	~13	37.2	~24

Table 25: Parameters of the catalysts used.

METMABH ₄	m METMABH ₄ [g]	Solvent	DMMorOH conc.	m solution [g]
3 wt.% H ₂	9.6627	KOH	0.5 M	18

Table 26: Parameters of the ionic liquid investigated.

Temperature [°C]	Time [min]
30	0
40	15
50	27
60	40
70	55
Gas flow	[ml/min]
Working electrode N ₂	100
Counter electrode H ₂	100
Catalyst added	At the start

Table 27: Setting of the METMABH₄ investigation at different temperatures.

From the established Arrhenius plot the activation energy could be deducted once again, leading to 20.1 kJ/mol H₂. This value would be much too low, if not for the viscosity reasons explicated in the section above. Since METMABH₄ has much inferior viscosity behaviour than DMMorBH₄, temperature is affecting it a lot more. Therefore, both the slope of the Arrhenius plot and the activation energy calculated from the Arrhenius-equation are distinctly smaller.

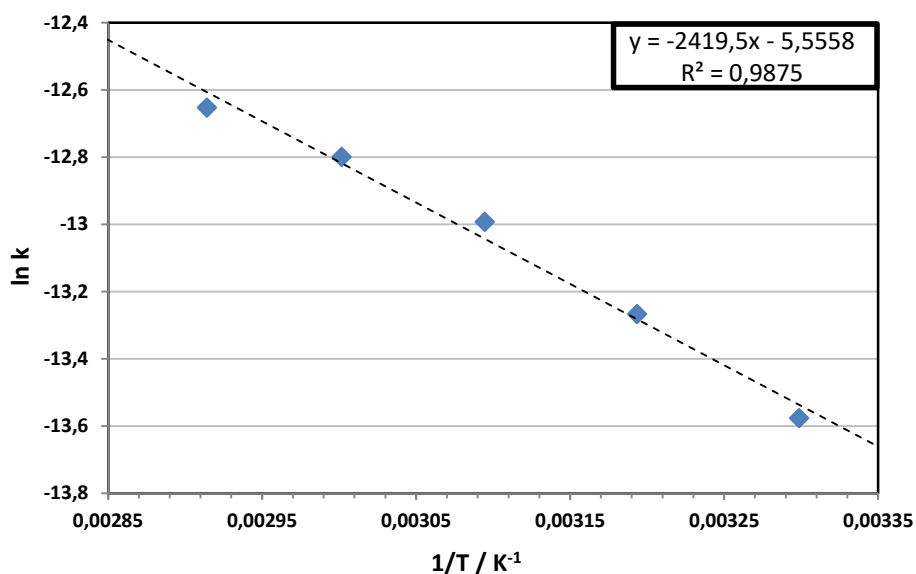


Figure 35: Arrhenius plot of METMABH₄ (in KOH) hydrolysis with Co-W-B/Ni-foam catalyst at 30°C, 40°C, 50°C, 60°C and 70°C.

Activation Energy (E _A) per mol H ₂ [kJ/mol]	Activation Energy (E _A) per mol BH ₄ [kJ/mol]	Standard deviation
20.1	80.5	+/- 0.37

Table 28: Activation energy of METMABH₄ hydrolysis via Co-W-B/Ni-foam catalyst.

5.2.2.3 METMABH₄ in 0.1 M NaOH

Since the outcomes of the previous HRR measurement with METMABH₄ at increased temperatures did not bring the expected values, or rather the experiment did not seem to work as hoped, another attempt was made, using the standard base for dissolving borohydrides: sodium hydroxide. In order to exclude the catalyst as possible cause for the unsatisfying results, CGr80_10^{3rd} was replaced by CGr78^{3rd}. Additionally, for each temperature value a particular test was conducted, because those results are generally better suited for comparison, more representative and less influenced by fluctuations. The following figures summarize the recorded data from the four experiments:

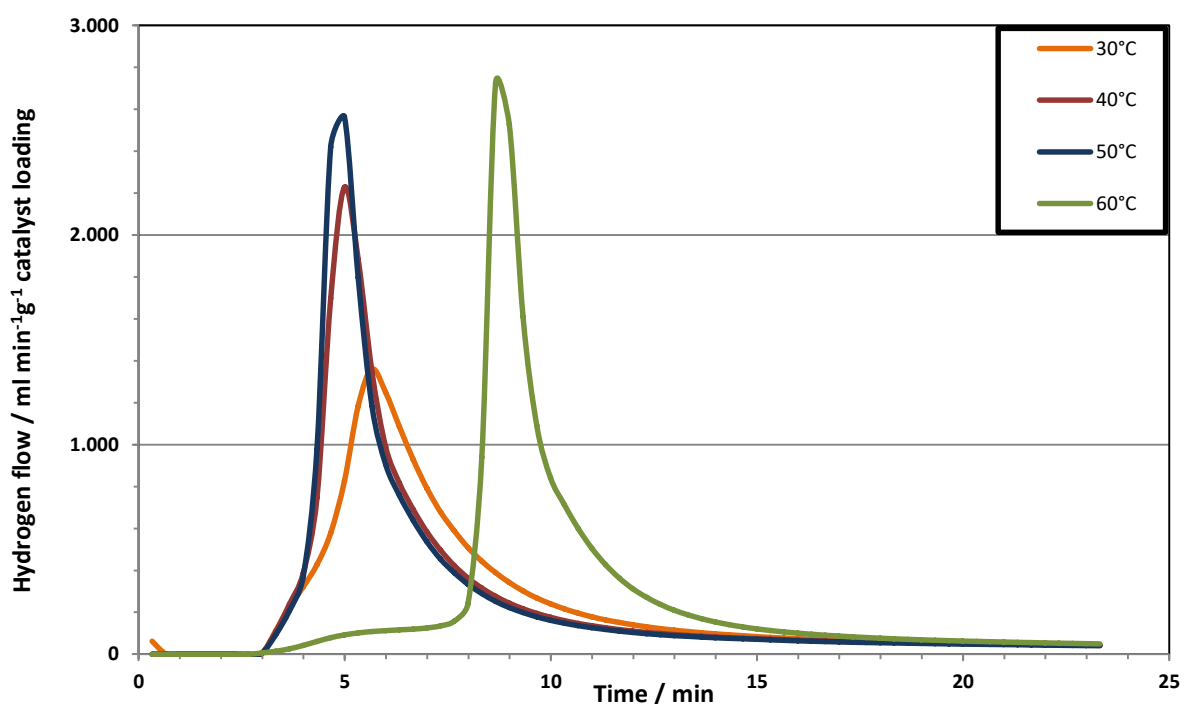


Figure 36: HRR per gram catalyst from METMABH₄ solution (3 wt.% H₂) with Co-W-B/Ni-foam catalysts at different temperatures, analysed by electrochemical approach.

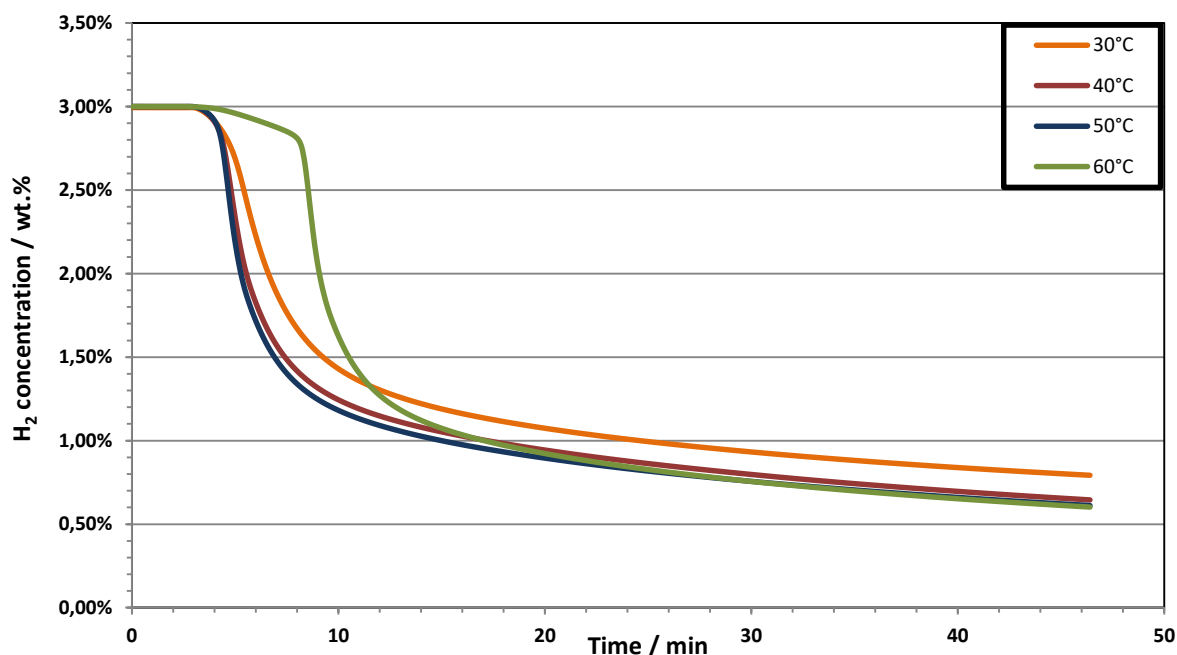


Figure 37: Concentration profile of METMABH₄ solution (3 wt.% H₂) during hydrogen release with Co-W-B/Ni-foam catalysts at different temperatures, analysed by electrochemical approach.

Name	Size [cm ²]	Heating rate [°C/min)	m (Ni-foam) [mg]	m (catalyst) [mg]	m (loading) [mg]
CGr78 ^{3rd}	1	1	45	94.7	49.7

Table 29: Parameters of the catalysts used.

METMABH ₄	m METMABH ₄ [mg]	Solvent	NaOH conc.	Volume [ml]
3 wt.% H ₂	563.1	NaOH	0.1 M	1

Table 30: Parameters of the ionic liquid investigated.

The activity peak points of this second attempt have been between approx. 1400 ml/min and 2700 ml/min per gram Co-W-B-loading and hence in an expected range. A very noticeable feature of the 60°C test was the broad shoulder before the peak within the graph, or rather the 4-minute delay preceding the climax. Since every catalyst needs to be activated before any testing can begin, the lagging period could have come from a lack of activation, due to human error or an expired borohydride solution. Although the H₂ generation was not nearly as effective as it has been with sodium borohydride, more hydrogen could be yielded from METMABH₄ than from DMMorBH₄, which by itself was quite surprising. Usually DMMorOH behaves less reluctant regarding hydrogen release, which could be an indicator for the latent activity loss of CGr80_10^{3rd}. However, even if the catalyst was probably partially responsible for the outcome, the base concentration of the solution should not be ignored either. Reducing to base content within a borohydride solution to a fifth, does raise the tendency to express hydrogen.

Since the performance of METMABH₄ in 0.1 M NaOH did surpass the first attempt, where 0.5 M KOH had been used, the slope of the Arrhenius plot and thus the deduced activation energy were lower.

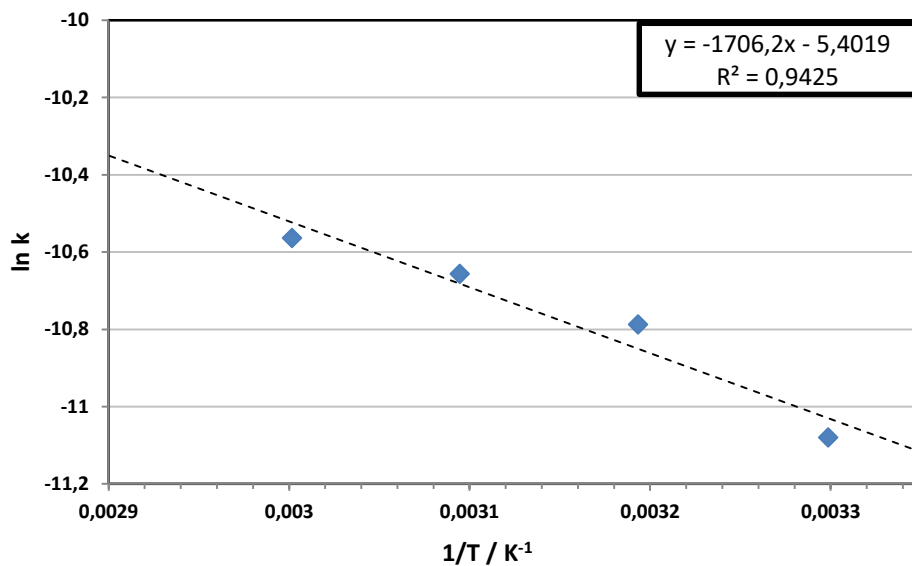


Figure 38: Arrhenius plot of METMABH₄ (in NaOH) hydrolysis at 30°C, 40°C, 50 °C, 60°C and 70°C.

Activation Energy (E _A) per mol H ₂ [kJ/mol]	Activation Energy (E _A) per mol BH ₄ [kJ/mol]	Standard deviation
14.2	56.7	+/- 0.23

Table 31: Activation energy of METMABH₄ hydrolysis via Co-W-B/Ni-foam catalyst.

5.3 Self-regulating Compact Hydrogen Expression System

The key questions concerning the self-regulating compact hydrogen activation system have been:

- Does it work?
- Is it also possible to interrupt the hydrogen expression as often and as long as needed?
- How much hydrogen can be produced?
- Does it also work for more stable ionic liquids?

Answering the first question took the most effort and was by far the most time consuming step within this thesis. Numerous initial struggles had to be overcome, since the first attempt, in order to make the system work. Said former attempt envisioned an internal pressure setting, by determining an accurate amount of borohydride in the release chamber and an accurate amount of headspace in the tank at the start. The build-up pressure from the first catalyst borohydride contact should have pushed the liquid back into the tank. Therefore, the free headspace of the tank would have been compacted

to a fraction of its initial volume, thus creating a starting pressure of a few bar inside the tank and rendering the reaction chamber free of the reactant. This should have led to a small hydrogen pressure within both cells and resulting in a self-regulating hydrogen generation system. However, since every time the reactant and the catalyst came in touch with each other, pressure of a little over 5 bar was build up very fast, resulting in a lot of hydrogen gas getting pumped into the tank. The hydrogen crossover would not have been a problem, because in the end it would have gotten into the reaction chamber and consequently to the detector, if not for the fact that the calculated headspace within the tank and hence the pressure varied with different gas volumes. With more hydrogen ending up in the headspace of the tank, less pressure could be generated, since pressure is volume-dependent. Several creative attempts for improvement had been made, but this approach had to be condemned as unsatisfying.

Finally, with the help of externally applied system pressure, the approach explained in section 4.2.4 appeared promising and with a few fine tuning adjustments, e.g. choosing the appropriate transition point of the safety valves, a self-regulating system could be accomplished. In order to find answers for the other key questions, the following testing series for the compact hydrogen expression system had been established, which consisted of four parts: Continuous and discontinuous operation with sodium borohydride and with DMMorBH₄. Two parameters have been investigated during the operation of the system, i.e. hydrogen flow and pressure. This refers to the pressure measured on the releasing end of the system, or rather at the reaction chamber, not the pressure inside the tank. However, the two pressure levels were closely connected and should never have been diverging more than approx. 0.7 bar. Since the aim of this experiment was to achieve a self-regulating mechanism with relatively high hydrogen yields, a large amount of catalyst has been used. Subsequently some significant results are represented and discussed as examples; a display for all the outcomes is reproduced in the appendix.

Name	Size [cm ²]	Heating rate [°C/min]	m (Ni-foam) [mg]	m (catalyst) [g]	m (loading) [g]
CGr82 ^{3rd}	~37	1	~1.8	~3.5	~1.7

Table 32: Parameters of the catalysts used.

5.3.1 Continuous operation

The settings for the continuous operation mode was very simple: a certain hydrogen consumption was adjusted via needle valve and pressure, as well as flow behaviour have been observed. With the employed amount of catalyst this resulted in a maximum hydrogen flow of 1000 ml/min from sodium borohydride and 500 ml/min for the kinetically unfavoured DMMorBH₄. Successful outcomes could be

accomplished by applying the following hydrogen demands at ambient temperature and are assembled in the appendix:

Hydrogen carrier	[ml/min]	[ml/min]	[ml/min]
NaBH ₄	100	500	1000
DMMorBH ₄	100	300	500

Table 33: Adjusted hydrogen demand measured.

5.3.1.1 NaBH₄ in 0.5 M NaOH

The highest hydrogen expression could be reached with sodium borohydride dissolved in 0.5 M sodium hydroxide. Figure 39 shows the H₂ flow to pressure behaviour of the 1000 ml/min measurement:

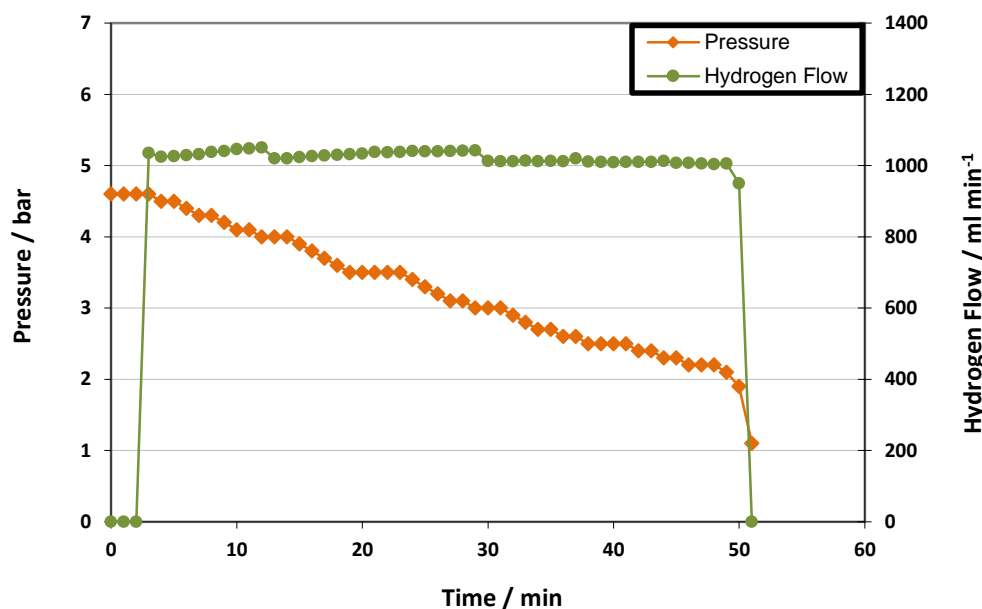


Figure 39: HRR and pressure profile of hydrolysis reaction from NaBH₄ solution (1.5 wt.% H₂) with Co-W-B/Ni-foam catalysts at ambient temperature, analysed by flow tracker. Hydrogen demand employed: 1000 ml/min.

At the beginning of this test a hydrogen pressure of 4.6 bar was applied to the reaction chamber and 4.6 bar of nitrogen pressure to the tank chamber. The system was able to produce a little over 1 L of hydrogen per minute for almost 50 minutes. Figure 39 depicts the relation between hydrogen flow and the pressure within the system, showing a slow and steady decay of pressure, while the hydrogen expression remains constant. This behaviour could be observed at any investigated hydrogen consumption. The pressure did constantly decay over time, but never increased again, due to the amount of borohydride pumped into the reaction chamber. Only a few millilitres sodium borohydride

per minute have been pushed from tank to release cell, in order to counteract the slow pressure drop. Since the transition points of the safety valves have been rather small, the system could respond very fast, but also very accurate to pressure drops with additional borohydride supply. Therefore, only the amount of borohydride solution needed to maintain a consistent hydrogen generation, has been delivered to the release cell. To achieve such an even decrease in pressure the catalyst-borohydride behaviour must be very reactive and the catalyst itself has to be very active. Otherwise the response time regarding borohydride supply is increased, leading to a temporary oversupply of reactant and thus also to a delayed rise of pressure. Since the hydrogen demand was set quite high for this setup the possible hydrogen generation was almost at its maximum, concerning the amount of catalyst employed in this test.

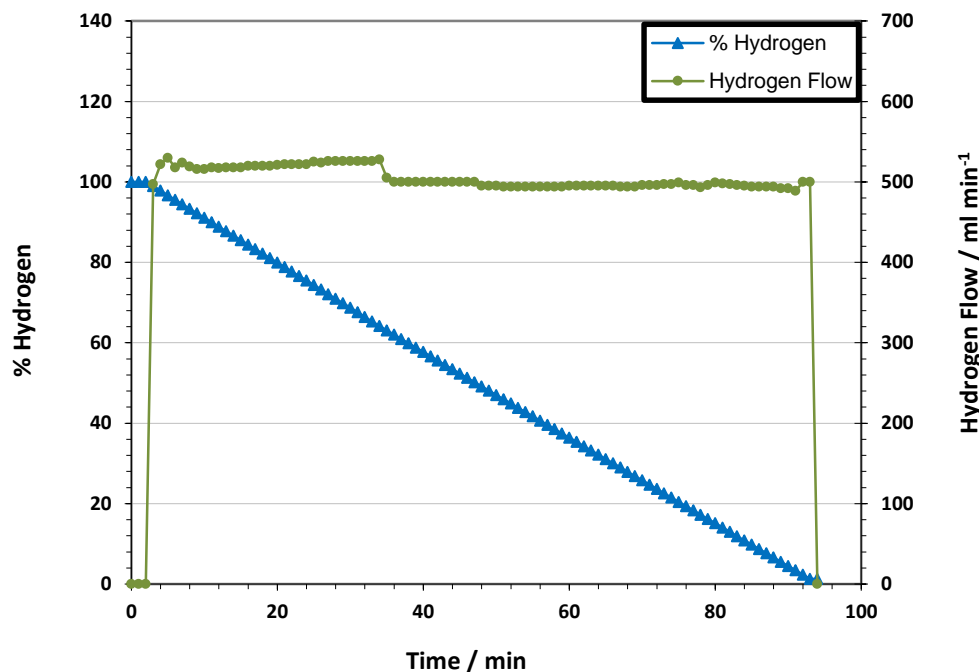


Figure 40: HRR and concentration profile of hydrolysis reaction from NaBH_4 solution (1.5 wt.% H_2) with Co-W-B/Ni-foam catalysts at ambient temperature, analysed by flow tracker. Hydrogen demand employed: 500 ml/min.

Within approx. 90 minutes this hydrogen expression setup was able to release all the hydrogen content from 230 ml of sodium borohydride. Figure 40 shows the connection between the set hydrogen flow of 500 ml/min and the concentration profile of the associated borohydride solution. Marginal fluctuations in the hydrogen flow occurred, because the needle valve had to be readjusted manually from time to time. Due to the very stable hydrogen generation with small fluctuations of max. 5 % (the largest step occurred between minute 34 and 35), the corresponding concentration profile is even more consistent. Given the fact that the hydrogen demand was relatively large, the hydrogen expression stopped within the minute upon reaching 0 wt.% H_2 concentration. In previous experiments

with borohydride solutions a significant drop in hydrogen release could be witnessed, if the hydrogen concentration went beyond a certain level. Nothing of the sort can be seen in the two figures above, leading to the conclusion that excessive amounts of catalyst have been employed.

Results of the measurements concerning the self-regulating hydrogen generation system have been plotted in three different ways: hydrogen flow versus hydrogen concentration, hydrogen flow versus pressure and pressure versus hydrogen concentration. The latter of the three is represented in figure 41.

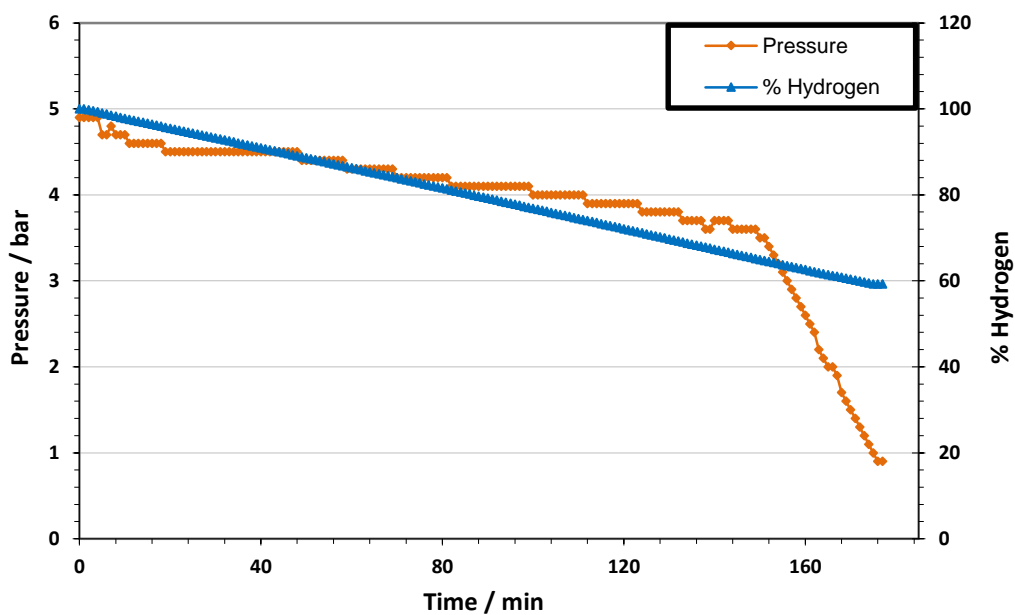


Figure 41: Concentration and pressure profile of hydrolysis reaction from NaBH_4 solution (1.5 wt.% H_2) with Co-W-B/Ni-foam catalysts at ambient temperature, analysed by flow tracker. Hydrogen demand employed: 100 ml/min.

The graphic above shows the relation between hydrogen concentration and pressure for the 100 ml/min investigation. At minute 147 the stopcocks between the two cell compartments have been closed, in order to stop the experiment, as it would have lasted approx. eight hours otherwise. The reason for the continued constant degasification after minute 147 was the permanent readjustment of the needle valve subsequently. The hydrogen expression afterwards has still been collected to see how much H_2 could be won from approx. 2.5 bar overpressure within the system. Although the volume could have been calculated, it was more reliable to measure the amount of hydrogen, due to the fact that the exact size of the complex piping system was not known. From the remaining 3.6 bar inside the system, approx. 3 l of hydrogen could be yielded. Upon reaching the 1 bar mark, hydrogen yield stops almost instantly. This was expected, since with a lack in overpressure there is no force to push the last bit of H_2 within the system to the detector and can be observed in figure 41, as well as in figure 39. For every test with sodium borohydride the solution below has been employed.

NaBH ₄	Solvent	NaOH conc.	Volume [ml]
1.5 wt.% H ₂	NaOH	0.1 M	230

Table 34: Parameters of the sodium borohydride solution used.

5.3.2 Discontinuous operation

5.3.2.1 NaBH₄ in 0.5 M NaOH

For the discontinuous operation mode, the setting was again very straightforward: a distinct hydrogen consumption was set for a certain time with the help of a needle valve, followed by a certain sleeping period, where no hydrogen demand was employed. Pressure and hydrogen flow have been monitored.

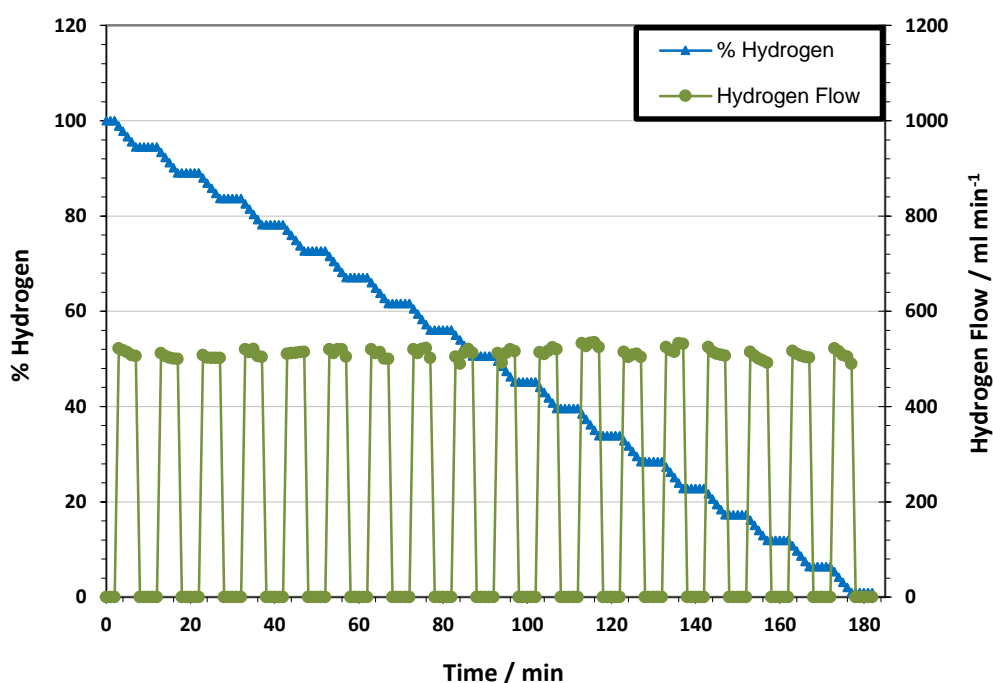


Figure 42: HRR and concentration profile of hydrolysis reaction from NaBH₄ solution (1.5 wt.% H₂) with Co-W-B/Ni-foam catalysts at ambient temperature, analysed by flow tracker. Hydrogen demand employed: 500 ml/min.

The discontinuous operation testing was conducted with a hydrogen consumption of 500 ml per minute every five minutes for five minutes. Small fluctuations in the range of a few percent were unavoidable, since the flow has been adjusted manually every five minutes and the needle valve needed a few minutes to become steady. Figure 42 shows the relation between concentration profile for this setup versus the hydrogen flow per minute. The degasification of the sodium borohydride was achieved within 3 hours, while half of that time no hydrogen has been consumed. When looking at the concentration profile, it is obvious that hydrogen release has been executed perfectly consistent. Because the concentration profile has been calculated from the measured hydrogen flow, which in

turn has been readjusted every 5 minutes, the steadiness of the decreasing H_2 content is explicable. The corresponding pressure profile in the appendix on the other hand shows an increase in pressure, if the flow had been terminated, and a decrease upon employing a certain consumption five minutes later.

5.3.2.2 DMMorBH₄ in 0.1 M DMMorOH

Due to the need of pausing the test overnight another property could be investigated, i.e. the ability to stop the reaction for many hours and start it up immediately once it was needed again.

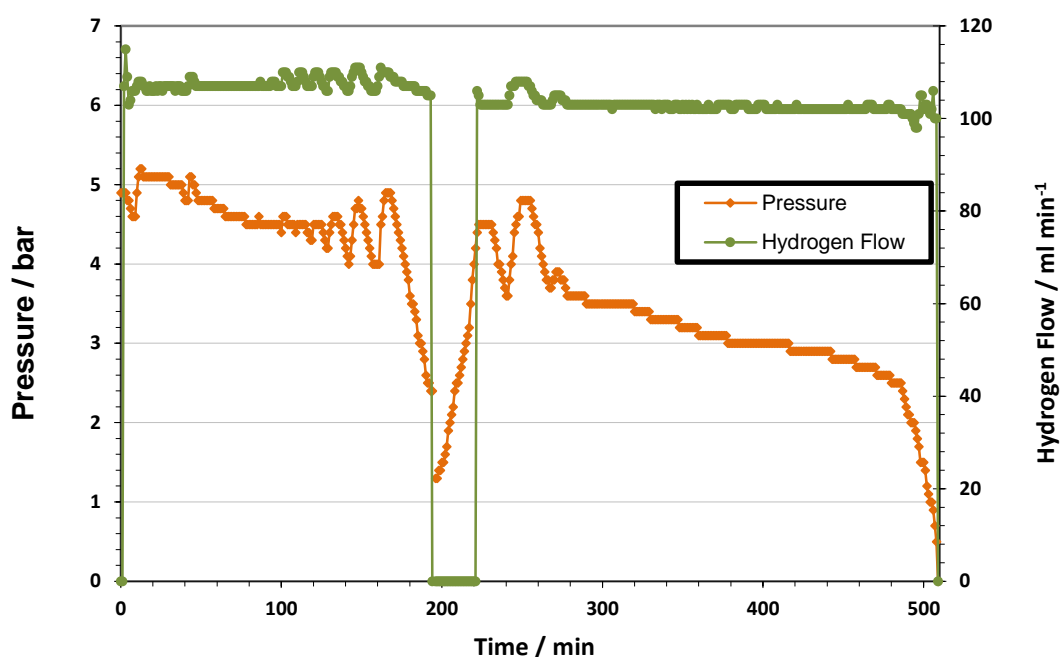


Figure 43: HRR and pressure profile of hydrolysis reaction from DMMorBH₄ solution (1.5 wt.% H₂) with Co-W-B/Ni-foam catalysts at ambient temperature, analysed by flow tracker. Hydrogen demand employed: 100 ml/min.

Figure 43 represents the hydrogen flow vs pressure profile for DMMorBH₄ in DMMorOH at a hydrogen consumption of 100 ml per minute and ambient temperature. The break from minute 193 to minute 222 was in reality much longer than 29 minutes, since the experiment has been stopped overnight. For graphical clarity reasons this 15-hour break has been depicted as only half an hour. At minute 161 the stopcocks between the two cells have been closed, but hydrogen was still consumed, in order to release the majority of the hydrogen pressure due to safety concerns. Approx. 1 bar of pressure had been lost during the night break. Therefore, at first only the stopcock leading to the reaction chamber was opened, until enough pressure had built up to continue the test. At minute 222 both the other stopcock, as well as the needle valve were opened and the measurement has been continued. Even though the overall pressure behaviour was not as smooth as during the sodium borohydride tests and

mediocre fluctuations could be observed, the fact that the system could be shut down and started up again safely and quickly after a long break was a substantial success.

DMMorBH₄ measurement have been conducted with solutions possessing the parameters below:

DMMorBH₄	Solvent	DMMorOH conc.	Volume [ml]
1.5 wt.% H ₂	DMMorOH	0.1 M	230

Parameters of the DMMorBH₄ solution used.

6. Conclusion and Outlook

The aim of this thesis was the design and assembly of a self-regulating system, capable to release significant amounts of hydrogen via catalytic hydrolysis from borohydride solutions with the aid of non-noble transition metal catalysts. To accomplish this task, the catalyst itself has been investigated in order to increase catalytic performance. Through comparing the effects of different heating rates for thermal treatment in addition to optimizing the number of electro-less plating steps, the initial Co-W-B/Ni-foam catalyst could be improved significantly. Further investigations into the specific surface processes during catalyst deposition are required.

Outcomes of this work also indicated a higher activity for a lower number of Co-W-B deposition cycles. By further optimizing the thermal treatment a distinct improvement in hydrolysis activity was provided. While the initial HRR was in the range of 2000 millilitres per minute per gram catalyst, upgraded catalyst preparation led to values of approx. 5500 ml/min/g Co-W-B. Compared to literature data regarding non-noble metal catalysts those results are among the most active.

Moreover, to determine the HRR a novel electrochemical method to quantify hydrogen has been introduced and tested thoroughly. With the aid of a potentiostat and an in-house fabricated hydrogen release cell, the electrodes of a fuel cell have been used to measure the directly generated hydrogen gas in an electrochemical way.

Subsequent efforts have been made towards borohydride based ionic liquids. Due to the superior gravimetric hydrogen storage capacity of liquid salts like METMABH₄ and DMMorBH₄, they provide a promising alternative to sodium borohydride for future applications, considering the American DoE requirements for hydrogen storage technologies. Furthermore, the increased long-term stability of these substances yields an additional advantage. Unfortunately, the kinetics of the hydrolysis reaction are unfavourably affected by higher stability as well. In order to counteract this distinct drawback, an examination of various bases for stabilizing the borohydride in solution has been conducted. Using the water displacement method, attempts to find the base most prone to release hydrogen under the influence of a Co-W-B/Ni-foam catalyst have been launched. The resulting data with consecutive temperature dependent measurements have enabled a practical evaluation of the activation energies for hydrolysis from METMABH₄ and DMMorBH₄.

Ultimately a self-regulating hydrogen expression system has been designed and fabricated. After several approaches concerning the starting setup of the system, a promising way to generate on demand hydrogen in a safe and simple manner was found. With the help of an externally applied pressure of a few bars to the system, larger quantities of hydrogen could be produced. A variety of hydrogen generating systems have already been presented, but every hydrogen generator until now

had to rely on supplementary devices, e.g. pumps, whereas the herein presented technology does not. Even though the system does require a light inflation after filling up the tank, this process is part of the refilling cycle and is not needed during operation mode. The system is regulated by a simple button or tap. Nevertheless, H₂ yields of over one Litre per minute could be accomplished from sodium borohydride hydrolysis, while exhibiting a very fast response behaviour regarding gas demand due to demonstrating a negative feedback. This technology is also applicable for ionic liquids. Hydrogen flow rates of up to 500 ml/min could be produced from DMMorBH₄ on a permanent basis.

The build scale of the device is in the size of a regular PC tower and can be easily transported. Expanding both the 500 ml tank, as well as the catalyst amount is a very simple and effective improvement, resulting in even larger hydrogen yields per minute. Since the borohydride solutions inquired for the compact release system held a low hydrogen concentration of 1.5 wt.% H₂, approx. 50 L of hydrogen have been stored. Given that borohydride solutions exhibit significantly higher H₂ storage capacities, this volume can easily be multiplied.

7. References

- [1] C. S. Watson, N. J. White, J. A. Church, M. A. King, R. J. Burgette, and B. Legresy, "Unabated global mean sea-level rise over the satellite altimeter era," *Nat. Clim. Chang.*, vol. 5, pp. 565–568, 2015.
- [2] S. reinsurance company Ltd., "Natural catastrophes and man-made disasters in 2008," *Swiss Re Sigma*, vol. 9, 2009.
- [3] IPCC5 WGII, *Climate Change 2013*. .
- [4] S. Rahmstorf and H. J. Schellnhuber, *Der Klimawandel*, 6th editio. C. H. Beck, 2007.
- [5] C. Deser, J. E. Walsh, and M. S. Timlin, "Arctic sea ice variability in the context of recent atmospheric circulation trends," *J. Clim.*, vol. 13, no. 3, pp. 617–633, 2000.
- [6] UNFCCC. Conference of the Parties (COP), "Adoption of the Paris Agreement. Proposal by the President.," *Paris Clim. Chang. Conf. - Novemb. 2015, COP 21*, vol. 21932, no. December, p. 32, 2015.
- [7] "The Montreal protocol on substances that deplete the ozone layer.," in *Ozone Secretariat United Nations Environment Programme*, 1988.
- [8] A. Bocarsly, D. Micheal, and P. Mingos, *Fuel Cells and Hydrogen Storage*. 2011.
- [9] J. G. Aston and P. Mitacek Jr., "Structure of hydrides of palladium," *Nature*, vol. 195, pp. 70–71, 1962.
- [10] J. H. N. Van VUCHT, F. A. KUIJPERS, and H. C. A. M. BRUNING, "REVERSIBLE ROOM-TEMPERATURE ABSORPTION OF LARGE QUANTITIES OF HYDROGEN BY INTERMETALLIC COMPOUNDS," *Philips Res. Repts*, vol. 25, pp. 133–140, 1970.
- [11] U. Eberle, M. Felderhoff, and F. Schuth, "Chemical and physical solutions for hydrogen storage," *Angew. Chemie - Int. Ed.*, vol. 48, no. 36, pp. 6608–6630, 2009.
- [12] K. O'Malley, G. Ordaz, J. Adams, K. Randolph, C. C. Ahn, and N. T. Stetson, "Applied hydrogen storage research and development: A perspective from the U.S. Department of Energy," *J. Alloys Compd.*, vol. 645, no. S1, pp. S419–S422, 2015.
- [13] R. T. Yang, "Hydrogen storage by alkali-doped carbon nanotubes-revisited," *Carbon N. Y.*, vol. 38, no. 4, pp. 623–626, 2000.
- [14] C. Liu et al., "Hydrogen storage in carbon nanotubes revisited," *Carbon N. Y.*, vol. 48, pp. 452–455, 2010.
- [15] S. S. Kaye, A. Dailly, O. M. Yaghi, and J. R. Long, "Impact of preparation and handling on the hydrogen storage properties of $Zn_4O(1,4\text{-benzenedicarboxylate})_3$ (MOF-5)," *J. Am. Chem. Soc.*, vol. 129, no. 46, pp. 14176–14177, 2007.

- [16] P. Chen, Z. Xiong, J. Luo, J. Lin, and K. L. Tan, "Interaction of hydrogen with metal nitrides and imides," *Nature*, vol. 420, pp. 302–304, 2002.
- [17] K. M. Eblagon, D. Rentsch, O. Friedrichs, A. Remhof, A. Zuetzel, A. J. Ramirez-Cuesta, and S. C. Tsang, "Hydrogenation of 9-ethylcarbazole as a prototype of a liquid hydrogen carrier," *Int. J. Hydrogen Energy*, vol. 35, no. 20, pp. 11609–11621, 2010.
- [18] T. He, Q. Pei, and P. Chen, "Liquid organic hydrogen carriers," *J. Energy Chem.*, vol. 24, no. 5, pp. 587–594, 2015.
- [19] D. R. Palo, R. A. Dagle, and J. D. Holladay, "Methanol steam reforming for hydrogen production," *Chem. Rev. 107 3992-4021*, vol. 107, no. PNNL-SA-53246, pp. 3992–4021, 2007.
- [20] B. Bogdanović and M. Schwickardi, "Ti-doped alkali metal aluminium hydrides as potential novel reversible hydrogen storage materials," *Journal Alloy. Compd.*, vol. 253–254, pp. 1–9, 1997.
- [21] C. M. Jensen and K. J. Gross, "Development of catalytically enhanced sodium aluminum hydride as a hydrogen-storage material," *Appl. Phys. A Mater. Sci. Process.*, vol. 7, no. 2, pp. 213–219, 2001.
- [22] J. Chen, N. Kuriyama, Q. Xu, T. H. Takeshita, and T. Sakai, "Reversible hydrogen storage via titanium-catalyzed LiAlH₄ and Li₃AlH₆," *Int. J. Phys. Chem. B*, vol. 105, no. 45, pp. 11214–11220, 2001.
- [23] F. Schüth, B. Bogdanović, and M. Felderhoff, "Light metal hydrides and complex hydrides for hydrogen storage," *Chem. Commun.*, vol. 20, pp. 2249–2258, 2004.
- [24] S. C. Amendola, S. L. Sharp-Goldman, M. S. Janjua, M. T. Kelly, P. J. Petillo, and M. Binder, "An ultrasafe hydrogen generator: Aqueous, alkaline borohydride solutions and Ru catalyst," *ACS Div. Fuel Chem. Prepr.*, vol. 44, no. 4, pp. 864–866, 1999.
- [25] P. Krishnan, S. G. Advani, and A. K. Prasad, "Cobalt oxides as Co₂B catalyst precursors for the hydrolysis of sodium borohydride solutions to generate hydrogen for PEM fuel cells," *Int. J. Hydrogen Energy*, vol. 33, no. 23, pp. 7095–7102, 2008.
- [26] U.S. DOE Hydrogen Program, "Go / No-Go Recommendation for Sodium Borohydride for On-Board Vehicular Hydrogen Storage," 2007.
- [27] P. Wasserscheid and W. Keim, "Ionic Liquids - New Solutions for Transition Metal Catalysis," *Angew Chem Int*, vol. 39, pp. 3772–3789, 2000.
- [28] R. Kalb, "Method of Use of an Ionic Liquid for Storing Hydrogen," *WO 2010/081657 A1*, 2010.
- [29] R. Kalb and A. Kraynov, "Use of an Ionic Liquid for Storing Hydrogen," *WO 2013/113452 A1*, 2013.
- [30] C. Grimmer, J. Senn, T. Friedrich, D. Woisetschläger, N. Mayer, R. Kalb, M. Koncar, J. Wagner,

- and V. Hacker, "Borohydride based Ionic Liquids as novel Hydrogen Storage," *5th Eur. PEFC H2 Forum*, vol. B0503, 2015.
- [31] E. K. H. I. Schlesinger, Herbert C. Brown, A. E. Finholt, James R. Gilbreath, Henry R. Hoekstra, "Sodium Borohydride, Its Hydrolysis and its Use as a Reducing Agent and in the," *J. Am. Chem. Soc.*, vol. 75, no. 3, pp. 215–219, 1953.
- [32] S. S. Muir and X. Yao, "Progress in sodium borohydride as a hydrogen storage material: Development of hydrolysis catalysts and reaction systems," *Int. J. Hydrogen Energy*, vol. 36, no. 10, pp. 5983–5997, 2011.
- [33] Y. Kojima, K. I. Suzuki, K. Fukumoto, Y. Kawai, M. Kimbara, H. Nakanishi, and S. Matsumoto, "Development of 10 kW-scale hydrogen generator using chemical hydride," *J. Power Sources*, vol. 125, no. 1, pp. 22–26, 2004.
- [34] D. Gervasio, S. Tasic, and F. Zenhausern, "Room temperature micro-hydrogen-generator," *J. Power Sources*, vol. 149, no. 1–2, pp. 15–21, 2005.
- [35] R. Aiello, J. H. Sharp, and M. A. Matthews, "Production of hydrogen from chemical hydrides via hydrolysis with steam.," *Int. J. Hydrog. Energy*, vol. 24, pp. 1123–1130, 1999.
- [36] S. Murugesan and V. Subramanian, "Effects of acid accelerators on hydrogen generation from solid sodium borohydride using small scale devices," *J Power Sources*, vol. 187, no. 216–223, 2009.
- [37] B. H. Liu, Z. P. Li, and S. Suda, "Solid sodium borohydride as a hydrogen source for fuel cells," *J Alloy. Compd*, vol. 468, pp. 493–498, 2009.
- [38] C. Cento, P. Gislou, and P. P. Prosini, "Hydrogen generation by hydrolysis of NaBH₄," *Int. J. Hydrogen Energy*, vol. 34, no. 10, pp. 4551–4554, 2009.
- [39] P. Kurzweil, *Brennstoffzellentechnik*. Springer Vieweg, 2013.
- [40] J. Larminie and A. Dicks, *Fuel Cell Systems Explained*, vol. 93. 2001.
- [41] C. Hartnig and C. Roth, *Polymer Electrolyte Membrane and Direct Methanol Fuel Cell Technology*. Woodhead Publishing, 2012.
- [42] Y.-S. Ye, J. Rick, and B.-J. Hwang, "Water Soluble Polymers as Proton Exchange Membranes for Fuel Cells," *Polymers (Basel)*, vol. 4, pp. 913–963, 2012.
- [43] Y. Wang, K. S. Chen, J. Mishler, S. C. Cho, and X. C. Adroher, "A review of polymer electrolyte membrane fuel cells: Technology, applications, and needs on fundamental research," *Appl. Energy*, vol. 88, no. 4, pp. 981–1007, 2011.
- [44] Y. J. Wang, N. Zhao, B. Fang, H. Li, X. T. Bi, and H. Wang, "Carbon-Supported Pt-Based Alloy Electrocatalysts for the Oxygen Reduction Reaction in Polymer Electrolyte Membrane Fuel Cells: Particle Size, Shape, and Composition Manipulation and Their Impact to Activity," *Chem.*

Rev., vol. 115, no. 9, pp. 3433–3467, 2015.

- [45] V. Hacker and S. Mitsushima, “Advanced Studies of Polymer Electrolyte Fuel Cells - 5th International Summer School,” *in.*, p. 20–24., 2012.
- [46] V. Hacker and E. wallnöfer-Ogris, “Advanced Studies of Polymer Electrolyte Fuel Cells - 4th International Summer School,” *in.*, pp. 11–15, 2011.
- [47] H. B. Dai, Y. Liang, P. Wang, X. D. Yao, T. Rufford, M. Lu, and H. M. Cheng, “High-performance cobalt-tungsten-boron catalyst supported on Ni foam for hydrogen generation from alkaline sodium borohydride solution,” *Int. J. Hydrogen Energy*, vol. 33, no. 16, pp. 4405–4412, 2008.
- [48] C. Grimmer, S. Nestl, J. Senn, and V. Hacker, “Selective real-time quantification of hydrogen within mixtures of gases via an electrochemical method,” *Int. J. Hydrogen Energy*, vol. 40, no. 4, pp. 2055–2061, 2015.
- [49] E. Ramschak, V. Peinecke, and P. Prenninger, “Online stackmonitoring tool for dynamically and stationary operated fuel cell systems,” *Fuel Cells Bull.*, p. 12, 2006.
- [50] C. F. Yao, L. Zhuang, Y. L. Cao, X. P. Ai, and H. X. Yang, “Hydrogen release from hydrolysis of borazane on Pt- and Ni-based alloy catalysts,” *Int. J. Hydrogen Energy*, vol. 33, no. 10, pp. 2462–2467, 2008.
- [51] P. Dupiano, D. Stamatis, and E. L. Dreizin, “Hydrogen production by reacting water with mechanically milled composite aluminum-metal oxide powders,” *Int. J. Hydrogen Energy*, vol. 36, no. 8, pp. 4781–4791, 2011.
- [52] C. Grimmer, “EFCF-2015_Paper_B0503_Borohydride based Ionic Liquids as novel Hydrogen Storage Technology_Grimmer_Christoph_final.” .
- [53] Z. Jiang, H. Yang, Z. Wei, Z. X. Xie, W. Zhong, and S. Wei, “Catalytic properties and structures of nano-amorphous Ni–B alloys affected by annealing temperatures,” *Appl Catal A Gen*, no. 279, pp. 165–171, 2005.
- [54] J. Liang, Y. Li, Y. Huang, J. Yang, H. Tang, Z. Wei, and P. K. Shen, “Sodium borohydride hydrolysis on highly efficient Co-B/Pd catalysts,” *Int. J. Hydrogen Energy*, vol. 33, no. 15, pp. 4048–4054, 2008.
- [55] Y. Liang, P. Wang, and H. Bin Dai, “Hydrogen bubbles dynamic template preparation of a porous Fe-Co-B/Ni foam catalyst for hydrogen generation from hydrolysis of alkaline sodium borohydride solution,” *J. Alloys Compd.*, vol. 491, no. 1–2, pp. 359–365, 2010.
- [56] D. R. Kim, K. W. Cho, Y. Il Choi, and C. J. Park, “Fabrication of porous Co-Ni-P catalysts by electrodeposition and their catalytic characteristics for the generation of hydrogen from an alkaline NaBH₄ solution,” *Int. J. Hydrogen Energy*, vol. 34, no. 6, pp. 2622–2630, 2009.
- [57] J. H. Kim, K. T. Kim, Y. M. Kang, H. S. Kim, M. S. Song, Y. J. Lee, P. S. Lee, and J. Y. Lee, “Study

on degradation of filamentary Ni catalyst on hydrolysis of sodium borohydride," *J. Alloys Compd.*, vol. 379, no. 1–2, pp. 222–227, 2004.

- [58] H. Tian, Q. Guo, and D. Xu, "Hydrogen generation from catalytic hydrolysis of alkaline sodium borohydride solution using attapulgite clay-supported Co-B catalyst," *J. Power Sources*, vol. 195, no. 8, pp. 2136–2142, 2010.

8. Appendix

8.1 Results of hydrogen release experiments using the self-regulating system

8.1.1 NaBH₄ in 0.1 M NaOH

100 ml/min:

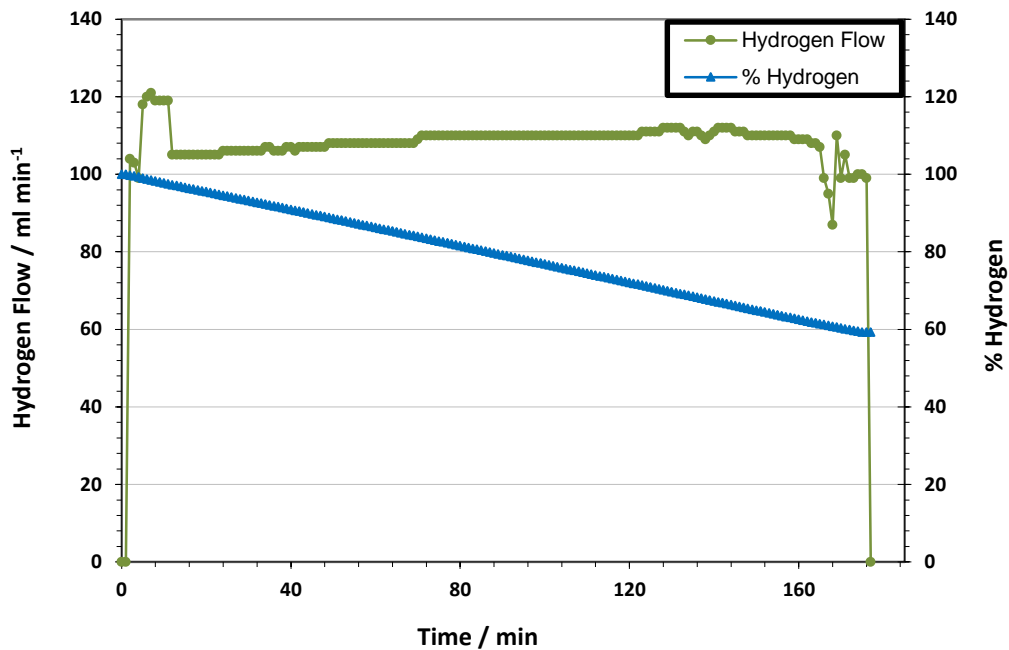
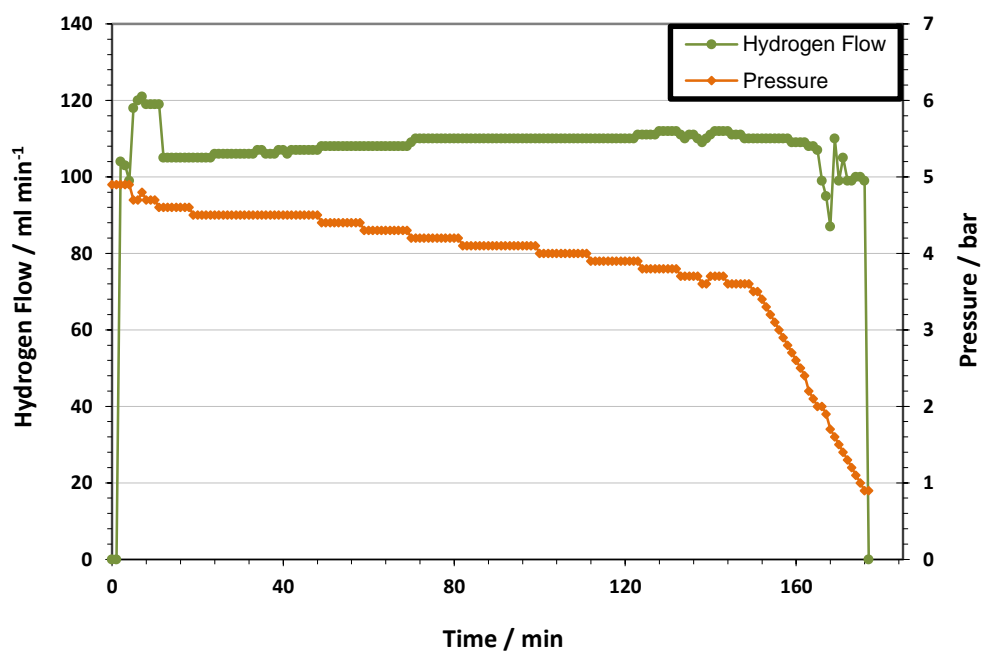
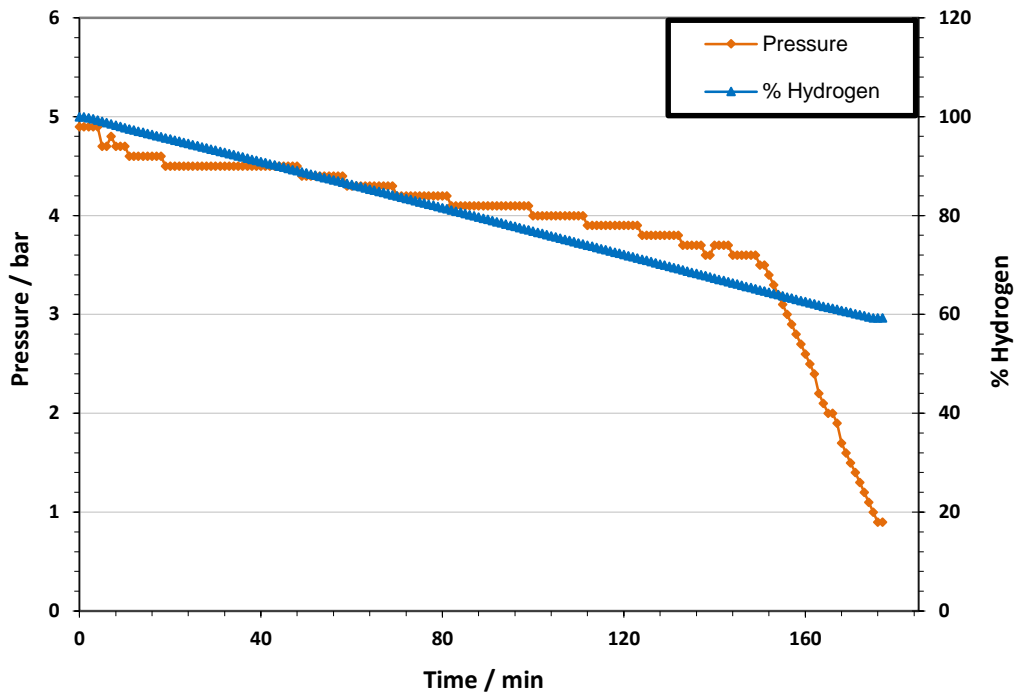


Figure 44: HRR and concentration profile of hydrolysis reaction from NaBH₄ solution (1.5 wt.% H₂) with Co-W-B/Ni-foam catalysts at ambient temperature, analysed by flow tracker. Hydrogen demand employed: 100 ml/min.

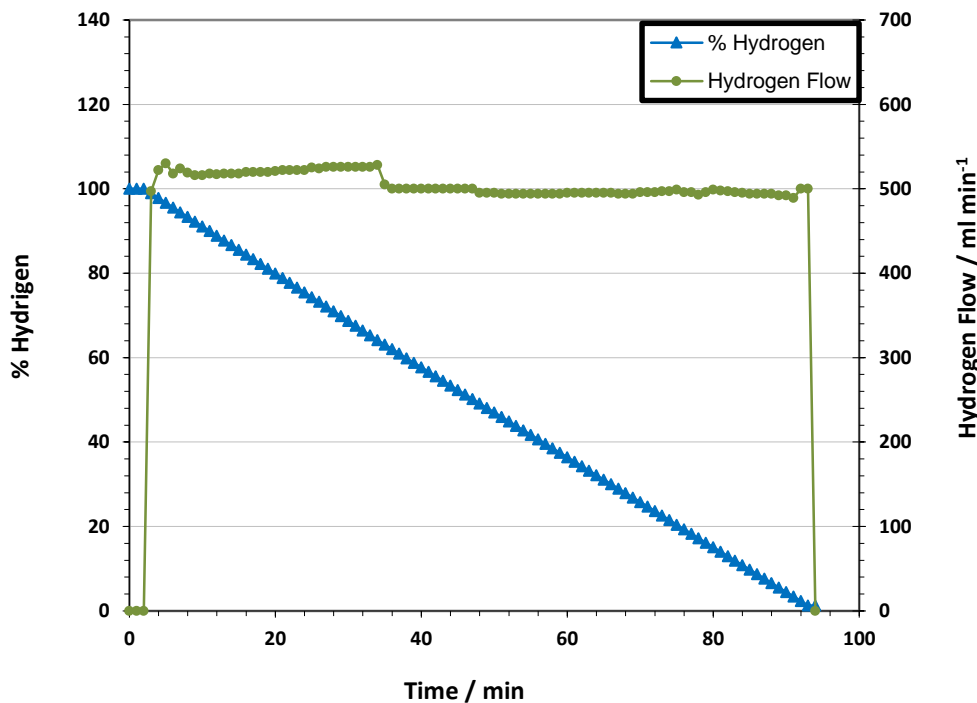


HRR and pressure profile of hydrolysis reaction from NaBH₄ solution (1.5 wt.% H₂) with Co-W-B/Ni-foam catalysts at ambient temperature, analysed by flow tracker. Hydrogen demand employed: 100 ml/min.

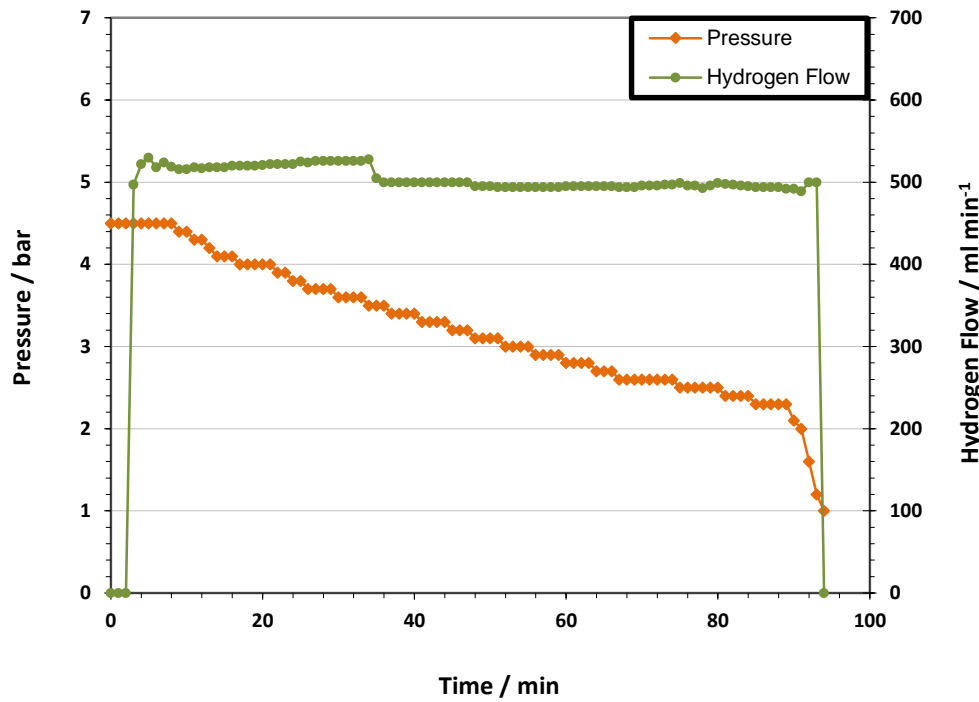


Concentration and pressure profile of hydrolysis reaction from NaBH₄ solution (1.5 wt.% H₂) with Co-W-B/Ni-foam catalysts at ambient temperature, analysed by flow tracker. Hydrogen demand employed: 100 ml/min.

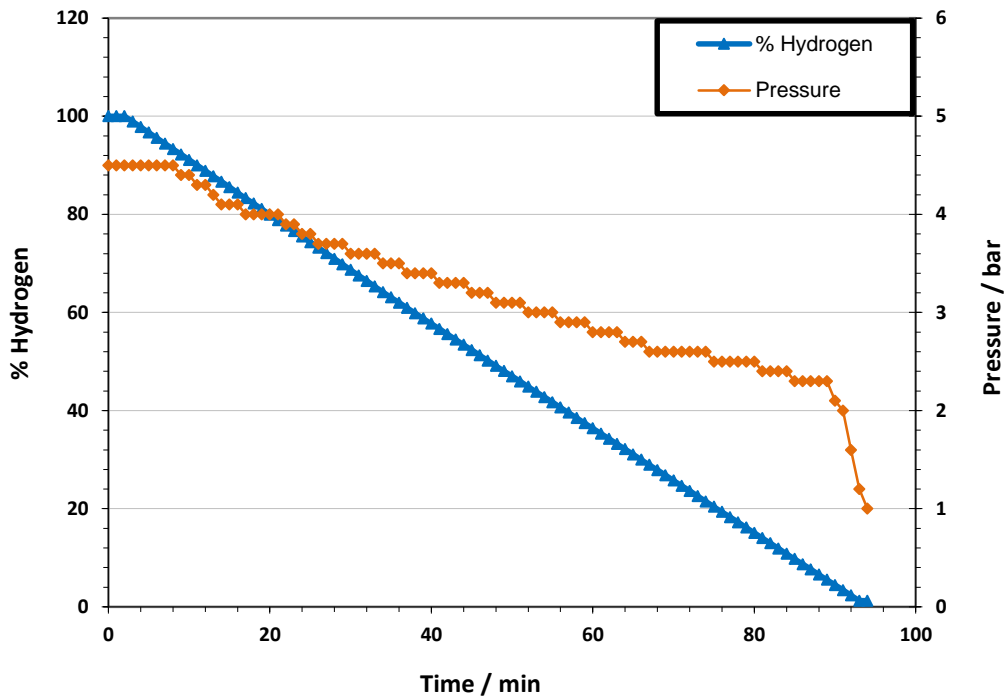
500 ml/min:



HRR and concentration profile of hydrolysis reaction from NaBH₄ solution (1.5 wt.% H₂) with Co-W-B/Ni-foam catalysts at ambient temperature, analysed by flow tracker. Hydrogen demand employed: 500 ml/min.

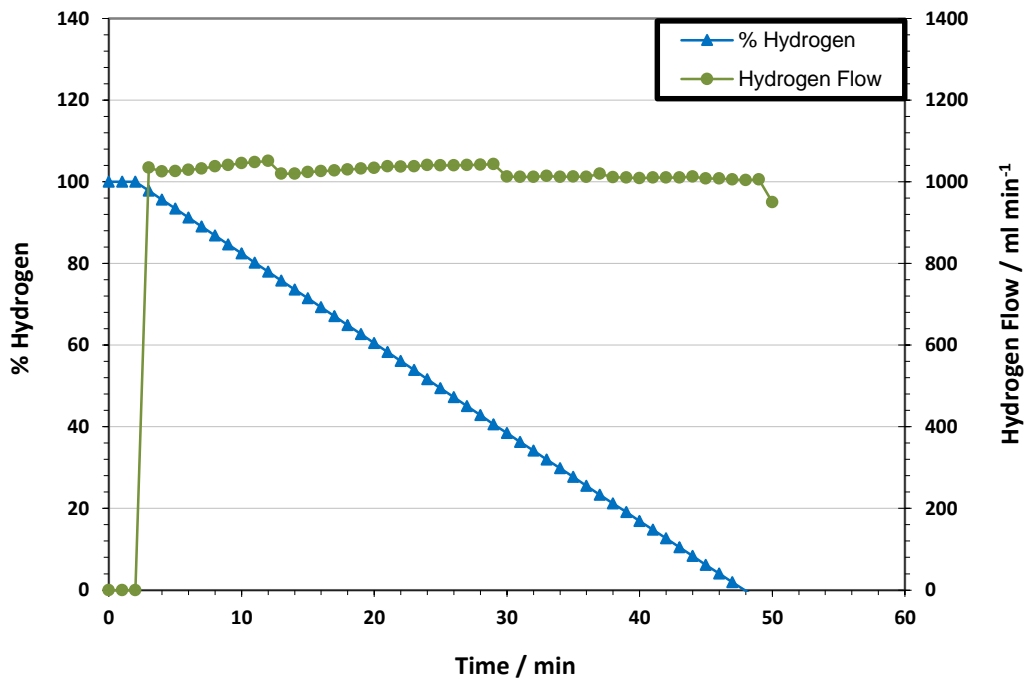


HRR and pressure profile of hydrolysis reaction from NaBH₄ solution (1.5 wt.% H₂) with Co-W-B/Ni-foam catalysts at ambient temperature, analysed by flow tracker. Hydrogen demand employed: 500 ml/min.

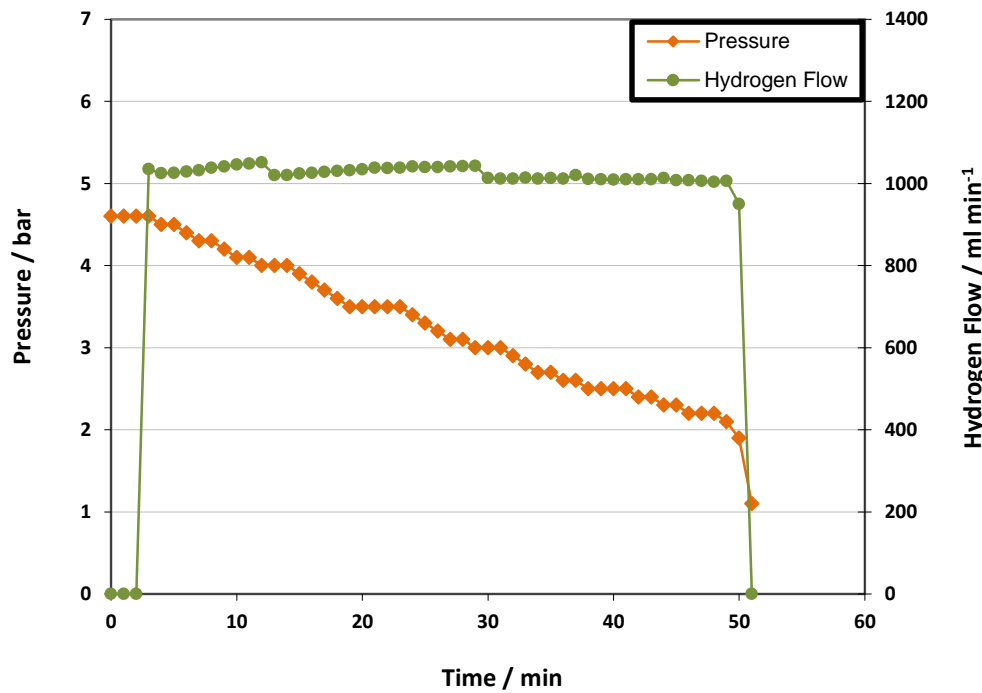


Concentration and pressure profile of hydrolysis reaction from NaBH₄ solution (1.5 wt.% H₂) with Co-W-B/Ni-foam catalysts at ambient temperature, analysed by flow tracker. Hydrogen demand employed: 500 ml/min.

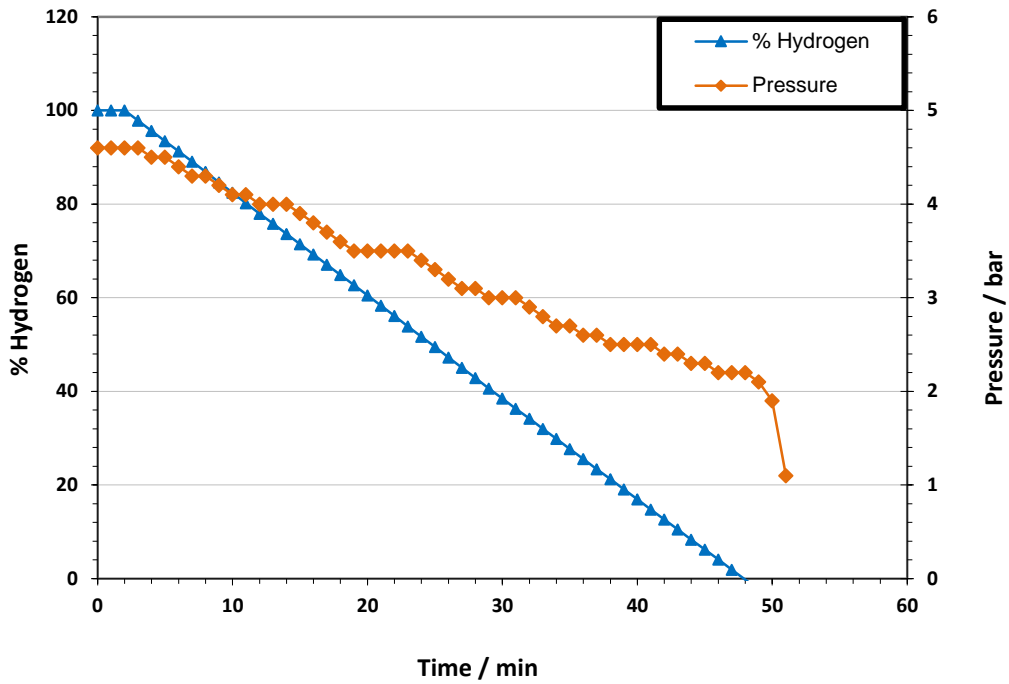
1000 ml/min:



HRR and concentration profile of hydrolysis reaction from NaBH₄ solution (1.5 wt.% H₂) with Co-W-B/Ni-foam catalysts at ambient temperature, analysed by flow tracker. Hydrogen demand employed: 1000 ml/min.

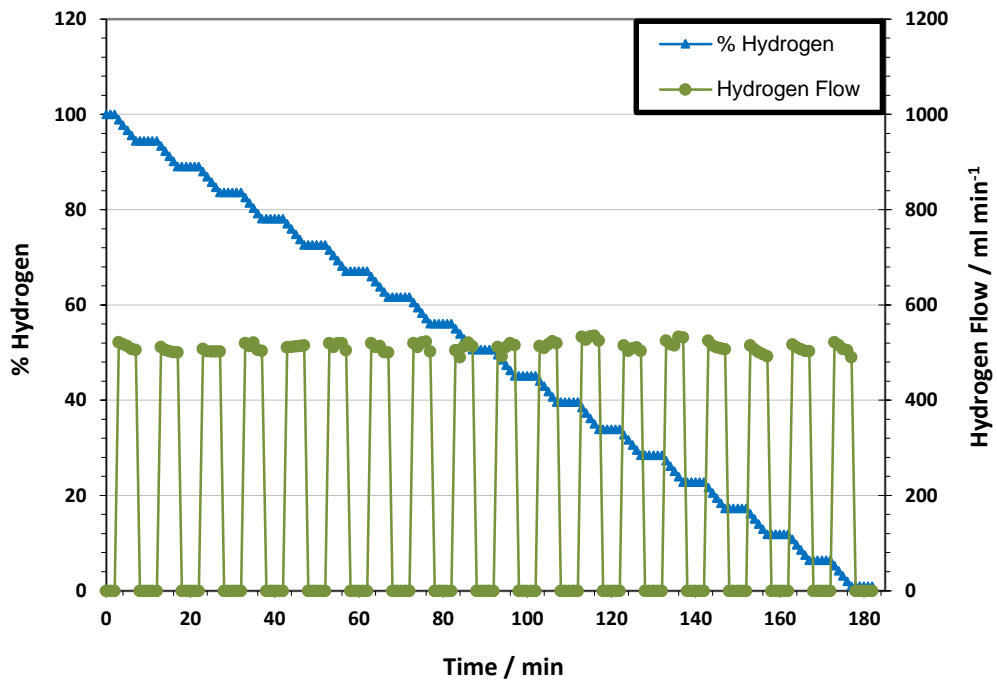


HRR and pressure profile of hydrolysis reaction from NaBH₄ solution (1.5 wt.% H₂) with Co-W-B/Ni-foam catalysts at ambient temperature, analysed by flow tracker. Hydrogen demand employed: 1000 ml/min.

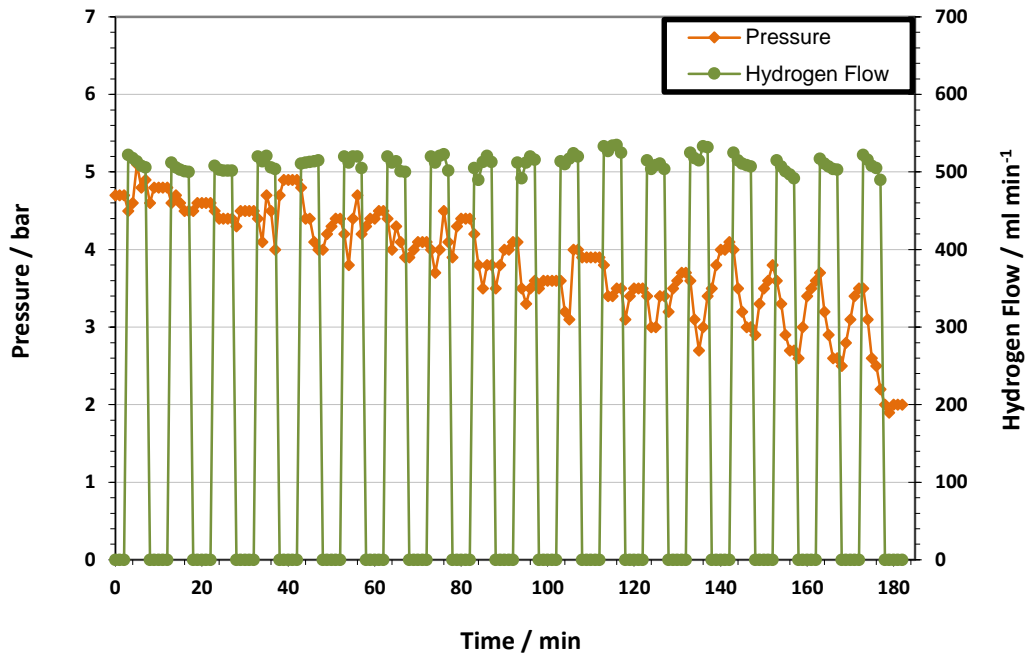


Concentration and pressure profile of hydrolysis reaction from NaBH_4 solution (1.5 wt.% H_2) with Co-W-B/Ni-foam catalysts at ambient temperature, analysed by flow tracker. Hydrogen demand employed: 1000 ml/min.

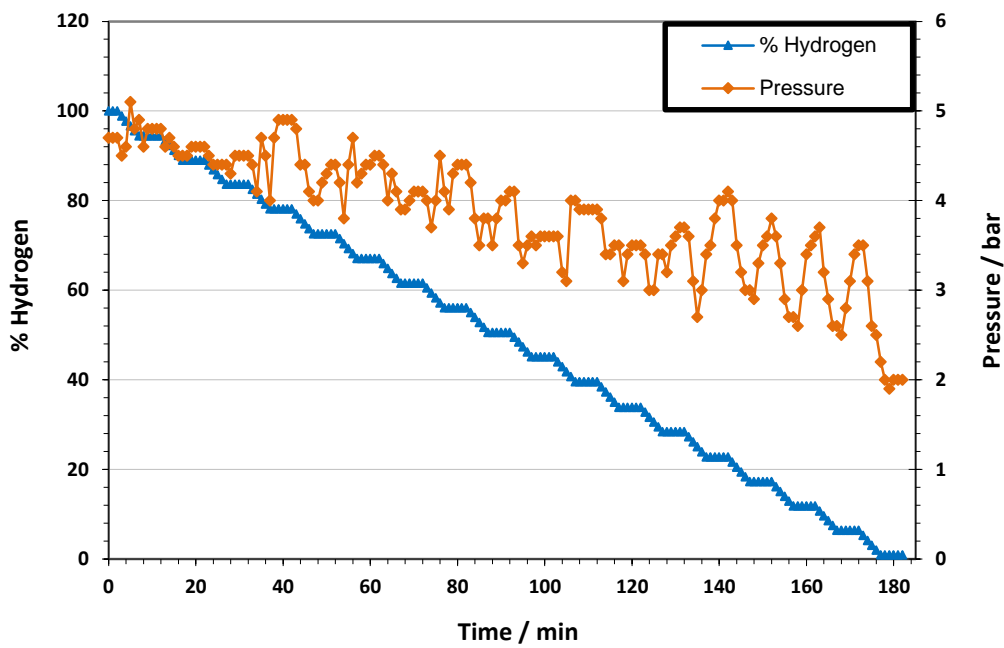
500 ml/min, start/stop operation:



HRR and concentration profile of hydrolysis reaction from NaBH_4 solution (1.5 wt.% H_2) with Co-W-B/Ni-foam catalysts at ambient temperature, analysed by flow tracker. Hydrogen demand employed: 500 ml/min.



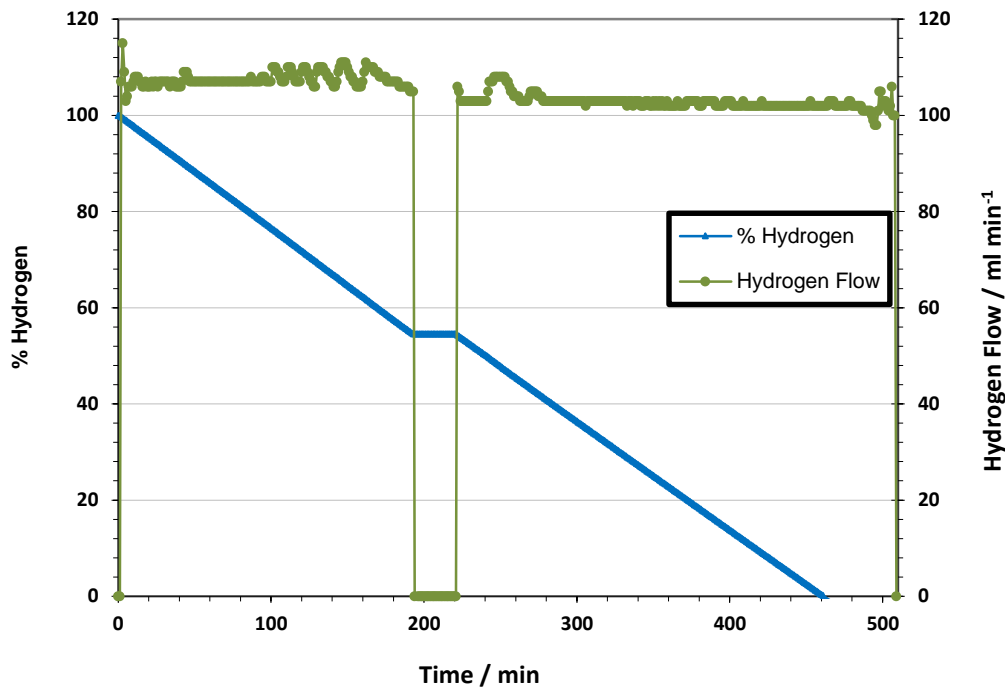
HRR and pressure profile of hydrolysis reaction from NaBH₄ solution (1.5 wt.% H₂) with Co-W-B/Ni-foam catalysts at ambient temperature, analysed by flow tracker. Hydrogen demand employed: 500 ml/min.



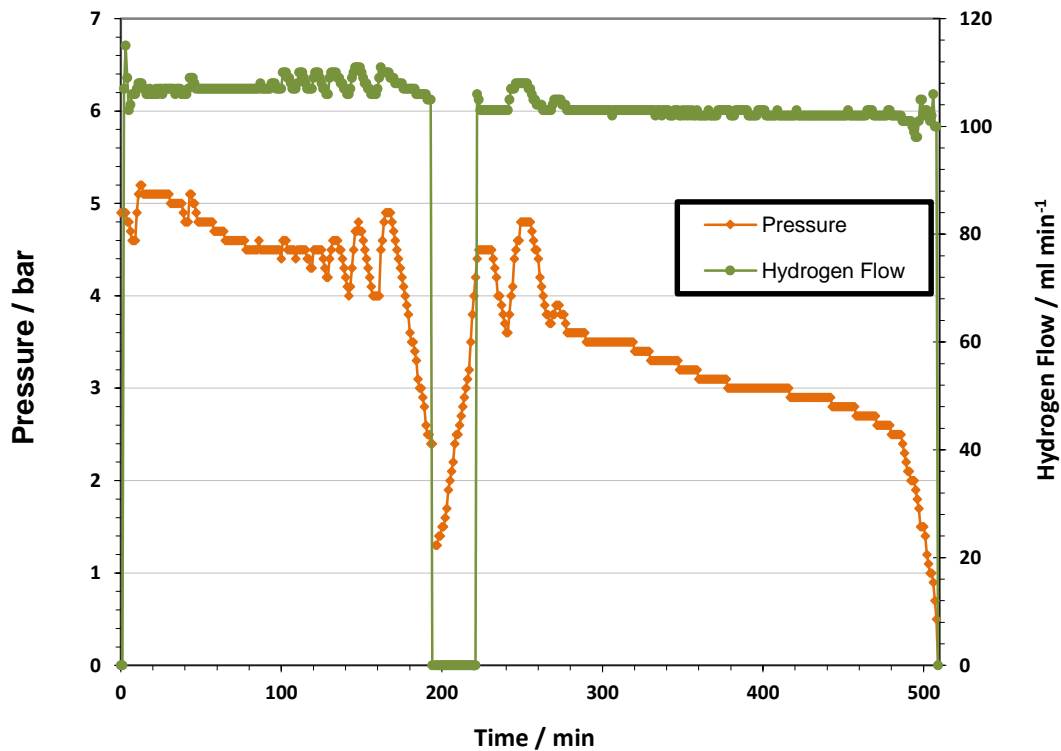
Concentration and pressure profile of hydrolysis reaction from NaBH₄ solution (1.5 wt.% H₂) with Co-W-B/Ni-foam catalysts at ambient temperature, analysed by flow tracker. Hydrogen demand employed: 500 ml/min.

8.1.2 DMMorBH₄ in 0.1 M DMMorOH

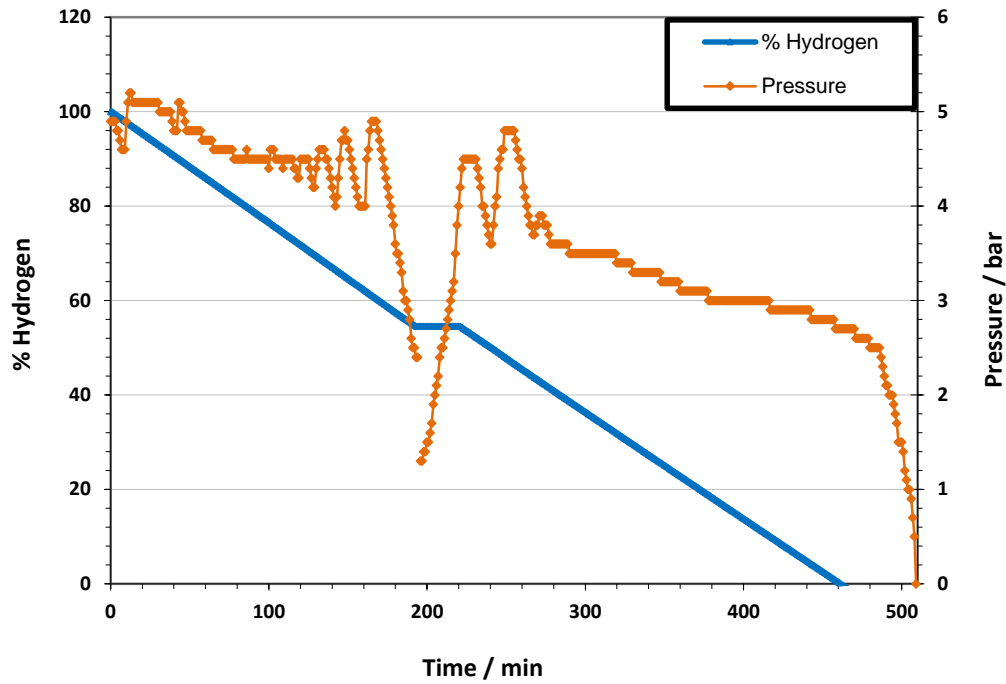
100 ml/min:



HRR and concentration profile of hydrolysis reaction from DMMorBH₄ solution (1.5 wt.% H₂) with Co-W-B/Ni-foam catalysts at ambient temperature, analysed by flow tracker. Hydrogen demand employed: 100 ml/min.

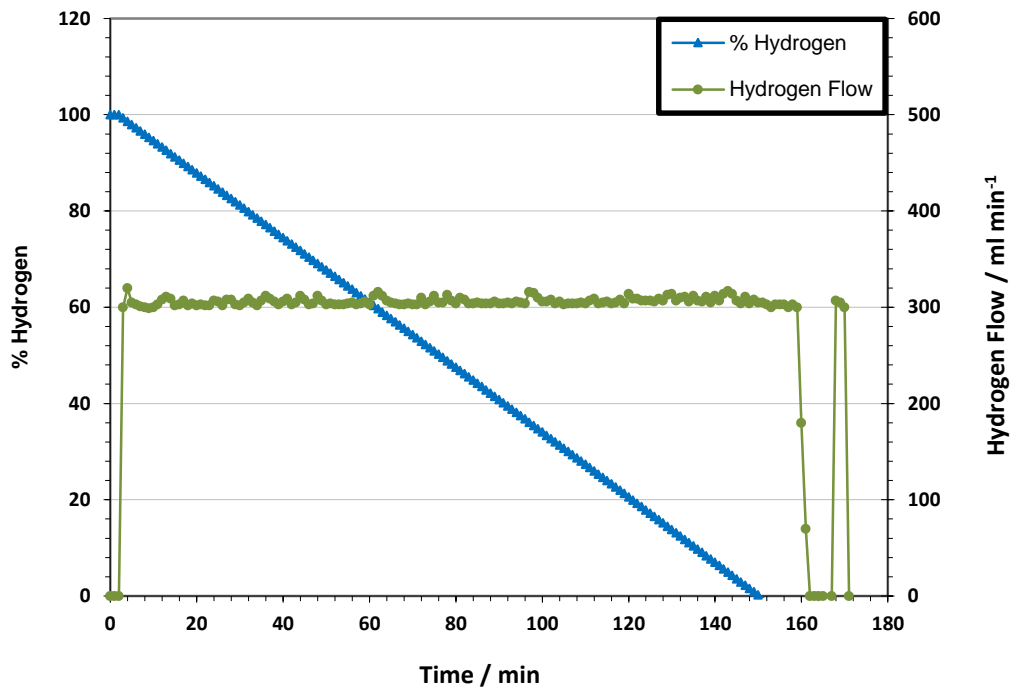


HRR and pressure profile of hydrolysis reaction from DMMorBH₄ solution (1.5 wt.% H₂) with Co-W-B/Ni-foam catalysts at ambient temperature, analysed by flow tracker. Hydrogen demand employed: 100 ml/min.

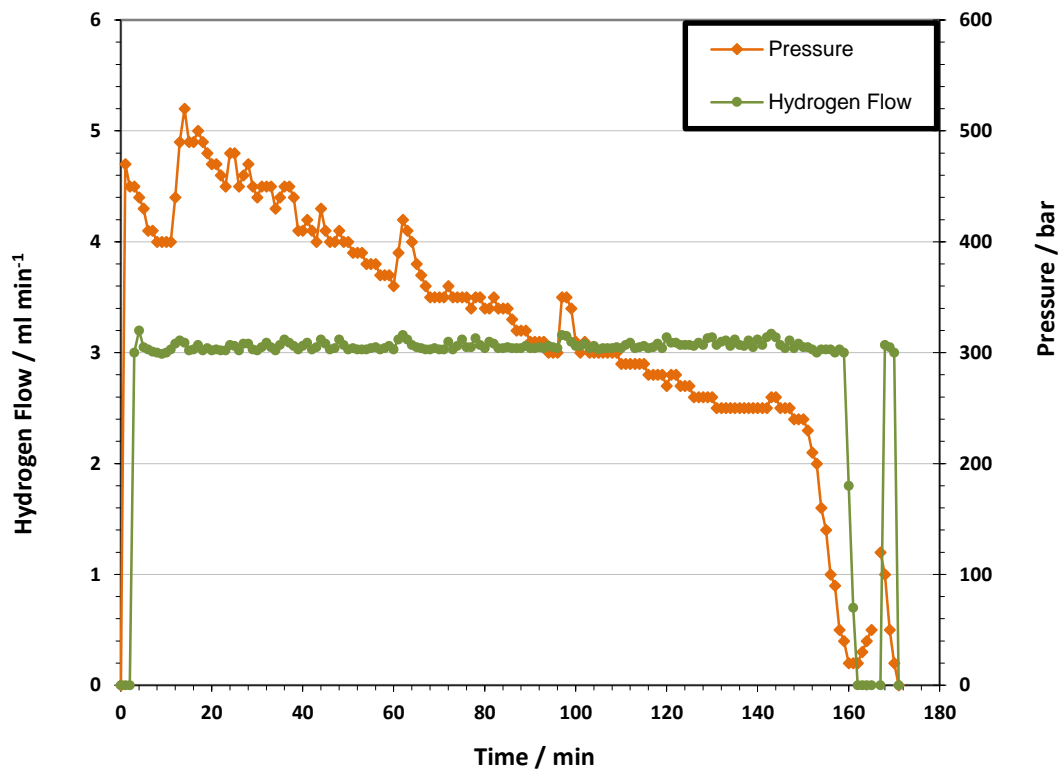


Concentration and pressure profile of hydrolysis reaction from DMMorBH_4 solution (1.5 wt.% H_2) with Co-W-B/Ni-foam catalysts at ambient temperature, analysed by flow tracker. Hydrogen demand employed: 100 ml/min.

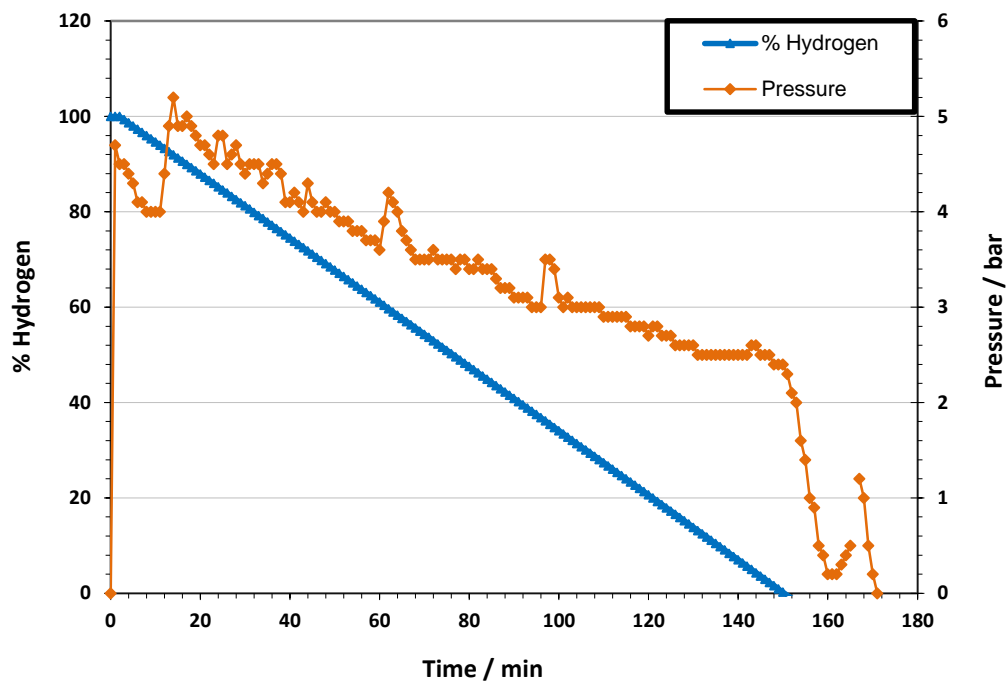
300 ml/min:



HRR and concentration profile of hydrolysis reaction from DMMorBH_4 solution (1.5 wt.% H_2) with Co-W-B/Ni-foam catalysts at ambient temperature, analysed by flow tracker. Hydrogen demand employed: 300 ml/min.

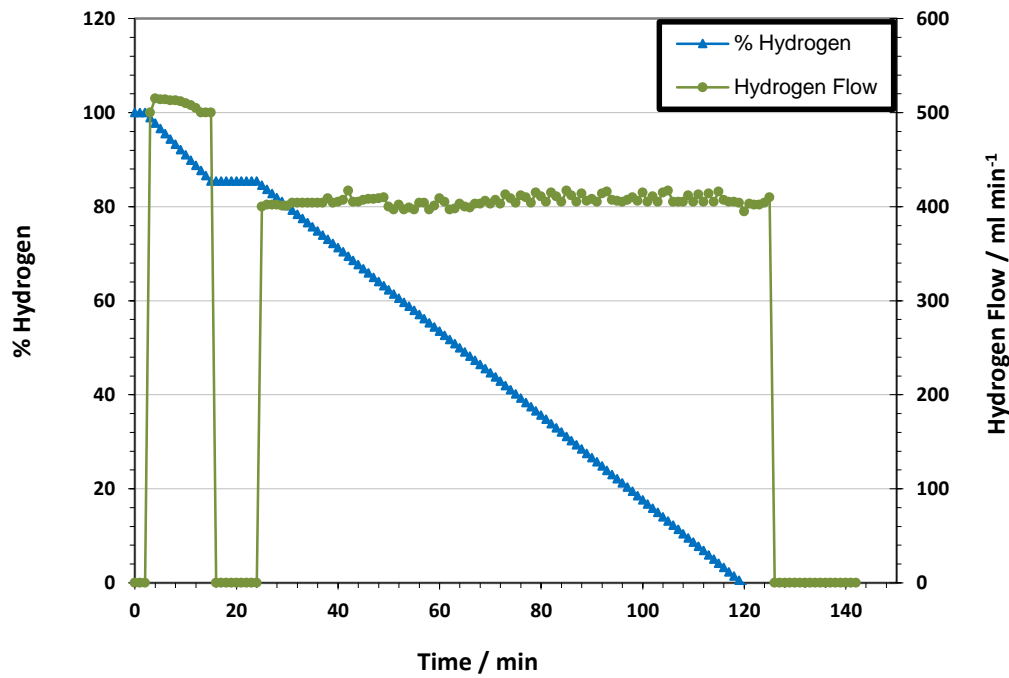


HRR and pressure profile of hydrolysis reaction from DMMorBH₄ solution (1.5 wt.% H₂) with Co-W-B/Ni-foam catalysts at ambient temperature, analysed by flow tracker. Hydrogen demand employed: 300 ml/min.

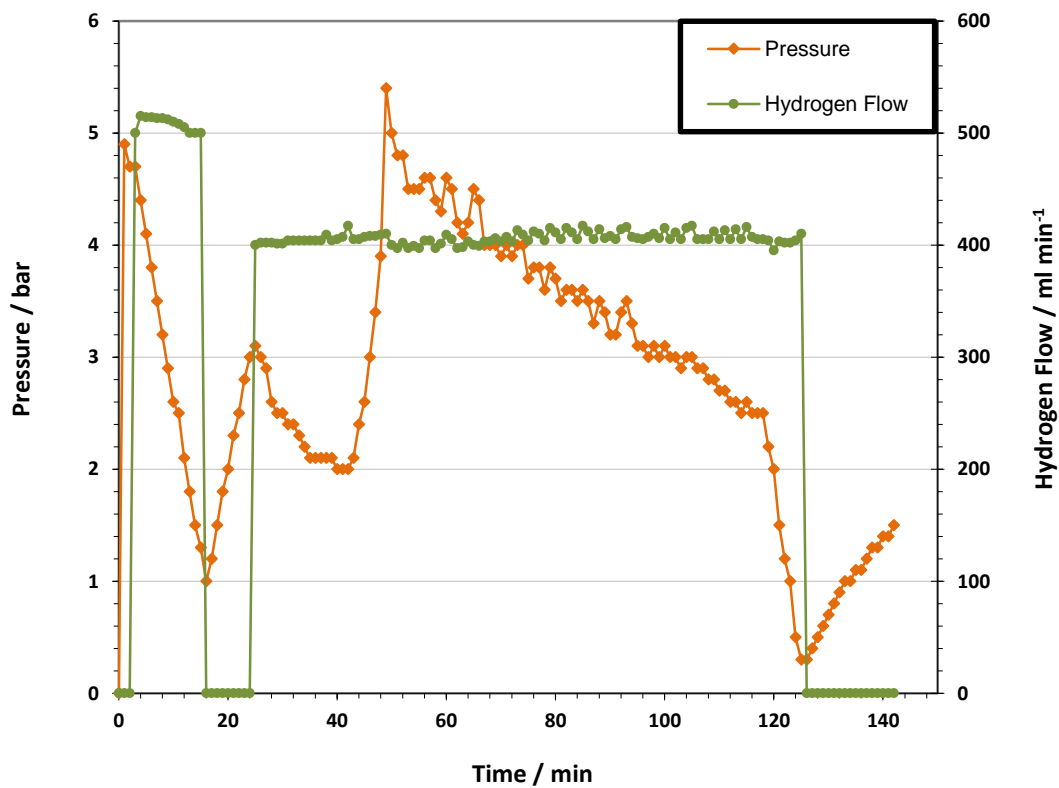


Concentration and pressure profile of hydrolysis reaction from NaBH₄ solution (1.5 wt.% H₂) with Co-W-B/Ni-foam catalysts at ambient temperature, analysed by flow tracker. Hydrogen demand employed: 300 ml/min.

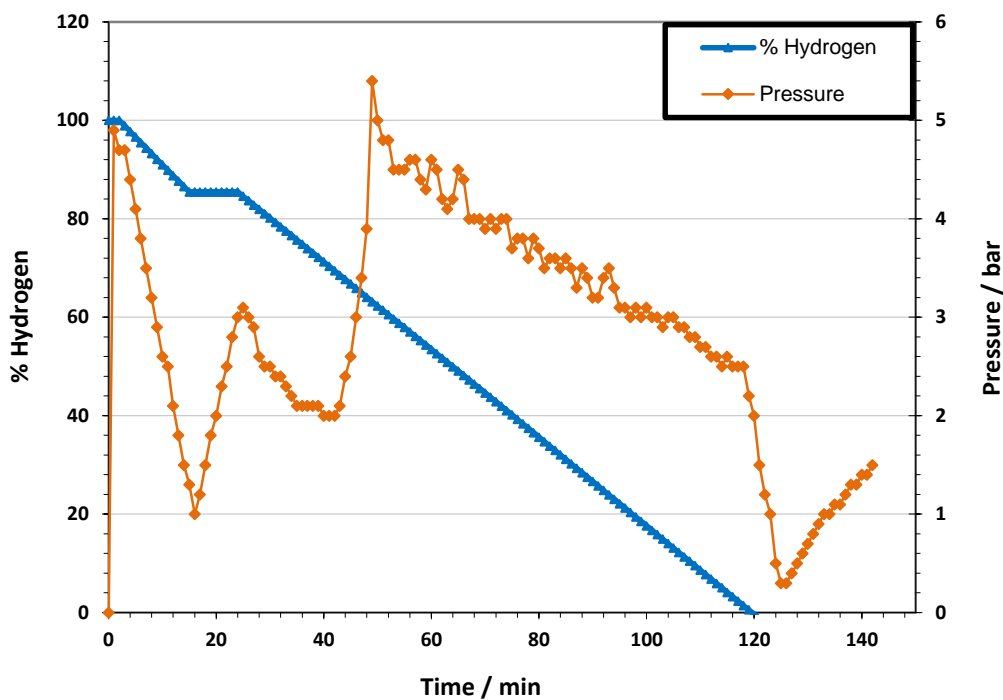
500 ml/min:



HRR and concentration profile of hydrolysis reaction from DMMorBH₄ solution (1.5 wt.% H₂) with Co-W-B/Ni-foam catalysts at ambient temperature, analysed by flow tracker. Hydrogen demand employed: 500 ml/min.



HRR and pressure profile of hydrolysis reaction from DMMorBH₄ solution (1.5 wt.% H₂) with Co-W-B/Ni-foam catalysts at ambient temperature, analysed by flow tracker. Hydrogen demand employed: 500 ml/min.



Concentration and pressure profile of hydrolysis reaction from NaBH₄ solution (1.5 wt.% H₂) with Co-W-B/Ni-foam catalysts at ambient temperature, analysed by flow tracker. Hydrogen demand employed: 500 ml/min.

8.2 Complementary Information

Ionic liquid	M [g/mol]
METMABH ₄	133.04
DMMorBH ₄	130.8
NaBH ₄	37.83
METMAOH	135.208
DMMorOH	133.190

Molecular weight of ionic liquids and bases used.

8.3 List of figures

<i>Figure 1: Hydrogenation/dehydrogenation of 9-ethylcarbazole as an example for LOHC [17].</i>	<i>9</i>
<i>Figure 2: Scheme of continuous flow hydrogen generator [33].</i>	<i>14</i>
<i>Figure 3: Scheme for an acid electrolyte fuel cell [40].</i>	<i>15</i>
<i>Figure 4: Scheme of a PEMFC (1) and of a DMFC (2) [42].</i>	<i>17</i>

<i>Figure 5: Scheme of a PEMFC electrode with gas diffusion layer (left), active layer (middle) and electrolyte (right) [40].</i>	18
<i>Figure 6: Example structure of Nafion® (a), 3MTM-PFSA (b) and Aquivion® (c) [41].</i>	18
<i>Figure 7: Advantages and applications of different types of fuel cells [40].</i>	21
<i>Figure 8: Raw nickel foam (left), during catalyst deposition (middle) and catalyst after calcination on nickel foam (right).</i>	25
<i>Figure 9: Scheme of the in-house made hydrogen release cell.</i>	25
<i>Figure 10: In-house made hydrogen release cell; spare parts (left) and assembled cell (right).</i>	26
<i>Figure 11: Measurement setup consisting of: hydrogen release cell, fuel cell and potentiostat [48].</i>	26
<i>Figure 12: Setup for volumetric water displacement method.</i>	29
<i>Figure 13: Glass cylinders during the measurement (left), double-neck flasks submerged into the thermostat (right).</i>	30
<i>Figure 14: Profile of hydrogen storage and hydrogen release chamber (left), front of hydrogen storage chamber (right), without piping and pressure controlling implemented.</i>	31
<i>Figure 15: Scheme of the system setup, with borohydride tank (left) and hydrogen release chamber (right).</i>	32
<i>Figure 16: Scheme of the self-regulating hydrogen supply system before the start of hydrogen evolution.</i>	33
<i>Figure 17: Scheme of the self-regulating hydrogen supply system during operation.</i>	34
<i>Figure 18: SEM images of the raw nickel foam support material (left) and the completed Co-W-B/Ni-foam catalyst (right) [52].</i>	36
<i>Figure 19: HRR from NaBH₄ solution (1 wt.% H₂) with four differently loaded Co-W-B/Ni-foam catalysts at 30°C, analysed by electrochemical approach.</i>	37
<i>Figure 20: HRR per gram catalyst from NaBH₄ solution (1 wt.% H₂) with four differently loaded Co-W-B/Ni-foam catalysts at 30°C, analysed by electrochemical approach.</i>	38
<i>Figure 21: Concentration profile of NaBH₄ solution (1 wt.% H₂) during hydrogen release of four differently loaded Co-W-B/Ni-foam catalysts at 30°C, analysed by electrochemical approach.</i>	38
<i>Figure 22: HRR from NaBH₄ solution (1 wt.% H₂) with four differently calcined Co-W-B/Ni-foam catalysts at 30°C, analysed by electrochemical approach.</i>	40
<i>Figure 23: HRR per gram catalyst from NaBH₄ solution (1 wt.% H₂) with four differently calcined Co-W-B/Ni-foam catalysts at 30°C, analysed by electrochemical approach.</i>	40
<i>Figure 24: Concentration profile of NaBH₄ solution (1 wt.% H₂) during hydrogen release of four differently calcined Co-W-B/Ni-foam catalysts at 30°C, analysed by electrochemical approach.</i>	41

<i>Figure 25: HRR from NaBH₄ solution (1 wt.% H₂) of the Co-W-B/Ni-foam catalysts at BOL and after 720 hours of non-stop operation at EOL, analysed by electrochemical approach at 30°C.</i>	<i>42</i>
<i>Figure 26: Concentration profile of NaBH₄ solution (1 wt.% H₂) during hydrogen release of the Co-W-B/Ni-foam catalysts at BOL and at EOL, analysed by electrochemical approach at 30°C.....</i>	<i>43</i>
<i>Figure 27: SEM images of a freshly manufactured catalyst at BOL (left) and after 720 hours of operation at EOL (right) [52].</i>	<i>44</i>
<i>Figure 28: HRR per gram catalyst from DMMorBH₄ solution (3 wt.% H₂) with different bases at ambient conditions, analysed by water displacement method.</i>	<i>45</i>
<i>Figure 29: Concentration profile of DMMorBH₄ solutions (3 wt.% H₂) made from different bases during hydrogen at ambient conditions, analysed by water displacement method.</i>	<i>46</i>
<i>Figure 30: Concentration profile of METMABH₄ solutions (3 wt.% H₂) made from different bases during hydrogen at ambient conditions, analysed by water displacement method.</i>	<i>47</i>
<i>Figure 31: HRR per gram catalyst from DMMorBH₄ solution (3 wt.% H₂) with Co-W-B/Ni-foam catalysts at different temperatures, analysed by electrochemical approach.</i>	<i>48</i>
<i>Figure 32: Arrhenius plot of DMMorBH₄ hydrolysis with Co-W-B/Ni-foam catalyst at 30°C, 40°C, 50 °C and 60°C.</i>	<i>50</i>
<i>Figure 33: Viscosity behaviour in dependence of the temperature of DMMorBH₄ in DMMorOH.....</i>	<i>51</i>
<i>Figure 34: HRR per gram catalyst from METMABH₄ solution (3 wt.% H₂) with Co-W-B/Ni-foam catalysts at different temperatures, analysed by electrochemical approach.</i>	<i>52</i>
<i>Figure 35: Arrhenius plot of METMABH₄ (in KOH) hydrolysis with Co-W-B/Ni-foam catalyst</i>	<i>53</i>
<i>Figure 36: HRR per gram catalyst from METMABH₄ solution (3 wt.% H₂) with Co-W-B/Ni-foam catalysts at different temperatures, analysed by electrochemical approach.</i>	<i>54</i>
<i>Figure 37: Concentration profile of METMABH₄ solution (3 wt.% H₂) during hydrogen release with Co-W-B/Ni-foam catalysts at different temperatures, analysed by electrochemical approach.....</i>	<i>55</i>
<i>Figure 38: Arrhenius plot of METMABH₄ (in NaOH) hydrolysis at 30°C, 40°C, 50 °C, 60°C and 70°C. ..</i>	<i>56</i>
<i>Figure 39: HRR and pressure profile of hydrolysis reaction from NaBH₄ solution (1.5 wt.% H₂) with Co-W-B/Ni-foam catalysts at ambient temperature, analysed by flow tracker. Hydrogen demand employed: 1000 ml/min.</i>	<i>58</i>
<i>Figure 40: HRR and concentration profile of hydrolysis reaction from NaBH₄ solution (1.5 wt.% H₂) with Co-W-B/Ni-foam catalysts at ambient temperature, analysed by flow tracker. Hydrogen demand employed: 500 ml/min.</i>	<i>59</i>
<i>Figure 41: Concentration and pressure profile of hydrolysis reaction from NaBH₄ solution (1.5 wt.% H₂) with Co-W-B/Ni-foam catalysts at ambient temperature, analysed by flow tracker. Hydrogen demand employed: 100 ml/min.</i>	<i>60</i>

<i>Figure 42: HRR and concentration profile of hydrolysis reaction from NaBH₄ solution (1.5 wt.% H₂) with Co-W-B/Ni-foam catalysts at ambient temperature, analysed by flow tracker. Hydrogen demand employed: 500 ml/min.</i>	<i>61</i>
<i>Figure 43: HRR and pressure profile of hydrolysis reaction from DMMorBH₄ solution (1.5 wt.% H₂) with Co-W-B/Ni-foam catalysts at ambient temperature, analysed by flow tracker. Hydrogen demand employed: 100 ml/min.</i>	<i>62</i>
<i>Figure 44: HRR and concentration profile of hydrolysis reaction from NaBH₄ solution (1.5 wt.% H₂) with Co-W-B/Ni-foam catalysts at ambient temperature, analysed by flow tracker. Hydrogen demand employed: 100 ml/min.</i>	<i>71</i>

8.4 List of tables

<i>Table 1: Examples for liquid organic hydrogen carriers [11].</i>	<i>10</i>
<i>Table 2: Properties of the ionic liquids METMABH₄ and DMMorBH₄ [21], [22].</i>	<i>13</i>
<i>Table 3: Efficiency limits based on HHV for hydrogen fuel cells [33].</i>	<i>20</i>
<i>Table 4: Parameters of nickel foam support material.</i>	<i>23</i>
<i>Table 5: Composition of the two solutions used for electrochemical deposition of the catalyst [40]. ...</i>	<i>24</i>
<i>Table 6: Parameters for HRR measurements.</i>	<i>27</i>
<i>Table 7: Equipment used for HRR measurements.</i>	<i>28</i>
<i>Table 8: Equipment for volumetric water displacement method.</i>	<i>29</i>
<i>Table 9: Equipment used for the simulation of non-stop operation.</i>	<i>30</i>
<i>Table 10: Setting parameters used for on demand hydrogen production.</i>	<i>34</i>
<i>Table 11: Equipment used for on demand hydrogen production.</i>	<i>35</i>
<i>Table 12: Parameters of the catalysts for electrochemical deposition optimization.</i>	<i>36</i>
<i>Table 13: Parameters for HRR measurement regarding electro-less deposition optimization.</i>	<i>37</i>
<i>Table 14: Parameters of the catalysts for thermal treatment optimization.</i>	<i>39</i>
<i>Table 15: Parameters for HRR measurement regarding thermal treatment optimization.</i>	<i>41</i>
<i>Table 16: Parameters of the catalysts for long-term experiments, m (foam) and M (loading) have been estimated.</i>	<i>42</i>
<i>Table 17: Parameters for BOL and EOL HRR measurement.</i>	<i>42</i>
<i>Table 18: Parameters of the catalyst used for volumetric performance characterization.</i>	<i>45</i>
<i>Table 19: Parameters of the various DMMorBH₄ solutions investigated.</i>	<i>46</i>
<i>Table 20: Parameters of the various METMABH₄ solutions investigated.</i>	<i>47</i>
<i>Table 21: Parameters of the catalysts used.</i>	<i>49</i>

<i>Table 22: Parameters of the ionic liquid investigated.</i>	49
<i>Table 23: Setting of the DMMorBH₄ investigation at different temperatures.</i>	49
<i>Table 24: Activation energy of DMMorBH₄ hydrolysis via Co-W-B/Ni-foam catalyst.</i>	50
<i>Table 25: Parameters of the catalysts used.</i>	52
<i>Table 26: Parameters of the ionic liquid investigated.</i>	52
<i>Table 27: Setting of the METMABH₄ investigation at different temperatures.</i>	53
<i>Table 28: Activation energy of METMABH₄ hydrolysis via Co-W-B/Ni-foam catalyst.</i>	53
<i>Table 29: Parameters of the catalysts used.</i>	55
<i>Table 30: Parameters of the ionic liquid investigated.</i>	55
<i>Table 31: Activation energy of METMABH₄ hydrolysis via Co-W-B/Ni-foam catalyst.</i>	56
<i>Table 32: Parameters of the catalysts used.</i>	57
<i>Table 33: Adjusted hydrogen demand measured.</i>	58
<i>Table 34: Parameters of the sodium borohydride solution used.</i>	61